EFFECTS OF AMMONIA EMISSIONS FROM AGRICULTURAL SOURCES ON AIR QUALITY AND SENSITIVE ECOSYSTEMS IN THE UNITED STATES

A Dissertation
Presented to
The Academic Faculty

by

Yilin Chen

In Partial Fulfillment
of the Requirements for the Degree
Doctor of Philosophy in the
School of Civil and Environmental Engineering

Georgia Institute of Technology
August 2020

EFFECTS OF AMMONIA EMISSIONS FROM AGRICULTURAL SOURCES ON AIR QUALITY AND SENSITIVE ECOSYSTEMS IN THE UNITED STATES

Approved by:

Dr. Armistead G. Russell, Advisor
School of Civil and Environmental Engineering
Georgia Institute of Technology

Dr. Jennifer Kaiser
School of Civil and Environmental Engineering
Georgia Institute of Technology

Dr. James A. Mulholland
School of Civil and Environmental Engineering
Georgia Institute of Technology

Dr. Yongtao Hu
School of Civil and Environmental Engineering
Georgia Institute of Technology

Dr. Rodney J. Weber
School of Earth & Atmospheric Sciences
Georgia Institute of Technology

Date Approved: 06/16/2020

ACKNOWLEDGEMENTS

I would like to express my sincere appreciation to all the wonderful people that I met during my graduate study. I would like to thank my advisor, Dr. Armistead Russell, for his guidance and support for my research, for his motivation, critical thinking, and immerse knowledge in air quality modeling. Besides my advisor, I would also like to thank my committee members, Dr. Rodney Webber, Dr. James Mulholland, and Dr. Jennifer Kaiser, for serving on my Ph.D. committee and providing insightful comments and criticism for my work. My sincere thanks also go to all the collaborators I had worked with, Dr. Jhih-Shyang Shih from Resources for the Future, Shuai Shao from Syracuse University, Dr. Amir Hakami and Dr. Shunliu Zhao from Carleton University, and Dr. Shannon Capps from Drexel University, for their expertise and valuable inputs to my research. I would like to thank Russell group members from whom I benefit a lot through discussions, group meetings, and daily companions. I would like to thank the funding sources for my research and graduate study, U.S. EPA and China Scholarship Council. Finally, I would like to acknowledge my family for their continuous support and for the delights they bring into my life. To my mom, for your unwavering support in my life whenever I needed you. To my husband, Huizhong, for sharing all the good and bad times with patience and trust. To my boy, Lucas, for your smiling faces and sweet hugs that make me feel fulfilled each day.

TABLE OF CONTENTS

LIST OF TABLES

LIST OF FIGURES

deposition is grouped for 10 level I ecoregions defined by the Commission for Environmental Cooperation, including Northern Forests (NF), Great Plains (GP), Northwestern Forested Mountains (NFM), Marine West Coast Forest (MWCF), North American Deserts (NAD), Mediterranean California (MC), Southern Semiarid Highlands (SSH), Temperate Sierras (TS), and Tropical Wet Forests (TWF).

LIST OF SYMBOLS AND ABBREVIATIONS

Nr	reactive nitrogen
CMAQ	Community Multiscale Air Quality Model
NEI	National Emission Inventory
EGU	energy generation unit
Nr-oxi	oxidized form reactive nitrogen
Nr-red	reduced form reactive nitrogen
CONUS	contiguous United States
USGS	US Geological Survey
4D-Var	four-dimensional variational assimilation
IMB	iterative mass balance
LWC	liquid water content
USDA	U.S. Department of Agriculture
WRF	Weather Research and Forecasting
GISS	Goddard Institute for Space Studies
RH	relative humidity
TNH_x	total ammonium

CASTNET	Clean Air Status and Trends Network
AMoN	Ammonia Monitoring Network
SEARCH	Southeast Aerosol Research and Characterization network
NMB	normalized mean bias
NRMSE	normalized root mean square errors
NVC	non-volatile cations
CL	critical loads
ACM2	asymmetric convective model version 2
CESM1	Community Earth System Model version 1
SSP	Shared Socio-Economic Pathway
NCLD	National Critical Loads Database
ANC	acid neutralization capacity
SPARROW	SPAtially Referenced Regressions On Watershed
CAFO	concentrated animal feeding operations
IASI-NH_3	Infrared Atmospheric Sounding Interferometer NH_3 column density
CrIS	Cross-track Infrared Sounder
TES	Tropospheric Emission Spectrometer
LST	local standard time

Ω_o	mean column density
σ	relative error
NARR	North American Regional Reanalysis
E_t	new emission estimates
E_a	*a priori* emission estimates
ε	scaling factor
J	cost function
S_a	error covariance matrices for the *a priori* emission estimates
S_o	error covariance matrices for the *IASI-NH3 retrievals*
$F(\varepsilon)$	CMAQ simulated NH_3 column density sampled at the satellite passing
γ	regularization factor
NADP	National Atmospheric Deposition Program

SUMMARY

Anthropogenic ammonia (NH_3) emissions significantly disturb the global nitrogen cycle, causing a series of adverse impacts on air quality, human health, and ecosystem well-being. Sources of NH_3 emissions include, predominantly, agricultural practices including fertilizer application and livestock waste management, as well as automobile exhaust and industrial operations. Despite its rising environmental impact, the future response of air quality and nitrogen loading in sensitive ecosystems to agricultural NH_3 emission increases are not well understood. The impact assessments are hindered by the large uncertainty in emission inventories and a lack of routine measurements to constrain NH_3 abundance. This thesis presents the development, evaluation, and application of an integrated modeling framework to estimate the future response of $PM_{2.5}$ (particulate matter with an aerodynamic diameter of 2.5 micrometers or less) formation and reactive nitrogen (Nr) deposition to the rising agricultural NH_3 emission in the United States when other conventional pollutants are being further regulated. Present-day and future scenarios are designed to reflect emission and meteorological condition changes between 2011 and 2050. Both agricultural NH_3 emission increase and reduction of conventional pollutants including sulfur dioxide (SO_2) and oxides of nitrogen (NO_x) are considered, as well as the impact of global change.

First, ambient $PM_{2.5}$ acidity, mass concentration, and chemical speciation are simulated for present-day and future scenarios using the Community Multiscale Air Quality Model (CMAQ). Additional sensitivity scenarios are tested to explore the response of aerosol formation, composition, and pH to different levels of anthropogenic SO_2 emission control and boundary conditions. The simulation results show that the aerosol

will remain acidic in the future even with an aggressive reduction in anthropogenic SO_2 emissions and increases in NH_3 emissions in the U.S., because of the buffering effect of NH_3-ammonium (NH_4^+), as well as the increasing relative contribution from background sulfate (SO_4^{2-}). One consequence of this is that, rising agricultural NH_3 emissions and SO_2 reductions will not cause nitrate substitution in most of North America, contrary to the common belief, although it will possibly happen in the central parts of the country if NH_3 and NO_x emissions are not further controlled. Second, the impact of Nr deposition on sensitive ecosystems is evaluated by comparing the simulated Nr deposition with critical loads targeting both acidification and biodiversity. The evaluation identifies that areas with intensive NH_3 emission from agricultural practices will remain in exceedance despite effective NO_x emission control. Reducing the nitrogen deposition level below the critical loads requires simultaneous control of NH_3 emissions from agriculture activities and NO_x emissions from fossil fuel combustion. The Nr deposition is further linked with a water quality model to locate watersheds vulnerable to agricultural NH_3 emission increase. The results provide valuable information to help guide regulation priorities for NH_3 emission regulation in the U.S.

As noted above, NH_3 emission are viewed as highly uncertain. In response, the thesis constrains the NH_3 emission estimates from the National Emission Inventory (NEI) using satellite observations and hybrid inverse modeling. The adjoint of CMAQ is applied for the first time to emission optimization. The optimized NH_3 emission in April is 46% higher than the NEI estimates with large spatial differences. Model evaluation against independent ground observations including NH_3 concentrations and particulate NH_4^+ concentrations, both suggest the optimized NH_3 emissions reduce model bias. Re-evaluation of $PM_{2.5}$

concentrations and Nr deposition with the optimized NH_3 emissions shows the optimization can partly close the gap between simulated and observed $PM_{2.5}$ concentration by reducing the bias in simulated ammonium nitrate (NH_4NO_3). The Nr deposition in sensitive ecosystems might be underestimated by 40% in April due to the low bias in NH_3 emission. The optimized NH_3 emission and NEI estimates are in good agreement in July and October.

Overall, the integrated framework and simulations presented in this thesis provide valuable information by identifying the regions where agricultural NH_3 emissions are and/or will be a major contributor to air quality degradation and ecosystem harm. The capability of inverse modeling using satellite observations to constrain NH_3 emission estimates and improvement in model performance is demonstrated.

CHAPTER 1. INTRODUCTION

Ammonia (NH_3) emissions cause a series of adverse environmental impacts on ambient air quality, soil and water quality, and sensitive ecosystem well-being. NH_3 can condense onto particle surface through thermodynamic partitioning and form ammonium sulfate ($(NH_4)_2SO_4$), ammonium bisulfate (NH_4HSO_4), and ammonium nitrate (NH_4NO_3) (Seinfeld and Pandis 2016), contributing to $PM_{2.5}$ (particulate matter with an aerodynamic diameter of 2.5 micrometers or less) mass. NH_3 can also condense onto freshly nucleated particles and support rapid particle growth (Wang et al., 2020). Exposure to $PM_{2.5}$ is known to be associated with cardiovascular disease, respiratory disease, and premature mortality (Cohen et al., 2017; USEPA 2019c). After depositing on terrestrial surfaces, NH_3 and NH_4^+ can cause acidification and eutrophication due to the excessive nitrogen load received by the ecosystems (Fowler et al., 2013; Galloway et al., 2003). The soil and water quality degradation can further reduce biodiversity (Bobbink and Hicks 2014; Porter et al., 2013).

Excess NH_3 emissions mainly stem from agricultural practices. It is estimated that livestock waste management contributes to over 50% of total NH_3 emission, followed by 30% from fertilizer application, and together the two practices account for over 80% of the anthropogenic NH_3 emission in the U.S. (Battye et al., 2003; Paulot et al., 2014). Not being considered as a criteria pollutant, no direct regulations target atmospheric NH_3 emission from agricultural practices. During the past two decades, NH_3 emission stayed stagnant even though nitrogen use efficiency has been improved, pushed up by the growth of both domestic and export food demand (Galloway et al., 2007; NRC 2008). More fertilizer nitrogen is applied to the cropland to achieve higher yield while the nitrogen recovery

efficiency remains largely unchanged, resulting in more Nr loss to the environment (Conant et al., 2013). Increased meat consumption also raises NH_3 emission from animal manure handling (Zeng et al., 2019). The NH_3 emission from agriculture sources is expected to rise in the foreseen future, as more food is needed to sustain a growing population. The rising temperature under climate warming will also favor the release of NH_3 from vegetation, soil surface, and farms (Bash et al., 2013; Massad et al., 2010; Sutton et al., 2013).

In contrast, SO_2 and NO_x emissions have been decreasing due to successful emission control of mobile sources, energy generation units (EGUs), and other sources (Dallmann and Harley 2010; Kim et al., 2006; Li et al., 2016). Further reduction of SO_2 and NO_x emissions from fossil fuel combustion is expected to continue in the near future with more stringent air quality and emission standards (Campbell et al., 2018). Despite the reduction of $PM_{2.5}$ under successful emission controls of SO_2 and NO_x, a few areas remain in nonattainment of the National Ambient Air Quality Standards. The marginal cost to further reduce $PM_{2.5}$ through those traditional control programs are expected to be high (USEPA 2011). Controlling NH_3 emission from agriculture sources possibly provides a more cost-effective alternative solution to reduce $PM_{2.5}$ in the future. Some studies suggest that NH_3 emission control may be more effective to reduce $PM_{2.5}$ as aerosol composition shifted from sulfate to nitrate dominated (Pinder et al., 2007).

Beyond its air quality and human health impacts, NH_3 emission will affect ecosystem well-being through atmospheric deposition of reactive nitrogen (Nr). It is observed that the Nr deposition pattern has shifted from being dominated by Nr-oxi (oxidized form of reactive nitrogen) to being dominated by Nr-red (reduced form of reactive nitrogen) dominated because of the coupled NO_x emission reduction and NH_3 emission increase

during the past two decades (Dallmann and Harley 2010; Kim et al., 2006; Li et al., 2016). This undermines the efforts to reduce excessive Nr deposition in sensitive ecosystems and pose an even higher risk to the vegetations because their normal function will be impaired when exposed to too much ammonium in soil and water (Bobbink and Hicks 2014).

Building upon the accumulated pieces of evidence finding the importance of NH_3 emission control, this thesis seeks to quantify the impacts of increasing NH_3 emissions on air quality and ecosystem well-being in the U.S. under future conditions using chemical transport modeling. Further, the research lays out how global change acts together with emissions changes to modify the composition and acidity of aerosols.

The ability of models to simulate aerosol formation or Nr deposition largely depends on the input emissions inventory. However, there is a large uncertainty associated with NH_3 emission estimates. The national total NH_3 emission estimates reported by different inventories vary by a factor of 2 (Paulot et al., 2014). Comparison between top-down emission estimates using satellite observations and the bottom-up inventories developed by using estimates of human activities and emissions factors suggest that the inventoried emission strength is generally underestimated by a factor of 10 to 100 for large point sources (Dammers et al., 2019; Van Damme et al., 2018). A lack of detailed information for emission factors and agricultural activity level obscure the development of a bottom-up emission inventory with high spatial and temporal resolution. Numerous factors can influence the NH_3 emission from agricultural practices, including the facility temperature, management practices for different animal types, nitrogen in the feed for livestock waste management and soil temperature, amount and timing for fertilizer application, application method for crop production (Cooter et al., 2012; McQuilling and Adams 2015).

A historical lack of NH_3 monitoring data further limits our ability to constrain the emission estimates using inverse modeling technique. The routine monitoring of ambient NH_3 concentration did not start until 2007 in the U.S. and only 107 operational monitoring sites are providing bi-weekly averages, 39 of which are collocated with NH_4^+ monitoring sites, providing much less data than what is required to capture the spatial and temporal distribution of NH_3 emissions. The increasing availability of satellite observations of NH_3 columns provides a great opportunity to fill the gap with high spatial coverage and semi-daily temporal resolution (Clarisse et al., 2009; Shephard et al., 2020; Van Damme et al., 2015b; Warner et al., 2016).

This thesis first evaluates the present and future environmental impacts of NH_3 emission by assessing 1) the response of aerosol acidity, $PM_{2.5}$ mass concentration, and chemical speciation to co-occurring emissions and climatological changes; 2) the change in Nr deposition amount and relative abundance of Nr-red. In this first section of the thesis, emission estimates from the National Emission Inventory (NEI) are adopted as the emission input data for the Community Multiscale Air Quality Model (CMAQ) (USEPA 2015). Given the recognized uncertainty in the NH_3 inventories, the potential bias of the NH_3 emission estimates is then addressed by inverse modeling optimization using the adjoint of CMAQ and satellite retrieved NH3 column density from the Infrared Atmospheric Sounding Interferometer (IASI) (Van Damme et al., 2015b). The implications of the optimized NH_3 emission estimates are quantified by re-evaluating the change in $PM_{2.5}$ and Nr deposition. All research presented in this thesis focus on the contiguous United States (CONUS). A diagram of the integrated modeling framework for the thesis is

presented (Figure 1-1). A brief introduction to each chapter in this thesis is presented below.

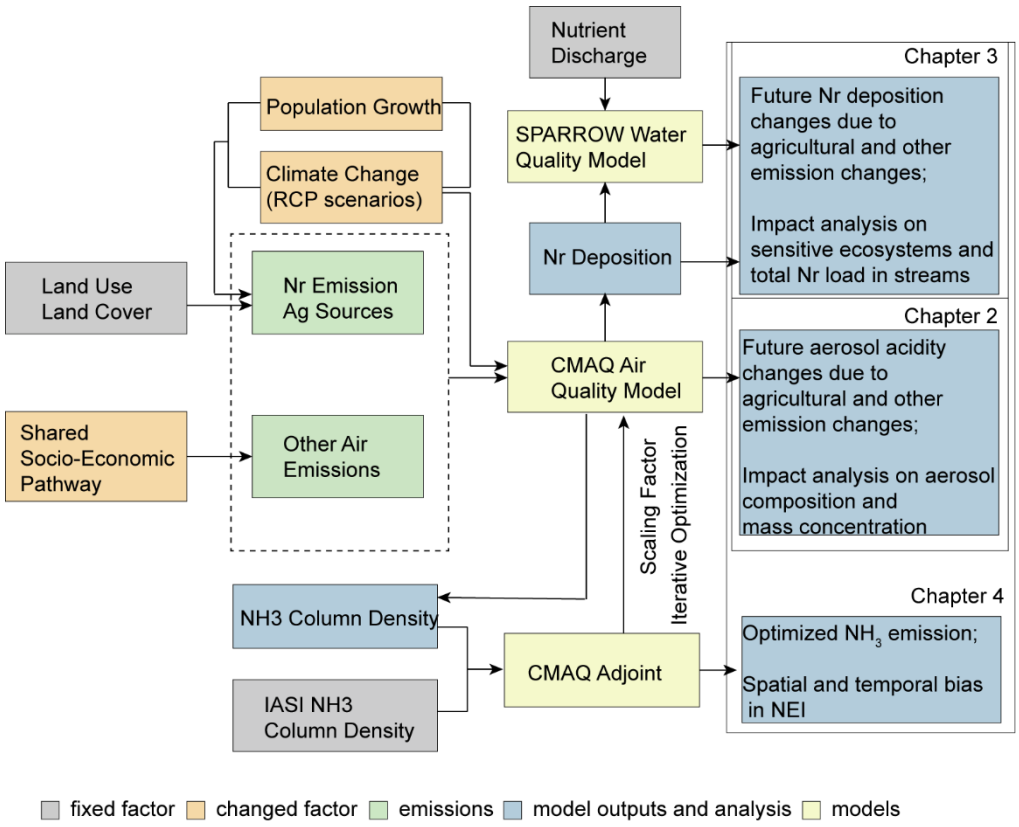

Figure 1-1 Flow chart of the integrated modeling framework and major outcomes of each chapter in this thesis

Chapter 2 presents current and future responses of aerosol pH and composition in the CONUS to declining SO_2 emissions and increasing NH_3 emissions. A set of sensitivity tests are performed by perturbing the SO_2 and NH_3 emissions based on projected baseline future emissions following representative concentration pathway (RCP) 4.5 and MiniCAM stabilization scenarios (Thomson et al., 2011). The aerosol pH and aerosol formation are

simulated using CMAQ v5.0.2, which incorporates the thermodynamic equilibrium model ISORROPIA-II (Fountoukis and Nenes 2007; USEPA 2014a). Results showed that the aerosol will remain acidic in the future even with an aggressive reduction of anthropogenic SO_2 emissions and an increase in agricultural NH_3 emissions in the US. Limited "nitrate substitution" occurs even if SO_2 emissions are further reduced drastically in the future. The projected NH_3 emission increase in the future will barely change the $PM_{2.5}$ mass load, even under the most extreme SO_2 emissions control scenario. A modified version of this chapter has been published in Environmental Science and Technology (Chen et al., 2019).

Chapter 3 presents the ecological impacts of Nr deposition at present-day and future levels by comparing the simulated Nr deposition with multiple critical loads targeting the protection of different sensitive ecosystems. The simulated deposition fields are integrated water with the US Geological Survey (USGS) water quality model, SPARROW, to qualitatively estimate the main source of total Nr load at the watershed level over the CONUS (Schwarz et al., 2006). The results show that the decline in nitrogen deposition achieved by NO_x emission control for power and transport sectors would be offset or even reversed by NH_3 emission increase from the agricultural sector. The assessment helps inform regulation priorities for NH_3 emission regulation in the country by identifying areas with Nr critical load exceedances and areas sensitive to atmospheric Nr deposition. A modified version of this chapter is under review in Earth's Future (Chen et al., 2020a).

Results from the second and third chapters evaluate the model performance of CMAQ simulation using NH_3 emission estimates from NEI.

Chapter 4 presents the optimization of NH_3 emission estimates using inverse modeling techniques and satellite retrieved NH_3 column density. A hybrid inverse modeling approach consisting iterative mass balance (IMB) optimization at coarse resolution followed by four-dimensional variational assimilation (4D-Var) optimization at fine resolution is applied for the first time to optimize NH_3 emissions. The 4D-Var optimization framework is developed in this thesis using the newly developed multiphase adjoint of CMAQ v5.0 and a steepest-descent optimization algorithm (Zhao et al., 2019). The optimization is performed in April, July, and October 2011 using IASI observations in the corresponding months. The 2011 NEI is used as the a priori emission inventory. The results find that total NH_3 emission is underestimated by 46% in April with a significant low bias in Southern states and a high bias in the Midwest. In July and October, the optimized NH_3 emission is only ~7% higher than the 2011NEI and the spatial distribution agrees well. Model evaluation using independent observations shows that the optimized emission estimates yield a better agreement between simulated and observed NH_3 concentration and particulate NH_4^+ concentrations, supporting that the optimized inventory is improved from top-down constrains. A re-evaluation of aerosol formation and Nr deposition using the optimized NH_3 emission show that the relative contribution of NH_4NO_3 to $PM_{2.5}$ is lower in Midwest and higher in Pacific West and the Rocky Mountains. The magnitude of change is larger than 10%, suggesting that the uncertainty of NH_3 emission inventory is a key factor for errors in the $PM_{2.5}$ simulation. The Nr deposition is generally higher in sensitive regions with the optimized NH_3 emission, implying an underestimated role of agricultural NH_3 emissions to the elevated Nr burden. A modified version of this chapter is under review in Atmospheric Chemistry and Physics (Chen et al., 2020b).

The final chapter concludes the thesis with a summary of major finding in the previous chapters as well as ideas for future work that will allow further applications of the integrated modeling framework developed in this thesis, and its application to studies involving agricultural NH_3 emissions on air, and water quality, and new observations worldwide from space.

CHAPTER 2. CURRENT AND FUTURE RESPONSES OF AEROSOL PH AND COMPOSITION IN THE US TO DECLINING SO_2 EMISSIONS AND INCREASING NH_3 EMISSIONS

2.1 Abstract

Aerosol pH can affect gas-particle partitioning of semi-volatile species, secondary aerosol formation, aerosol water uptake and growth, acid deposition and, potentially, aerosol toxicity. Despite its importance, aerosol pH projected in the near future has not been addressed explicitly while investigating the response of aerosol concentrations to emission regulations. In this study, we apply CMAQ to simulate aerosol pH in 2011 and 2050 across the continental US. We also assess the influence of two major emission trends, declining SO_2 emissions and rising NH_3 emissions, with a set of sensitivity simulations. Our results show that the aerosols will remain acidic with average pH typically ranging from 0.5 to 3.5 in 2050. Further reducing domestic SO_2 emissions does not significantly decrease aerosol acidity, even if SO_2 emissions were reduced to preindustrial level because of the nonlinear response of SO_4^{2-} concentration to SO_2 emissions, and the semi-volatile NH_3-NH_4^+ buffering effect. Aerosol pH response to NH_3 emission increase will remain minor. Consequently, future fine particulate matter control efficiency will not be undercut by additional nitrate aerosol formation even if SO_2 emissions from industry and electricity generation are aggressively controlled, though areas will see some substitution leading to nitrate increases if NO_x emissions are not reduced.

2.2 Introduction

Exposure to ambient fine particles (particulate matter with aerodynamic diameter of 2.5 micrometers or less i.e., $PM_{2.5}$) is linked to adverse health outcomes (Burnett et al., 2014; Nel 2005). $PM_{2.5}$ can also disturb the nutrient balance of ecosystems (Galloway et al., 2003), and impact climate (Ramanathan et al., 2001). While not directly observed, aerosol pH is critical because it not only influences the ambient concentration of $PM_{2.5}$ through mediating the formation pathways of organic and inorganic compounds (Cheng et al., 2016; Wang et al., 2016a), but also affects several other important chemical, physical, and radiative properties. The total mass of $PM_{2.5}$ formed and the chemical composition are affected by aerosol pH because it affects the gas-particle partitioning of semi-volatile species including ammonia (NH_3) and ammonium (NH_4^+), nitric acid (HNO_3) and nitrate (NO_3^-), and organic acids (Guo et al., 2016). The gas-particle partitioning further influences the amount and the spatial pattern of reactive nitrogen deposition because the deposition velocities of NH_3 and HNO_3 are much higher than particle bound NH_4^+ and NO_3^- (Sehmel 1980). Aerosol pH also influence the solubility of trace metals contained in particles (Fang et al., 2015). The mobility and oxidation state of trace metals such as iron, copper, and manganese, in acidic atmospheric particles may link to their toxicity and ecosystem impacts (Fang et al., 2015; Oakes et al., 2012). Secondary organic aerosol (SOA) formation is found to be enhanced at low pH (Marais et al., 2016; Surratt et al., 2007). Chamber studies also found that light-absorbing SOA is formed in the presence of highly acidic seeds as the formation process is accelerated at low pH (Moise et al., 2015; Song et al., 2013). Further, pH is associated with liquid water uptake (Guo et al., 2015).

Aerosol pH is defined as the negative of the base 10 logarithms of the hydrogen ion (H^+) activity in the particle water (Buck et al., 2002). It is determined by the thermodynamic

equilibrium between anions and cations in particles, as well as the particle liquid water content (LWC). Although aerosol pH is difficult to precisely measure directly because of the non-conservation of the hydrogen ion, thermodynamic equilibrium models including AIM2 (Clegg et al., 1998; Clegg and Pitzer 1992), SCAPE2 (Kim et al., 1993), EQUISOLV II (Jacobson et al., 1996), ISORROPIA-II (Fountoukis and Nenes 2007), E-AIM (Friese and Ebel 2010), and AIOMFAC (Zuend et al., 2011) can be used to estimate pH given the aerosol composition. Model evaluation studies show that they are capable of reproducing the measured gas-particle partitioning of semi-volatile species including NH_3 - NH_4^+ and HNO_3 - NO_3^- pairs, both of which are sensitive to pH prediction bias (Guo et al., 2016; Guo et al., 2015; Hennigan et al., 2015; Zhang et al., 2000).

Aerosols are found to be highly acidic across the continental United States (CONUS) with the average bulk aerosol pH consistently below 3 (Lawal et al., 2018). An evaluation of historical aerosol pH change over the past 15 years at a monitoring site in the southeastern US reveals that the pH remained below 2 while sulfate concentration decreased by 70% and predicts that the pH will remain low in the near future, even if sulfate concentrations are further reduced with other conditions unchanged (Weber et al., 2016).

Studies project decreasing anthropogenic emissions of air pollutants, including SO_2 and NO_x, and increasing emissions of NH_3 (Lee et al., 2016b; Pye et al., 2009; Trail et al., 2014). Further impacting aerosol pH, projections from global and regional climate models predict that temperatures will rise and relative humidity (RH) will decrease through most of the CONUS (Yahya et al., 2017). Expanding urban areas in the future may also impact aerosol pH due to the urban heat island effect (Battaglia et al., 2017).

Despite its importance, the responses of aerosol pH to future changes in emissions and meteorological conditions are not well understood. Scenario simulations and sensitivity tests with chemical transport models provide an effective way to project future aerosol pH change for the CONUS with widely varying emissions and meteorological conditions. In this study, we employ the Community Multiscale Air Quality Model (CMAQ) (Byun and Schere 2006), which incorporates ISORROPIA- II to compare simulated aerosol pH for both historical (2011) and future scenarios (2050) over the CONUS. For the future baseline scenario, future sectoral emissions changes in various pollutants, including SO_2 and NO_x, were projected according to the RCP 4.5 scenario (Thomson et al., 2011). In addition, NH_3 emissions from livestock, fertilizer application, and forest fires were estimated using forecasted land use changes, agricultural activity, and population growth. The sensitivity of aerosol pH to SO_2 emission changes is derived by simulating the future pH change at different SO_2 reduction levels starting from the baseline scenario. The relationship between NH_3 emission increases to changes in aerosol pH projected in the near future at varying SO_2 emission levels is also investigated. The implications for nitrate aerosol formation and human health impacts caused by aerosol pH in response to changing emissions are quantified.

2.3 Materials and Methods

2.3.1 Emissions and meteorological fields

Historical emissions were generated for the year 2011 from EPA 2011 air emissions modeling platform v6.1 based on the 2011 National Emissions Inventory (USEPA 2014b) using a 36 km by 36 km horizontal grid. Emissions of the future baseline scenario were

derived by applying sectoral annual-fixed adjustment factors for each species. Specifically, sector-specific growth factors of emissions of NO_x, SO_2, NH_3, CO, CH_4, VOC, elemental carbon (EC), organic carbon (OC), and other PM components were applied to six anthropogenic sectors (international shipping, mobile sources, residential and commercial use, power plants, industry, and solvents). The growth factors were calculated as the ratio of annual emissions between the year 2050 and year 2010 over the CONUS following the RCP4.5 pathway (Thomson et al., 2011) (Table A-1**)**. Future NH_3 emissions from livestock were projected based on historical and future animal populations by assuming constant emission factors for the source categories between 2011 and 2050. Animal-specific population regressions were performed for cattle, swine, and poultry production using historical and future livestock projection statistics from U.S. Department of Agriculture (USDA) (Figure A-1) (USDA 2018a; b). As future animal statistics were only available until 2027, linear growth was assumed afterward. Fertilizer application emissions for both historical and future scenarios were estimated using CMAQ with the NH_3 bidirectional exchange model and EPIC simulated fertilizer application associated with land-use types (Bash et al., 2013). Historical and future land-use data were derived from the LandCarbon Database under the Intergovernmental Panel on Climate Change A1B scenario (Zhu et al., 2010). The projected increase in agricultural NH_3 emissions assumes mitigation measures to improve NUE and abatement approaches to reduce atmospheric NH_3 emissions remain unchanged at present-day level.

While the baseline 2050 scenario already represents a 70% reduction in SO_2 emissions, a series of future reduction scenarios were simulated to test the sensitivity of aerosol pH change to future SO_2 reduction. Total SO_2 emissions were reduced to 25% and 6.25% of

the future baseline level for each grid within the study domain. For each SO_2 emission level, aerosol pH was simulated with both current and future NH_3 emission levels to explore the difference in the sensitivity of aerosol pH change to NH_3 emission changes at varying SO_2 emission levels. We also include two scenarios which exclude all anthropogenic SO_2 emissions to distinguish the effects of anthropogenic emissions on aerosol pH. All scenarios simulated in this study are summarized in Table 2-1.

Meteorological fields for use by CMAQ and emissions estimates were downscaled using the Weather Research and Forecasting (WRF) model using global fields from the Goddard Institute for Space Studies (GISS) ModelE2 (Trail et al., 2013) for the year 2010 and year 2050 Spectral nudging was used in WRF. Changes in temperature, RH, horizontal wind velocities, soil temperature and moisture, and surface pressure were considered. Single years of meteorological fields were used to focus the analysis on the impacts of emissions changes.

Table 2-1 Description of emissions and meteorological data for simulation scenarios. The emission year for different species and the year of meteorology for each scenario is provided. The values of annual emissions of SO_2 and NH_3 over the CONUS is provided in parentheses with the emission year.

Scenario	Description	Emission year for different species (annual emission values for the CONUS)			Year of meteorology
		SO_2 emissions	NH_3 emissions	Other emissions	
H	Historical scenario	2011 (6.1 Tg)	2011 (3.6 Tg)	2011	2011
FB	Future baseline scenario	2050 (1.8 Tg)	2050 (4.0 Tg)	2050	2050
FB_fixed NH_3	Future baseline scenario with fixed NH_3	2050	2011	2050	2050
FS1	Future sensitivity scenario 1	2050 (25% of baseline, 0.43 Tg)	2050	2050	2050

FS1_fixed NH_3	Future sensitivity scenario 1 with fixed NH_3	2050 (25% of baseline, 0.43 Tg)	2011	2050	2050
FS2	Future sensitivity scenario 2	2050 (6.25% of baseline, 0.11 Tg)	2050	2050	2050
FS2_fixed NH_3	Future sensitivity scenario 2 with fixed NH_3	2050 (6.25% of baseline, 0.11 Tg)	2011	2050	2050

2.3.2 Chemical transport model

Aerosol pH was simulated over the CONUS for historical (2011) and future (2050) years at a 36km by 36 km resolution using CMAQ 5.0.2 (USEPA 2014a). The model extends vertically up to around 15.9 km, though this study focuses on particles in the surface layer (~18m). For regional analysis, the CONUS was divided into northeastern, southeastern, central, and western US as defined in Figure A-2. All scenario simulations were run for one year with a 10-day spin-up. CMAQ default boundary conditions for chemical mechanism CB05 with AERO06 were used. These are designed to represent relatively

clean air in the eastern half of the US (Gipson 1999). The same boundary conditions were used for all simulations to focus on the emissions' influence on aerosol pH. Detailed model setup was described by a previous study (Trail et al., 2014).

Aerosol pH was estimated from the thermodynamic equilibrium of the simulated K^+ - Ca^{2+} - Mg^{2+} - NH_4^+ - Na^+ - SO_4^{2-} - NO_3^- Cl^- - H_2O system with ISORROPIA-II implemented in the aerosol module (AERO6) in CMAQ (Fountoukis and Nenes 2007). The "forward mode" and "metastable" aerosol option were chosen for ISORROPIA-II, given that the daily average RH in most grids over the CONUS is over 60% and particle gas concentrations are available. The model results from ISORROPIA-II are also more robust under the "metastable" mode, while coding errors have been identified in the "stable" mode (Song et al., 2018). The inclusion of crustal species allows for evaluation of the influence of sea salt and dust on aerosol pH. Some studies suggest that sea salt and dust emissions may change in the future due to climate change (Struthers et al., 2013; Tegen et al., 2004). Such changes are uncertain and were assumed to be constant between the current and future scenarios. In addition to its implementation directly in CMAQ, ISORROPIA-II was also run offline with gas and condensed phase species concentrations from CMAQ to test the sensitivity of aerosol pH to temperature and RH. When computing aerosol pH using ISORROPIA-II, fine mode particles including both the Aitken mode and the accumulation mode are considered, and the particles are assumed to be internally mixed and independent of the particle size (Fountoukis and Nenes 2007). Daily average aerosol pH values were calculated using daily average equilibrium H^+ concentrations and LWC based on the CMAQ hourly output. Seasonal and annual average aerosol pH were then calculated by

averaging the daily aerosol pH. It is worth noticing that different ways of averaging will lead to different pH values (Figure A-3).

2.3.3 Ambient data for model evaluation

Although the model performance of CMAQ to simulate $PM_{2.5}$ concentrations over the US has been examined before (Struthers et al., 2013; Tegen et al., 2004; Trail et al., 2014; USEPA 2018), its ability to simulate aerosol pH has not been as extensively evaluated, especially over the entire CONUS domain. We compared the predicted and observed partitioning of semi-volatile species including NH_3 - NH_4^+ and HNO_3 - NO_3^- pairs as a proxy because they are very sensitive to pH (Guo et al., 2016; Guo et al., 2015). The partitioning ratios ($\varepsilon(NH_4^+)$ and $\varepsilon(NO_3^-)$) were defined as the molar ratio of NH_4^+ and NO_3^- to total ammonium ($TNH_x = NH_3$ (g) + NH_4^+) and total nitrate ($TNO_3 = HNO_3$ (g) + NO_3^-), respectively. The observational data for HNO_3, NO_3^-, and NH_4^+ were obtained from the Clean Air Status and Trends Network (CASTNET) and data for NH_3 were obtained from collocated Ammonia Monitoring Network (AMoN) and CASTNET sites for the year 2011. Data for NH_3 and NH_4^+ from three sites of the Southeast Aerosol Research and Characterization (SEARCH) network were also included. The time resolution chosen for model evaluation was determined by the time resolution of available monitoring data. For the HNO_3 - NO_3^- pairs, there are 82 sites in total with weekly average concentrations reported. For the NH_3 - NH_4^+ pair, there are 42 sites in total and the bi-weekly average was taken, as that is the temporal resolution of NH_3 concentration reported for AMoN. Reanalysis meteorology fields and emissions generated for the year 2011 were used as inputs to CMAQ. The weekly average of HNO_3 and NO_3^- concentrations, as well as the biweekly average of NH_3 and NH_4^+ concentrations, were extracted from CMAQ outputs

for each grid covering the monitoring sites. Annual average aerosol pH from CMAQ simulations was also compared with that predicted from ISORROPIA-II offline provided from a recent study (Lawal et al., 2018). The estimates are based on measured gas and particle species concentration, temperature, and RH measured at CASTNET, AMoN, and SEARCH. When comparing the simulated results in this study with measurements, the bias is defined as the deviation of simulated values from the measurements, meaning a low bias indicates the simulated value is lower than the measurement and vice versa. Limited by available information, this study has not considered the potential systematic offsets between different monitoring networks with different site setup and methods. Future model development and evaluation will benefit from more spatially extensive and species-comprehensive measurements.

We also employed a second evaluation method, assessing model simulated $PM_{2.5}$ compositions against ambient monitoring network data (Nolte et al., 2015). The modeled and measured annual and daily average concentrations of SO_4^{2-}, NO_3^-, NH_4^+, and non-volatile cations (NVC, referring to Na^+, K^+, Ca^{2+}, and Mg^{2+} in this study) were compared.

2.4 Results and Discussion

2.4.1 Model evaluation

CMAQ's ability to capture the variability in aerosol pH is shown by comparing the observed and simulated partitioning ratio of semi-volatile species, which are sensitive proxies of pH variation. Comparison between simulated and monitored $PM_{2.5}$ composition concentrations further support the model's ability to capture the overall aerosol pH spatial trend. Annual average partitioning ratios ($\varepsilon(NH_4^+)$ and $\varepsilon(NO_3^-)$ are calculated based on

simulated and measured gas and particle concentrations (Figure 2-1). Normalized mean bias (NMB) and normalized root mean square errors (NRMSE) are calculated to evaluate the spatial variation of partitioning ratios at the monitoring sites. Overall, CMAQ successfully captures the spatial trend of $\varepsilon(NH_4^+)$ and $\varepsilon(NO_3^-)$ over the CONUS, e.g., the high $\varepsilon(NH_4^+)$ in the eastern US and lower ratios in the central and western US. The NMB was 8.3%, although the predicted concentrations for NH_3 and NH_4^+ are both biased low compared to monitoring results (Figure A-4). The low bias in NH_3 and NH_4^+ is consistent with the finding that TNHx wet deposition is underestimated after precipitation adjustment in CMAQ version 5.0 when including the bi-directional NH_3 flux (Bash et al., 2013). For $\varepsilon(NO_3^-)$, the model is biased low (40%) because of the low bias in NO_3^- (Figure A-4). Several factors have been hypothesized for the low bias in NO_3^-, including a bias in NO_3^- fraction between fine and coarse mode (Nolte et al., 2015), decreased reliability of ISORROPIA-II at low RH (Guo et al., 2016), and lower ambient NH_3 predicted using CMAQ with bi-directional NH_3 flux (Bash et al., 2013). Simulated pH in this study is generally lower (more acidic) than the pH calculated based on observed concentrations, temperature, and RH at the monitoring sites (Figure 2-1). The absolute difference between annual average pH varies from 0.04 to 3.7 units. However, the relative difference is under 40% for 25 out of the 32 sites. For the four sites with relative differences over 60%, the measured NVC concentrations were among the highest of all sites. However, CMAQ failed to reproduce such high NVC concentrations, and the simulated values were only 3% to 11% of the measured values. This can be tied to a potential low bias in the emissions or the fine-mode size distribution of dust and sea salt (Appel et al., 2013; Gantt et al., 2015).

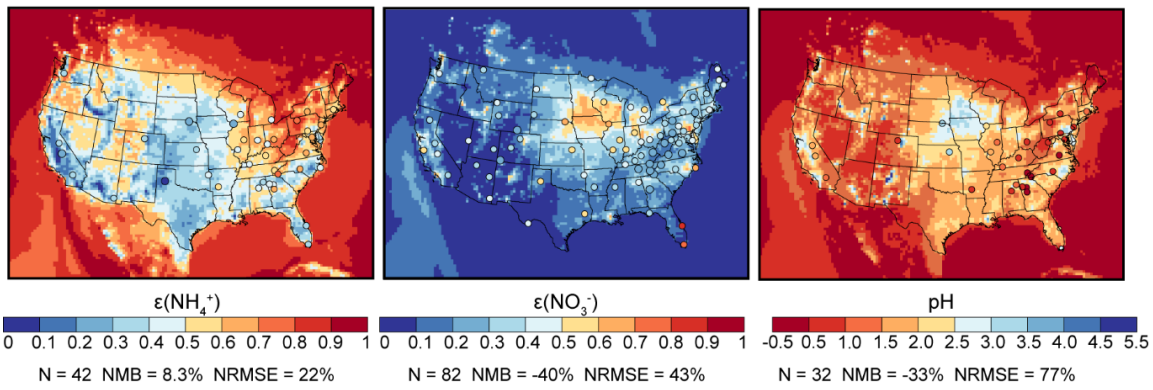

Figure 2-1 Overlay of annual mean gas-particle partitioning ratios, $\varepsilon(NH_4^+)$ and $\varepsilon(NO_3^-)$, and aerosol pH calculated based on simulated (color map) and observed (colored dots) concentrations over the study domain. The number of monitoring sites (N), NMB, and NRMSE are provided along the plots.

Comparison between simulated and observed biweekly average concentrations of NH_3 (g) and NH_4^+, and weekly average concentrations of HNO_3 and NO_3^- for all sites shows most of the data pairs scattered around the 1:1 line (Figure A-3). The data pairs of NH_3 and NO_3^- deviate from the one and five times the range when the simulated concentrations approach the low end, especially below 0.1 $\mu g/m^3$. This indicates that CMAQ tends to have a low bias in aerosol pH in areas with lower reactive nitrogen emissions, though the measured values are also subject to larger uncertainties when they are close to the instruments' minimum detection limits (Puchalski et al., 2011; Solomon et al., 2014). A clear dependence of NO_3^- and hence $\varepsilon(NO_3^-)$ bias on RH is found (Figure A-5). Including RH as an explanatory variable increases the adjusted R^2 for NO_3^- and $\varepsilon(NO_3^-)$. The low bias in NO_3^- and $\varepsilon(NO_3^-)$ suggests that the estimated pH calculated within CMAQ is less accurate in the Rocky Mountains area of the US where both the RH and emissions are low, and the relative dust contribution is a higher fraction of the total (Guo et al., 2016).

The spatial pattern of simulated SO_4^{2-} concentration agrees well with observations with an R^2 of 0.8. For NO_3^- and NH_4^+, the simulated concentrations also agree well with observations, except for several monitoring sites in western coastal areas in California (Figure A-6), where low biases in NO_3^- and NH_4^+ concentrations were found. Two factors influence this. First, as discussed above, the simulated concentration of NVC is biased low in California, which in turn leads to underestimation of aerosol pH. Although increasing NVC concentrations to observed levels would yield higher NO_3^- concentrations, simulated NH_4^+ concentrations would be more biased. Second, NH_3 emissions in California may be underestimated (Nowak et al., 2012; Zhu et al., 2013). Simultaneously increasing NVC concentrations and TNHx would result in a better agreement between simulated and monitored NO_3^- and NH_4^+ concentrations in the western coastal sites in California. The results for comparison between daily average concentrations are provided in the Supporting Information (Figure A-7).

Given the uncertainties in the measurements, emissions and meteorological fields model evaluation results using data from the four monitoring networks support that CMAQ v5.0.2 simulates aerosol pH over the CONUS with skill and captures the impacts of varying emissions and meteorological conditions. Simulating pH in some regions (e.g., coastal areas, Rocky Mountains) is more challenging because of the high impact from NVCs and/or low RH and pollutant concentrations.

2.4.2 Emission changes between 2011 and 2050

Overall, total NH_3 emissions are predicted to increase by 12% between 2011 and 2050, while SO_2 and NO_x emissions will be reduced by 52% and 70%, respectively. The increase

in NH_3 emissions derived here is lower than the estimate of the RCP4.5 scenario (20%) (Thomson et al., 2011). The NH_3 emission from livestock are projected to increase by 10% in this study instead of 24% in the RCP4.5 scenario. The results here are derived from estimated livestock counts where no further emission control measures are assumed. The decreasing percentage of SO_2 and NO_x emissions are comparable to predictions for the US with expected future air quality regulations for electricity generation units and mobile sources, and climate change mitigation measures to constrain fossil fuel consumption (Lee et al., 2016b). All regions except the northeastern US had lower SO_2 emissions (based on equivalents) than NH_3 emission equivalents in the year 2011 (Figure A-8). The forecasted reductions in SO_2 emissions and increase of NH_3, in the year 2050 lead to lower SO_2 emission equivalents than NH_3. For the SO_2 emissions reduction scenarios, total SO_2 emissions were 0.43 and 0.11 Tg for FS1 and FS2, respectively, with nearly 75% reduction from industrial (55%) and electricity generation (19%) activities. In fact, even if we remove all the SO_2 emissions from anthropogenic sources in the year 2050, SO_2 emissions only from forest fires are 0.15 Tg, which is higher than anthropogenic SO_2 emissions in the FS2 scenario. The ultra-low level of anthropogenic emissions in the FS2 scenario allows us to test how chemical composition and ambient aerosol pH would respond if SO_2 emissions were reduced to "pre-industrial" levels.

2.4.3 Aerosol pH change in 2050

The spatial patterns of annual average aerosol pH are similar between the historical and future baseline scenarios (Figure 2-2). Overall, the aerosol pH remains below 3 for most parts of the CONUS despite the variation of emissions and meteorological conditions. The central region with larger amounts of N fertilizer application has the highest aerosol pH.

The aerosol pH is above 3 near livestock farming areas in the Midwest US and California. The northeastern US has the lowest aerosol pH in the spring, summer, and autumn with an average below 1 and 1.5 for the historical and future baseline scenarios, respectively. Although the NH_3 emissions are higher in the spring and summer, the aerosol pH is highest in winter when NH_4NO_3 formation is thermodynamically favored due to low temperatures (Seinfeld and Pandis. 2016).

Compared to the historical scenario, aerosol pH increases in FB for most parts of the CONUS. Despite the significant decrease in SO_2 and NO_x emissions most parts of the CONUS only have an increase in pH ranging from 0 to 0.4, not likely causing major changes in aerosol chemical processes (Guo et al., 2017a; Guo et al., 2017b). The highest pH increases (0.6 ~ 0.8 unit) were seen in parts of the northeastern US where the aerosols are very acidic with pH below 1 in the historical scenario. These results further support the finding of Weber et al. (Weber et al., 2016) that fine particles will remain acidic, on average, not only in the southeastern US but the rest of the CONUS under a variety of emission and meteorological conditions. The seasonal average pH change is positive for all regions across the four seasons except the winter average for the western CONUS (Figure A-9). In the FB scenario, wintertime aerosol pH is as low as 1.5 in western CONUS, while the pH increase is under 0.25 in spring, summer, and fall, which is much smaller than in the other regions. The decrease of aerosol pH in winter and the small increase in the other seasons together lead to a decrease in annual average pH between historical and future scenarios for the western CONUS.

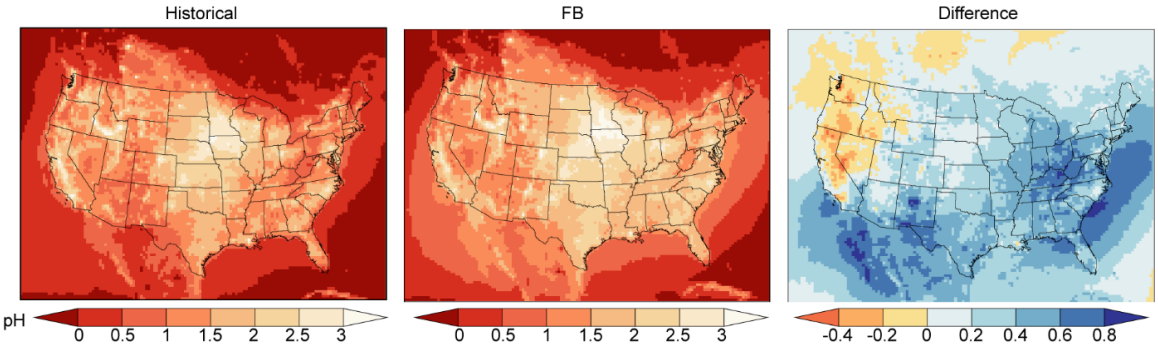

Figure 2-2 Comparison between the spatial distribution of CMAQ simulated annual average aerosol pH in historical (2011) and future (2050) scenarios. The lower panel displays the corresponding change of seasonal average aerosol pH for northeastern (NE), southeastern (SE), central (C) and western (W) US in 2011 (left) and 2050 (middle), as well as their differences (right). March, April, and May (MAM) are defined as spring. June, July, and August (JJA) are defined as summer. September, October, and November (SON) are defined as autumn. December, January, and February (DJF) are defined as winter.

Both emission changes and meteorological condition changes lead to the aerosol pH change between historical and future scenarios. To distinguish the contributions of the two factors, a set of three pH simulations were run with ISORROPIA-II offline using condensed phase concentrations of K^+, Ca^{2+}, Mg^{2+}, Na^+, Cl^-, SO_4^{2-}, NH_4^+, and NO_3^-, and gas phase concentrations of NH_3 and HNO_3 from CMAQ results and surface temperature and RH from WRF outputs. Simulation 1 (S_1) uses both CMAQ and WRF results from the historical scenario, simulation 2 (S_2) uses CMAQ results from the FB simulation and WRF results from the historical simulation, and simulation 3 (S_3) uses both CMAQ and WRF results from the FB simulation. The aerosol pH change between S_2 and S_1 approximates the contribution from emission changes, and the pH change between S_3 and S_2 approximates the contribution from meteorological changes. Using ISORROPIA-II offline allows us to better isolate the contribution of meteorological condition changes to

future aerosol pH changes in a computationally efficient way. It also allows us to clearly distinguish the impact of temperature and RH change through mediating the thermodynamic equilibrium. Emission changes lead to an increase in the aerosol pH in all the four regions across seasons (Figure A-10). The increase due to emission controls in the future is smallest in the western CONUS where the SO_2 emissions are already low and the reduction is less significant than in other regions. Meteorological changes generally lead to a decrease in the aerosol pH during winter in the northeastern and southeastern CONUS. The magnitude of pH decrease from meteorological condition changes is smaller than the pH increase from emission changes except during winter in the western CONUS. It is predicted that the winter time temperature will be ~3-4 K higher with lower RH for the western states in the future (Figure A-11) (Cayan et al., 2010; Trail et al., 2013). The warmer and dryer atmosphere results in the decrease of aerosol pH because the partitioning of ammonia to the condensed phase is less favored and liquid water decreases. Given the anticipated reduced RH in the future (Cayan et al., 2010; Overpeck and Udall 2010), further examining the meteorological impacts on aerosol pH and related NH_3 emission and deposition changes in the western CONUS is potentially important. It should be noted, however, that the impact of meteorological changes estimated from offline simulation results may deviate from a stand-alone WRF-CMAQ simulation with historical emissions and future meteorological conditions because the meteorologically-mediated emissions and reactions and changes in transport processes are not included. In addition, our historical and future simulations were run with two single-year meteorological fields (2010 and 2050) from the GISS ModelE2. Further investigation is needed to fully address the impact of meteorological changes on aerosol pH.

2.4.4 Sensitivity of aerosol pH change to SO_2 emission reductions

When total SO_2 emissions are further reduced to 25% and 6.25% of the future baseline value (FS1 and FS2), the annual average aerosol pH increased from 1.8 to 2.0 and 2.1, respectively (Figure 2-3). In comparison, removing all the anthropogenic SO_2 emissions also led to an average pH of 2.1, further supporting that controlling SO_2 emissions alone will not cause a drastic increase in aerosol pH in the CONUS. The increase is higher in the eastern CONUS, where there are more major SO_2 emission sources than in the central and western regions. The simulated pH from the FS2 scenario indicates that average aerosol pH over the CONUS would stay around 2 even if all anthropogenic SO_2 emission were eliminated while the emissions of other species remained relatively constant. There are three major factors leading to the low sensitivity of aerosol pH change to SO_2 emission reduction. First, partitioning of the NH_3 stabilized the aerosol pH because NH_4^+ will have a higher tendency to partition to the gas phase when SO_4^{2-} concentration decreases and aerosol pH increases (Weber et al., 2016). The NH_4^+ concentration generally tracks the decreasing trend of SO_4^{2-} concentration, even though NH_3 emissions stay constant among the three scenarios (Figure 2-3). Second, the decrease of SO_4^{2-} in response to SO_2 emission reduction is non-linear, especially when SO_2 emissions are reduced to a very low level within the CONUS and SO_4^{2-} transported into the domain starts to dominate. Figure A-12 displays the spatial distribution of normalized SO_4^{2-} concentration change in response to SO_2 emission reduction. The brute-force sensitivity is ~40% to 60% in the eastern CONUS and ~10% to 25% in the western CONUS between FB and FS1, and it drops to ~5% to 20% for the whole CONUS between FS1 and FS2. In fact, the surface concentration of SO_4^{2-} from the boundary condition (1.2 $\mu g/m^3$) is 4 times higher than the annual average

concentration in the western CONUS in the FS2 simulation (0.3 $\mu g/m^3$), indicating the strong contribution of SO_4^{2-} transport into the domain. By comparing the aerosol pH between our scenarios and a set of sensitivity simulations where the SO_2 and SO_4^{2-} concentration in the boundary conditions are reduced by half, we show that the aerosol pH will be increasingly more sensitive to the boundary conditions as SO_2 emissions are reduced (Figure A-13). The contribution from the transboundary transport is expected to dominate the aerosol pH change over half of the CONUS when domestic SO_2 emissions are reduced to the preindustrial level. With the ongoing SO_2 emission reductions in other countries, especially China (Craig et al., 2018), the influx of SO_2 and SO_4^{2-} is expected to decrease in the future, lowering the SO_4^{2-} concentrations in western North America, though this trend can be offset by increases in other countries, e.g., India (Heald et al., 2012). The resulting impact on aerosol pH warrants further investigation. It is also noted that concentrations of NH_4^+ and NVCs are not included in the boundary conditions, resulting in very acidic aerosols in areas close to the boundary. However, a sensitivity test assuming sulfate exists as ammonium sulfate on the boundary shows that the missing cations have little impact on aerosol pH estimation within the CONUS (Figure A-14).

Simulated aerosol pH may be biased due to model inputs and process descriptions. For example, by incorporating ISORROPIA-II, CMAQ only considers the inorganic compounds when calculating aerosol pH, though the impact of organics on pH prediction is believed to be minor even if the contribution of organics to total fine particle increases. Several studies have shown that organics have a minor impact on aerosol pH in the southeastern sites (Guo et al., 2015; Vasilakos et al., 2018) where organics are already high. Sensitivity analysis results by Vasilakos et al. (Vasilakos et al., 2018) show that the

conclusion stands even when organics are increased by 50%, although a larger impact might arise when phase separation exists in the aerosols (Pye et al., 2018). Our simulations have not considered the conversion of inorganic sulfate to organosulfates, which is expected to impact aerosol pH predictions because the conversion acts as a sink for inorganic sulfate, especially under acidic conditions (Surratt et al., 2007). In addition, as discussed in the model evaluation, the high bias in NVC concentration estimation at coastal regions will also bias the pH and corresponding sensitivity simulations. The "internally mixed" assumption may also introduce bias into the aerosol pH estimates as there exists a decreasing trend of aerosol acidity with growing particle size (Craig et al., 2018).

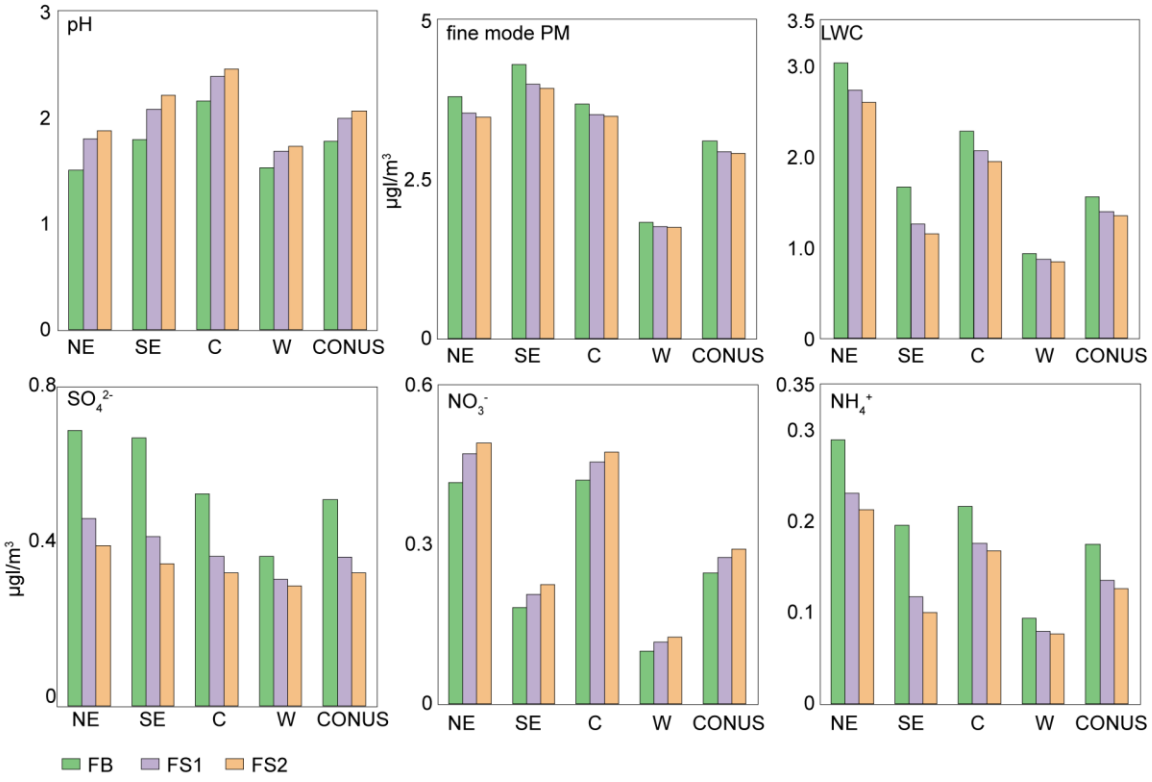

Figure 2-3 The sensitivity of aerosol pH, SO_4^{2-}, NO_3^-, NH_4^+, total fine mode PM mass concentration, and liquid water concent (LWC) to SO_2 emission reduction. The regional and CONUS annual average values for the three future scenarios (future baseline (FB), future sensitivity scenario 1 (FS1), and future sensitivity scenario 2 (FS2)) are plotted as colored bars.

2.4.5 Effects of SO_2 emissions control and NH_3 emissions increase on aerosol formation

There has been discussion that "nitrate substitution" may increase the formation of nitrate aerosols as SO_2 emissions are further decreased (Heald et al., 2012; Pye et al., 2009; Vayenas et al., 2005). As a result, $PM_{2.5}$ concentrations may not respond to reductions in SO_2 emissions as much as desired. Recent studies agree that the response of nitrate aerosol formation to aerosol composition change depends on aerosol acidity, and there exists a "sensitive window" (pH ranging from 0 to 3, with the exact range depending on specific thermodynamic conditions) where the nitrate gas-particle partitioning is sensitive to pH change (Vayenas et al., 2005). In this study, we show "nitrate substitution" occurs to a limited extent even if we aggressively reduce SO_2 emissions in the future over the CONUS. If the other emissions and meteorological conditions are unchanged, the increase of NO_3^- concentration is less than 20%, while SO_4^{2-} concentration decreased by over 35% from FB to FS2 on average over the CONUS (Figure 2-3). Still, partly due to the "substitution" effect, the reduction of total fine mode PM mass concentration from SO_2 emission reduction is limited, ranging from 4% in the western US to 9% in the northeastern and the southeastern US from FB to FS2. A brute force calculation of the sensitivity of nitrate to sulfate concentration change by taking the differences between scenarios reveals that the increase of nitrate in response to the reduction in sulfate concentration is limited. The mass ratio will approach or exceed 1 in the central US only when SO_2 emissions are further reduced to the preindustrial level in the future scenario (Figure A-15). The magnitude of substitution is very similar across the four seasons, although the formation of ammonium nitrate is expected to be more favorable under low-temperature conditions, possibly

because the pH increase is minor during winter. The limited increase in nitrate aerosol formation is expected because the aerosol pH increase is small in response to SO_2 emissions reduction and the process is only favored in a limited pH range. However, with the increase of nitrate and decrease of sulfate, the relative contribution of nitrate to total $PM_{2.5}$ mass load starts to outweigh sulfate in some regions. Most midwestern states have a nitrate to sulfate mass ratio of about 2 for FS1 and FS2, indicating that when SO_2 emissions are further reduced, the particles will shift from sulfate-dominated to nitrate-dominated in the more agriculture-intense regions where NH_3 and soil NO_x emissions from livestock and fertilizer application are abundant. A more comprehensive assessment of the future nitrate formation, however, will benefit from a carefully updated NVC emission inventory and the inclusion of organic nitrate formation. The significant reduction of SO_4^{2-} also reduce the LWC, especially in southeastern U.S., implying an extra benefit in improving the visibility.

The importance of NH_3 in determining aerosol pH and its consequent impact on secondary aerosol formation has also been widely discussed (Guo et al., 2017b; Pozzer et al., 2017; Wang et al., 2016b). Although aerosol pH predictions vary, estimates find that aerosol pH generally remains below 5 even in NH_3 abundant regions of the world and that excess NH_3 would mostly stay in the gas phase (Guo et al., 2017b). The results of this study further corroborate this conclusion. With the projected decrease of SO_2 emissions and increase of NH_3 emissions from the agriculture sector, most of the CONUS would have abundant NH_3 in the year 2050. However, the aerosol pH in most areas remains below 3, even in the central region where a significant amount of NH_3 is emitted from fertilizer application and livestock. The anticipated increase of NH_3 emission would result in a slight increase in aerosol pH, with a national average of 0.02 and a maximum of 0.25 under different SO_2

emission reduction scenarios (Figure A-16). The result is consistent with a previous sensitivity study that found 50% and 100% reductions of agriculture NH_3 emission will only lower the aerosol pH by 0.16 and 0.51 units, respectively (Ye et al., 2018). In fact, a regression of TNHx concentration change between scenarios with current and future NH_3 emission levels at different SO_2 emission reduction level indicates that it always takes 10 times increase of TNHx concentration to increase the aerosol pH by one (Figure A-17), as was found previously [56]. Consequently, the projected NH_3 emission increase in the future will barely change the $PM_{2.5}$ mass load over the CONUS, even under the most extreme SO_2 emissions control scenario.

There are a number of studies finding an association between exposure to "strongly acidic aerosols" and adverse respiratory outcomes (Dockery et al., 1996; Spengler et al., 1989). Recent studies investigating the linkage between $PM_{2.5}$ metals and the adverse health effects demonstrated that metals like iron can be mobilized into water-soluble forms, the more biologically accessible form, in acidic ambient aerosols (Ye et al., 2018). The atmospheric acid dissolution process increases the oxidative potential of aerosols, although most of the soluble transition metals are primarily emitted as insoluble forms (Fang et al., 2015; Fang et al., 2017). Thus, decreasing the total mass of sulfate and the frequency of days with highly acidic aerosols will potentially decrease the rate of respiratory and cardiovascular diseases. Here, we found that aerosols do become slightly less acidic with SO_2 controls. Further, the mass of acidic aerosol decreases. Both have the potential to provide widespread health benefits. Specifically, the number of days with daily average aerosol pH lower than 2 decreased from 206 days in 2011 to 54 days in 2050 in densely populated areas (grids with a population over 0.1 million) (Figure A-18), and the further

reductions of SO_2 emissions between FS1 and FS2 completely eliminates the days with aerosol pH below 2 in those areas. The shift is especially obvious for the eastern and central US, where the response of aerosol pH increase to SO_2 emissions reduction is higher.

2.5 Acknowledgements

This publication was made possible by funding from the US EPA under grants R83588001, the NSF PIRE Grant No.1243535, and China Scholarship Council (CSC) Grant #201606010393. Its contents are solely the responsibility of the grantee and do not necessarily represent the official views of the supporting agencies. Further, the US government does not endorse the purchase of any commercial products or services mentioned in the publication. We appreciate the help from Gertrude K Pavur and Nash Skipper for language editing.

CHAPTER 3. FUTURE REACTIVE NITROGEN DEPOSITION IN THE UNITED STATES DUE TO INCREASING AGRICULTURAL EMISSIONS

3.1 Abstract

Many sensitive ecosystems in areas protected for biodiversity conservation in the United States suffer from exposure to excess reactive nitrogen (Nr) released by fossil fuel combustion and agricultural practices and deposited onto the land surface and water bodies. The Community Multiscale Air Quality (CMAQ) model was applied over the contiguous United States to link emissions and climate change to reactive nitrogen deposition by simulating both present-day and future speciated Nr deposition to protected areas. Future conditions included examining the Representative Concentration Pathway 8.5 climate and the Shared Socio-Economic Pathway 5 emission scenarios. We further identify protected areas that would benefit most from better Nr management strategies by comparing the simulated deposition with multiple critical loads (CLs) for both biodiversity and acidification in terrestrial and aquatic ecosystems. Achieved by further NO_x emission reductions from the mobile and power generation sectors, future Nr deposition is expected to decrease. However, in regions with intensive fertilizer application or hosting concentrated animal feeding operations, the reduction may be offset by rising agricultural NH_3 emissions. The protected areas having CL exceedances in 2050 are expected to increase by 5.5% for empirical lichen-based CL, and by 11% and 22% for surface water and forest soil acidity, respectively, because of the agricultural NH_3 emission increase. By linking the deposition simulations with a water quality model, we identified that

atmospheric deposition is the dominant source of nitrogen for several remote watersheds, including several lakes in National Parks and National Wilderness areas in Colorado, Montana, and Minnesota.

3.2 Introduction

As one of the major elements for building proteins and DNA, nitrogen in reactive forms (Nr) is critical to all life. However, excessive release of Nr from human activities (e.g., food production and fossil fuel combustion) is now exerting adverse impacts on human and ecosystem health in many regions worldwide (Galloway et al., 2008; Galloway et al., 2014; Stevens 2019). The enormous amount of anthropogenic Nr input in intensified agriculture areas is believed to be far exceeded for a sustainable nitrogen cycle (Battye et al., 2017; Steffen et al., 2015). As it cascades through the environment, the same atom of nitrogen emitted into the atmosphere transforms into a sequence of different forms and causes multiple effects in series, including air quality degradation (via ozone and aerosol formation) and deposition leading to alterations in natural ecosystems productivity, acidification of soils and surface waters, eutrophication in freshwaters and coastal marine ecosystems, biodiversity loss, and production of N_2O (an important greenhouse gas) (Galloway et al., 2003).

During the past two decades, Nr deposition in the US has shifted from an oxidized Nr-dominated (Nr-ox, i.e. nitric oxide, nitrogen dioxide, nitrate radical, dinitrogen pentoxide , nitric acid, nitrous acid, peroxy-nitric acid, organic nitrate, peroxyacetyl nitrate, and nitrate) pattern to a reduced Nr-dominated (Nr-red, i.e. ammonia and ammonium) pattern because nitrate (NO_3^-) deposition has been decreasing due to successful emission controls of NO_x

from mobile sources, energy generation units, and other sources (Dallmann and Harley 2010; Kim et al., 2006; Li et al., 2016). Further reduction of Nr emissions from fossil fuel combustion is expected to continue in the near future with more stringent air quality and emission standards, as well as the shift to natural gas (Campbell et al., 2018; Paltsev et al., 2011). In contrast, ammonia (NH_3) emission from agricultural sources continues to rise, exacerbated by the growth of both domestic and export food demand (Galloway et al., 2007; NRC 2008). For crop production, the amount of surplus nitrogen remains high over the past decades despite an improved nitrogen-use efficiency (NUE) because a rising amount of fertilizer is applied, resulting in Nr-red loss to the environment (Zhang et al., 2015). Increased meat consumption also raises Nr emission and discharge from animal manure handling (Zeng et al., 2019). Greater contribution from agriculture sources to the environment Nr load is expected in the foreseen future, as more food is needed to sustain a growing population. The rising temperature under climate warming will also favor the release of NH_3 from vegetation, soil surface, and farms (Bash et al., 2013; Massad et al., 2010; Shen et al., 2019a; Sutton et al., 2013). Agricultural sources will contribute to Nr deposition to a larger extent if more energy needs will be met by biofuel (Davis et al., 2016). As a result, the decrease in Nr deposition achieved by controls on mobile sources and power generation may be canceled out by increasing Nr release from agricultural sources. How future changes in emission sources and climates will affect Nr deposition has only been sparsely investigated (Church and Van Sickle 1999; Ellis et al., 2013; Tagaris et al., 2008).

Although atmospheric deposition is a relatively minor nitrogen source to streams in urban and agricultural catchments, it is usually the dominant source of Nr in remote areas such

as headwater lakes and sensitive streams (Baron et al., 2011; Ellis et al., 2013). Knowing which watersheds may be more vulnerable to Nr deposition increase when agricultural emissions rise in the future can help identify the regions that will benefit more from agricultural Nr management.

Critical loads (CL) provide quantitative estimates of the thresholds below which the exposure to a pollutant is not expected to cause a significant adverse effect over the long term based on the current knowledge (Nilsson 1988). To understand the ecological impacts of Nr deposition, the deposition amounts are compared with the CLs and exceedances for CLs indicate the likelihood of an ecosystem suffering from excess nitrogen deposition under current and future scenarios (Ellis et al., 2013). It should be noted that a given location can have multiple CL values depending on the receptors and/or the biogeochemical process of concern. The CL values also vary by estimation approach, including empirical, steady-state and the dynamic modeling approaches (USEPA 2008a). There is a growing number of studies assessing the CL of nitrogen for the nutrient enrichment or acidification effects in surface water bodies and terrestrial ecosystems both at national and regional scales (McNulty et al., 2007; Pardo et al., 2011a; Scheffe et al., 2014). A National Critical Loads Database for nitrogen and sulfur was developed by the National Atmospheric Deposition Program to gather published critical loads (CL) data for the U.S (Lynch et al., 2017). CLs for different receptors and targeted ecological responses can vary by orders of magnitudes (Lynch et al., 2017). Hence, it is important to evaluate the Nr deposition against multiple CLs to better inform future Nr management to protect and maintain various functions and services of ecosystems.

Here, by incorporating population- and climate-driven Nr emission changes from agricultural sources and policy regulated Nr emission changes from fossil fuel combustion sources, we simulate historic (2010) and future (2030 and 2050) atmospheric Nr deposition over the contiguous United States (CONUS) under the Representative Concentration Pathway (RCP) $_{8.5}$ ($RCP_{8.5}$) scenario (a climate scenario generally representative of an intensely warming future). In addition, we link a water quality model with an atmospheric chemical transport model to estimate the impact of Nr deposition change on total Nr loading over the CONUS in 61117 watersheds (median size = 60 km^2) at the scale of 1:500000. The impacts of simulated Nr deposition is also examined in the context of CL datasets targeted for multiple ecological endpoints (e.g. surface water acidity, forest soil acidity, and biodiversity) to identify regions that were predicted to be adversely affected by Nr deposition. We further analyze the contribution of emission changes from agricultural sources to Nr deposition, mainly focusing on the identified vulnerable regions. Results of this study provide insights into spatially-resolved priorities to mitigate adverse impacts of Nr deposition by controlling Nr sources.

3.3 Materials and Methods

3.3.1 Modeling and Evaluating Reactive Nitrogen Deposition

The Community Multiscale Air Quality Modeling System (CMAQ) is a regional air quality model that has been widely applied to simulate the concentration and deposition of atmospheric pollutants (Appel et al., 2012; Appel et al., 2011; Byun and Schere 2006). In this study, CMAQ v5.0.2 is used to simulate Nr deposition (USEPA 2014a). The study domain covers the CONUS with a horizontal resolution of 36 km by 36 km and vertical

layers extending up to ~16 km. The specific model configurations including chemical mechanism and physical processes schemes are presented in Appel et al. (Appel et al., 2011). Particularly, we focus on the Nr deposition to protected areas for biodiversity conservation defined by USGS (referred to as protected areas hear after). The extent of protected areas in each simulated grid cell is derived from a GIS layer at 1 km by 1 km resolution (USGS 2018).

The meteorological fields in 2010, 2030, and 2050 are downscaled using the Weather Research and Forecasting (WRF) Model version 3.8.1 (Bruyere et al., 2014) from the bias-corrected climate projections under the $RCP_{8.5}$ (*IPCC*, 2014). $RCP_{8.5}$ is a climate scenario representative of an intensely warming future. The climate projections data are obtained from ensemble member #6, generated from the National Center for Atmospheric Research's Community Earth System Model version 1 (CESM1) (Monaghan et al., 2014). Spectral nudging is applied to temperature, geopotential heights, and horizontal winds. The downscaled meteorological fields showed average warming of 1.67 °C and reduced precipitation of 6.4 mm between 2010 and 2050 over the CONUS with great spatial variation (Figure B-1). The detailed downscaling techniques have been described in a previous study (Shen et al., 2019b).

The emissions in 2010 are generated from the EPA 2011 air emissions modeling platform v6.1 based on the 2011 National Emissions Inventory (NEI) (USEPA 2014b). Emissions in 2030 and 2050 are projected by sector. Two previous studies have projected emissions from agricultural sources based upon their response to climate factors and population growth. NH_3 emissions from fertilizer applications are obtained from Shen et al (Shen et al., 2019a), which estimated the change of emission-related processes and agricultural

practices in response to climate change using a coupled agroecosystem-air quality model (i.e., FEST-CMAQ with NH_3 bi-directional exchange model) (Yang 2017). The projection of livestock waste management emissions follows a previous study that used a regression model based on the growing population and demands for different animal groups to project future emission trends (Chen et al., 2019) (Figure B-2). Emission projections for both fertilizer application and livestock waste management assume the mitigation measures to improve NUE and abatement approaches to reduce atmospheric NH_3 emissions remain unchanged at present-day level. For other anthropogenic sources, the 2011 NEI emissions are used as the starting point, whereby sectoral-specific growth factors are applied based on the Shared Socio-Economic Pathway 5 (SSP5) (Kriegler et al., 2017) for projecting emissions. SSP5 represents a scenario featuring high fossil fuel consumption and food demand which will result in a radiative forcing pathway close to the $RCP_{8.5}$. Biogenic emissions are obtained from Shen et al (Shen et al., 2019b), which simulated present-day and future biogenic emissions with the Biogenic Emission Inventory System (Pierce 2002) (Figure B-3). Future Nr emissions from fires are adjusted based on the 2011 NEI emission data and the gridded future-to-current ratios of fire-induced column nitrogen loss predicted by CESM1 (NCAR 2011). Hereafter, we will refer to the future scenario with projections for all sources as "Ag_projected". In addition, we simulate a contrasting future scenario where all other sources are projected but the NH_3 emissions from agricultural sources remain unchanged after 2010 (Ag_fixed). The influence of agricultural NO_x emission is not included because it cannot be easily isolated from biogenic emissions from other land types in BEIS. Although the impact of agricultural NO_x emission can be high in agricultural

intensive areas (Almaraz et al., 2018), the contribution is expected to be minor on national scale.

To evaluate the model performance, the modeled concentration of Nr species are compared with the measured concentrations obtained from the Clean Air Status and Trends Network (CASTENET) (USEPA 2019b) (Figure B-4). The modeled NH_4^+ and NO_3^- depositions are compared with wet deposition measurements obtained from the National Atmospheric Deposition Program- National Trends Network (NADP-NTN) (NADP 2019) and dry deposition estimates from CASTENET (USEPA 2019b) (Figure B-5). The modeled total depositions (dry and wet) are also compared with the sum of dry deposition estimates from CASTNET and wet deposition measurements from NADP-NTN at collocated sites (Figure B-6). Meteorological fields derived from the North American Regional Reanalysis database (NOAA 2019) are used to drive the CMAQ simulations for evaluating model performance purpose. The CMAQ simulated concentrations agree well with the observations (Figure B-4), except for NO_3^-, which deviates from the observed concentrations when the relative humidity is below 60%. To eliminate the bias introduced by modeled precipitation, the measured precipitation is used to adjust the modeled wet deposition fields (Appel et al., 2011). Overall, CMAQ captures the spatial distribution of annual NH_4^+ and NO_3^- deposition in both dry and wet forms with a normalized mean bias ranging between 0.1 to -0.5 (Figure B-5), except for NO_3^- dry deposition. Prior studies suggest that the NO_3^- deposition may be biased due to overestimated dry deposition velocity for NO_3^- (Shimadera et al., 2014). Besides, the dry deposition estimates from CASTNET based on atmospheric concentrations and modeled deposition velocities are usually found to be biased low because 1) the weekly integrate sampling protocol of

atmospheric concentrations misses daily and diurnal variations (Fenn et al., 2009); 2) the modeled deposition velocities can be very inaccurate when influences from local meteorological condition, and terrain and canopy characteristics are complex (Weathers 2011); 3) NO_3^- and HNO_3 partitioning is biased due to the volatility of NH_4NO_3 particles on filters (Walker et al., 2019). There is a lack of routine measures to evaluate the modeled dry deposition of NH_3(g), but the modeled and observed NH_3 concentrations agree well (Figure B-4). In general, although the modeled total NO_3^- and NH_4^+ deposition agrees well with the dry and wet deposition sum from CASTNET and NADP-NTN collocated sites, more reliable measurements covering a wide range of landscapes and Nr species are needed to fully evaluate and constrain the uncertainties in the model-predicted Nr deposition amount (Walker et al., 2019).

In addition to Nr species, we also investigate other compounds that are associated with Nr deposition. Sulfate concentrations are expected to further decrease because of further emission controls of energy generation units, and this will modify Nr deposition because the abundance of sulfate will influence the gas and particle partitioning of ammonia/ammonium and nitric acid/nitrate (Paulot et al., 2013). We calculate the normalized brute-force sensitivity of total Nr deposition to sulfate concentration in each grid cell based on the SO_2 sensitivity scenarios developed by a previous study (Chen et al., 2019). The sensitivity is calculated using the equation below,

$$S_{Nr,SO_4^{2-}} = \frac{(Nr_{dep,baseline} - Nr_{dep,perturbation})/Nr_{dep,baseline}}{([SO_4^{2-}]_{baseline} - [SO_4^{2-}]_{perturbation})/[SO_4^{2-}]_{baseline}}$$

where $Nr_{dep,\ baseline}$ and $Nr_{dep,perturbation}$ represent the total Nr deposition amount in the baseline scenario and a sensitivity scenario in which SO_2 emissions are further reduced by

75%, respectively. $(SO_4^{2-})_{baseline}$ and $(SO_4^{2-})_{perturbation}$ represent the ambient sulfate concentration in the corresponding scenarios, respectively.

3.3.2 Critical Loads

To identify the areas requiring further Nr deposition reduction, we compare the amount of simulated Nr deposition with CLs associated with different biogeochemical and ecological endpoints including surface water acidity, forest soil acidity, and biodiversity in terrestrial ecosystems. The CL-approach has been widely applied to evaluate the ecological effects of acid depositions (Burns et al., 2008). Although the dose-response relationships between sensitive ecosystem well-being and atmospheric deposition are not established in some cases, most of them are non-linear with a threshold. It is because the ecosystems have certain ability to neutralize the acid deposition and assimilate nitrogen inputs.

The CL data in this study are obtained from the National Critical Loads Database (NCLD) for nitrogen and sulfur developed by the National Atmospheric Deposition Program (Lynch et al., 2017). CL data for surface water and forest soil acidity are mapped onto the 36 km by 36 km CMAQ grid employed here. The average and 10th percentile values are used for comparison, representing moderate and protective criteria, respectively (Figure B-7). The CL values for forest soil and aquatic acidity are combined for sulfur and nitrogen deposition, defined as a three-node linear CL function (Lynch et al., 2017). The CL for forest soil acidity is derived using a steady-state mass balance model (McNulty et al., 2007). The CL for freshwater acidity is derived using a steady-state water chemistry model (Scheffe et al., 2014). Major processes affecting base cations, anions, and nitrogen loading as well as the acid neutralization capacity (ANC) were considered in simulating the CLs.

It should be noted that although the variation in CLs among different sites within each grid cell is considered in this study, the uncertainty associated with CL estimates for each site is not incorporated. Both CL model estimates for forest soil and surface water acidification are subjected to high uncertainties in key model parameters such as soil base cation weathering rate and ANC (Li and McNulty 2007; Scheffe et al., 2014). The lichen-based CL was selected to represent the empirical CL for nitrogen for terrestrial ecosystems because the shift in dominant lichen species is a sensitive bioindicator of Nr level and community diversity loss in terrestrial ecosystems (Pardo et al., 2011b). The lower end of the empirical CL range reported for each ecoregion is adopted for CL exceedance assessment to provide a more conservative estimation. Steady-state CL and empirical CL values provide estimates of the deposition levels allowable to maintain ecosystem sustainability over the long term. Comparison between the deposition levels and CLs in this study thus provide insights into whether Nr deposition exceeds thresholds in the present-day or future scenarios, however, without considering the dynamic response of the ecosystem to changing Nr deposition.

3.3.3 Water quality modeling and total reactive nitrogen loads

We link the CMAQ deposition fields with the US Geological Survey (USGS) water quality model, SPARROW (SPAtially Referenced Regressions On Watershed), (Schwarz et al., 2006)) to qualitatively estimate the main source of total Nr load for each of 61117 watersheds over the CONUS. We also use the SPARROW model to simulate the mean annual flux of total Nr load in streams as a function of ten nutrient sources, six climatic and landscape factors that influence nutrient delivery to streams, and nutrient removal in streams and reservoirs. Nutrient sources include atmospheric deposition of nitrogen, urban

and population-related sources (i.e. industrial and municipal wastewater treatment plants, septic systems, and urban runoff), and eight sources in the runoff and subsurface flow based on the underlying surface, including forest, shrub, barren land, and animal farms and four types of cropland (corn and soybean, alfalfa, wheat, and other crops) (Alexander et al., 2008). The SPARROW model parameters are estimated based on a calibration to the long-term mean annual load of total nitrogen and total phosphorus at 425 stream monitoring sites in the CONUS. Overall, the modeled total nitrogen flux has an R^2 of 0.933 and root mean square error of 0.553 on log scale, which translates to a 95% confidence level of approximately a factor of two for flux predictions for individual stream reaches (Alexander et al., 2008). To quantify the impact of the change in atmospheric Nr deposition on total Nr loading in streams, we performed three SPARROW simulations using CMAQ-simulated Nr deposition fields from the "present-day", "Ag_projected", and "Ag_fixed" scenarios. Other variables, including urban population and agricultural land areas, and the corresponding source strengths remain unchanged at present-day level (USEPA 2019a; Wimalasekera 2015). The difference between the SPARROW simulations in "present-day" and "Ag_projected" scenarios characterizes the change in total Nr loading driven by the change in total deposition between 2010 and 2050. The difference between the SPARROW simulations in "Ag_projected" and "Ag_fixed" scenarios characterizes the change in total Nr loading driven by the change in deposition due to rising agricultural NH_3 emissions. The uncertainty in the predicted change in total Nr load mainly depends on the uncertainty of source coefficients for atmospheric nitrogen deposition (standard error =14.4%), which is smaller than the overall model uncertainties.

3.4 Results and Discussion

3.4.1 reactive nitrogen emissions changes between the present-day and future scenarios

We examine the changes in NH_3 emissions from agricultural sources, together with Nr emissions from other sources (i.e. NO_x emission from biogenic sources, NH_3, NO_x, and particulate NH_4^+ and NO_3^- emissions from agricultural waste burning, wildfire, mobile sources, energy generation, and other unspecified point and area sources) between 2010, 2030, and 2050. Emission trends follow the SSP5 socioeconomic pathway under the $RCP_{8.5}$ climate scenario. Agricultural emissions under $RCP_{8.5}$ represent a higher end of the emissions projected across RCP scenarios (*Shen et al.*, 2019b). In addition, the projections of agricultural NH_3 emissions do not include further adaptation to improve NUE in crop and livestock production under the changing climate. Adaptive measures such as replacement of urea with non-urea fertilizers, deep placement of fertilizers, optimizing feeding plans for animals are expected to lower the NH_3 emission in the future even under warmer conditions and higher food demand (*Kohn*, 2015; *Shen et al.*, 2019b). On the other hand, SSP5 generally exhibits a rapid decline in pollutant emissions from other anthropogenic sources due to pollution controls (Rao et al., 2017). In total, Nr emissions in the US are projected to decrease by 27%, from 7.7 Mt-N yr^{-1} in 2010 to 5.6 Mt-N yr^{-1} in 2030, and climb up back to 6.4 Mt-N yr^{-1} in 2050 in this specific case (i.e., $RCP_{8.5}$ + SSP5) (Figure 3-1(a)). The emissions of Nr-ox (mainly as NO) will decrease from 4.4 Mt-N yr^{-1} in 2010 to 2.1 Mt-N yr^{-1} in 2030. The emission rate in 2050 (2.6 Mt-N yr^{-1}) is higher than that in 2030 mainly because of the increase of NO_x from biogenic sources and fires caused by warming, part of which originated from the cropland emissions. In contrast, the total emission of Nr-red (mainly as NH_3) climbs up steadily from 3.2 Mt-N in 2010 to 3.8 Mt-N in 2050 because of emissions increases in agricultural sources associated with growing

food demand and warming. Besides, the NH_3 emissions from mobile and other fossil fuel combustion sources only decrease by ~3% between 2010 and 2050 while NO_x emissions from these sources are significantly reduced, resulting in an increase in the relative contribution of NH_3 emissions to total Nr emissions. The trend has already been identified in urban regions of CONUS (Sun et al., 2017). As a result, the emissions of Nr-red outweigh that of Nr-ox in 2050. Similar trends have been reported in previous studies (Lamarque et al., 2011; van Vuuren et al., 2011).

Spatially, Nr-red emissions from agricultural sources will make a major contribution to total Nr emissions in more widespread areas in the future in central and southeastern US, as well as California, while Nr emission reduction is expected to occur in populous metropolitan areas dominated by combustion sources. 63% of the land area over the CONUS will see increases in Nr emissions due to the emission increase from agricultural sources (Figure B-8). For these areas, NH_3 emissions account for 58% of the total emission of Nr. Even in areas with decreasing Nr emissions, the contribution from NH_3 will also increase from 32% in 2010 to 46% in 2050 (Figure 3-1). As a result, most areas will switch from Nr-ox-dominated in 2010 to Nr-red-dominated in 2050 (Figure B-9), and the percentage of areas dominated by agricultural Nr emissions will increase from 49% in 2010 to 67% in 2050.

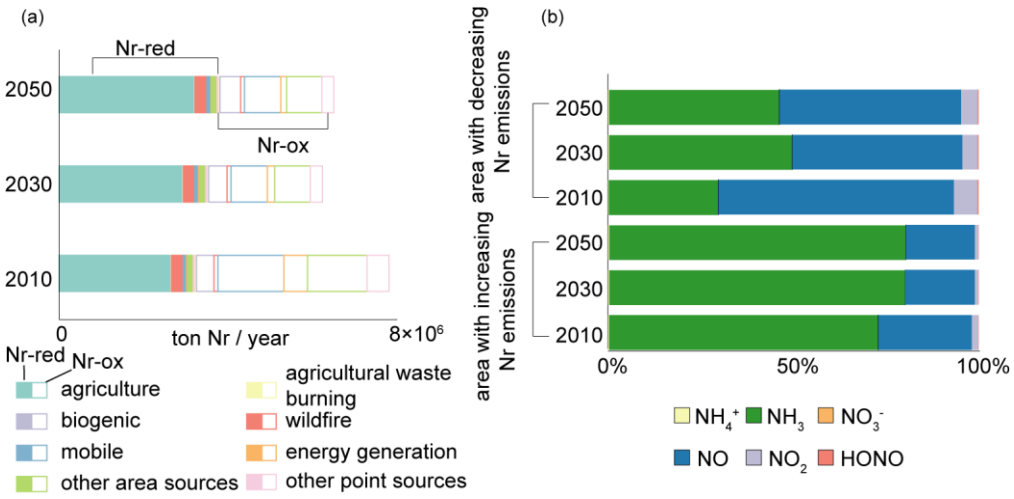

Figure 3-1 Sectoral Nr emissions changes between the present-day (2010) and future (2030 and 2050) scenarios. (A) shows the change in absolute amount of Nr emissions and the breakdown of oxidized and reduced forms of Nr from agricultural sources and other sources. (B) shows the change in Nr emission profiles for areas with increasing and decreasing Nr emissions, respectively. NH_3 emissions from agricultural sources are zero because they are aggregated as biogenic NO_x emissions in Biogenic Emission Inventory System (BEIS) model simulations.

3.4.2 reactive nitrogen deposition changes between the present-day and future scenarios

Nr deposition is simulated for 2010, 2030, and 2050 with a focus on protected areas. Generally, total Nr deposition over the protected areas declines during the projection period (Figure 3-2). From 2010 to 2030, the deposition amount shows a decrease of 23% mainly driven by a significant decrease in oxidized-Nr deposition (by 41% between 2010 and 2030). The decrease in Nr-red driven by other factors including emission changes from fossil fuel combustion sources is much smaller than the decrease in Nr-ox partly because NH_3 is being emitted as a byproduct for NO_x emission control when NO is over reduced,

which may contribute as a major source to Nr deposition in urban regions (Bettez and Groffman 2013; Fenn et al., 2018). However, the trend of the total Nr deposition becomes flat beyond 2030 when the decrease in oxidized-Nr deposition slows down and is offset by a steady increase in the reduced-Nr deposition. As a result, the increase in the Nr deposition is mostly in the reduced form consistent with the shift in compound profiles of the future Nr emissions (Figure B-9). The temporal trend for the CONUS is similar to that for the protected areas, although the magnitude of change is slightly smaller (Figure B-10). The increasing trend in reduced-Nr deposition and the decreasing trend in total Nr deposition are accordant with the observed historical trends which have shown an increase in NH_3 deposition since the 1980s and a decrease in total inorganic nitrogen deposition since the late 1990s (Du 2016; Li et al., 2016). Our projection of a specific scenario indicates that the decreasing historical trend in total Nr deposition could be reversed by the increase in reduced-Nr deposition due to growing agricultural emissions.

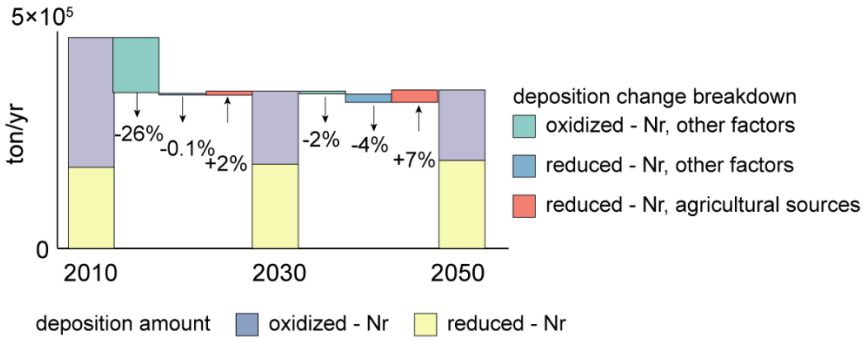

Figure 3-2 Projected changes in total deposition of Nr in protected areas over the CONUS from 2010 to 2050 in the "Ag_projected" scenario (stacked bars). The changes attributed to agricultural sources and other factors including emission changes in other sources and meteorological conditions are also displayed.

Due to further NO_x emission control in the future, the total Nr deposition is expected to decrease in most (91%) of the CONUS in 2050. For the rest of the areas, the estimated rise in total Nr deposition is driven by enhanced agricultural NH_3 emissions. Spatially, areas associated with concentrated animal feeding operations (CAFOs), especially for hogs and poultry, are hotspots showing the highest increases in Nr deposition during the projection period (Figure 3-3). These hotspots are concentrated in a few states, including Iowa, North Carolina, Georgia, and Arkansas (Figure 3-3). Large-scale increases in Nr deposition are found in the northern part of the Central U.S. because of the warming-induced increase in ammonia volatilization over cropland which outweighs the decrease in NO_x emissions. Across the CONUS, the proportion of land surface receiving more Nr-red than Nr-ox will increase from 37% in 2010 to 83% in 2050 (Figure B-11), emphasizing the ever-growing importance of Nr-red from agricultural sources for Nr deposition in our future scenario.

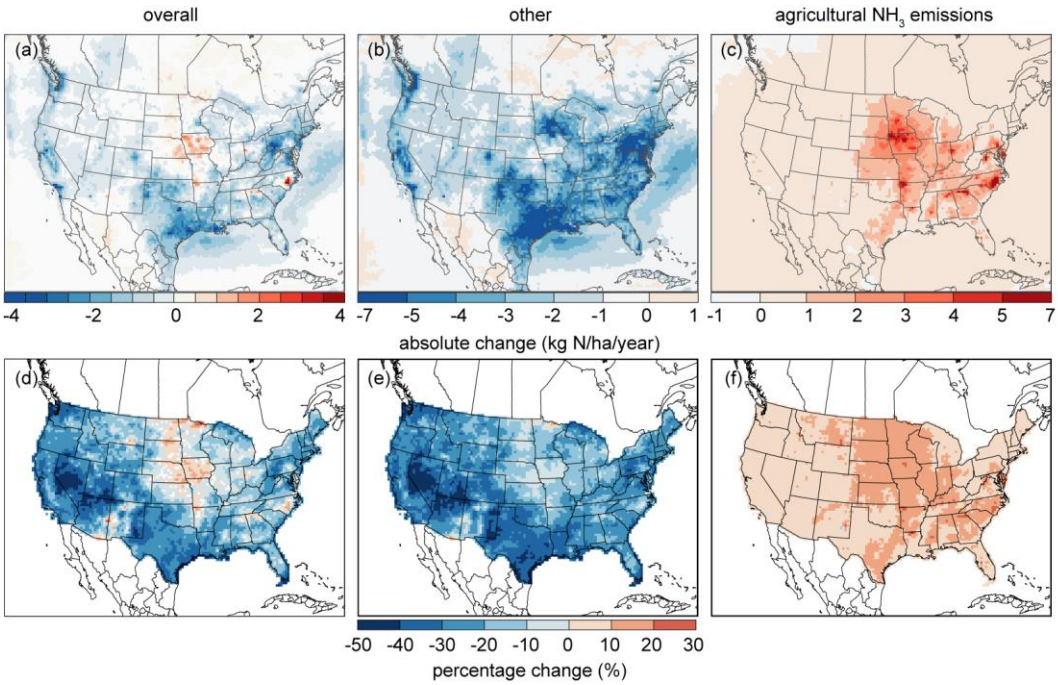

Figure 3-3 Changes in the spatial distribution of total Nr deposition between 2010 and 2050. The upper panel shows the absolute change of Nr deposition. The lower panel shows the percentage change. The overall change between the present-day and future scenario (Ag_projected) (left), changes attributable to agricultural NH_3 emissions (right), and other factors (middle) are shown.

In addition to the emissions changes of oxidized and reduced forms of Nr, the spatial pattern of Nr deposition responds to future regulations on SO_2 emissions. This is because SO_2 emissions can affect the gas-particle partitioning of Nr species, including NO_x and NH_3 (Nenes et al., 2020; Paulot et al., 2013; Weber et al., 2016). The gas-phase species tend to have much higher deposition velocities than their particle-phase counterparts (Sehmel 1980). The normalized brute-force sensitivity of total Nr deposition to sulfate concentration is positive in most parts of the Central U.S. with high emissions from agriculture sectors, indicating more localized Nr deposition impacts when less sulfate is available to form particles which tend to be more resistant to deposition (Figure B-12). In other words, the SO_2 emission reduction in the future limit the external cost of NH_3

emission through deposition in agricultural intensive regions rather than being exported downwind. However, the magnitude of the sensitivities to a 75% SO_2 emissions reduction is less than 15% in most areas of the CONUS, meaning that further control of SO_2 emissions will affect the spatial pattern of Nr deposition only moderately.

3.4.3 Comparison between reactive nitrogen deposition and empirical lichen-based CL for terrestrial ecosystems

Six of the ten ecoregions have empirical CLs available based on lichen community composition, including North American Deserts, Mediterranean California, Northern Forests, Northwestern Forested Mountains, Marine West Coast Forest, and Eastern Temperate Forest. The percentage of protected areas with exceedance of CL (referred to exceedance rate hereafter) were high (74% -93%) for all the ecoregions except for North American Deserts (Figure 3-4). The reduction in Nr-ox deposition can reduce the exceedance rate by ~30% in Marine West Coast Forest and Northern Forests to ~ 60% in Northwestern Forested Mountains and Mediterranean California between 2010 and 2050. The improvements will be largely offset by the additional Nr-red deposition with the expected NH_3 emission increase from agriculture sources in the future. The exceedance rate in Northern Forest will remain high mainly because of the intensified agriculture emissions. The other two ecoregions expect a significant impact from agricultural emission increase are Northwestern Forested Mountains and Eastern Temperate Forest. In particular, the decreasing trend in exceedances in Eastern Temperate Forest will be reversed after 2030 because of the combined increase in Nr-red and Nr-ox deposition. This finding is consistent with the conclusion that most national parks will remain in exceedance in eastern U.S. in a previous assessment national parks (Ellis et al., 2013).

As Nr-ox deposition further declines, controlling Nr-red deposition becomes even more important to reduce CL exceedances in the future. CL exceedance rate remains high in Northern Forest and Eastern Temperate Forest because of the NH_3 emission increase in the future. The relative contribution of Nr-red to total Nr deposition in these two ecoregions will rise from 48% and 50% in 2010 to 62% and 75% in 2050, respectively. Even if the Nr-ox deposition is zeroed in 2050, the Nr-red deposition will still exceed the CL in 50% and 12% of the sensitive areas, respectively.

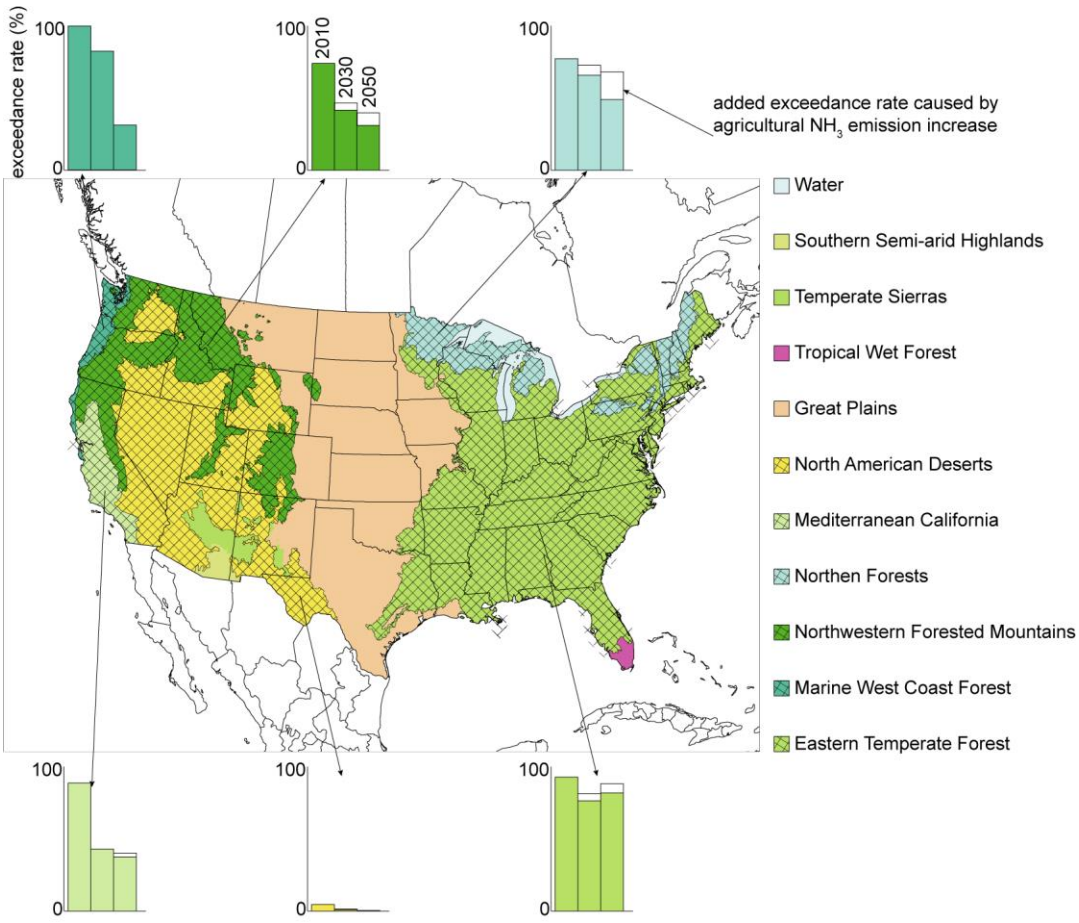

Figure 3-4 The percentage of area in exceedances of an empirical lichen-based critical load (exceedance rate) for nitrogen deposition. The map shows Level I ecoregions defined by the Commission for Environmental Cooperation. Ecoregions where empirical CL values are available are marked by checked patterns. Stacked bar charts show the CL exceedance rates in protected areas by comparing Nr deposition in each grid cell in 2010, 2030, and 2050 with the CL values, respectively. Colored bars indicate percentage of areas in exceedances in 2010 and "Ag_fixed" scenario in 2030 and 2050, in which agricultural NH_3 emissions are fixed at 2010 level and emissions from other sources as well as the meteorological fields are projected to 2030 and 2050 levels. Hollow bars indicate added exceedance rate due to increased agricultural NH_3 emissions between 2010 and 2030 or between 2010 and 2050.

3.4.4 Comparison between sulfur-nitrogen-combined deposition and CL based on freshwater acidity and forest soil acidity

Deposited nitrogen and sulfur, together, contribute to the acidity in aquatic and terrestrial ecosystems. In addition to nitric acid deposition, ammonium deposition will also contribute to the acidification with one proton released from the assimilation process or, in rare cases, two protons from the nitrification process if the soil is severely N saturated (Vanbreemen et al., 1982). NH_4^+ deposition was found to have greater ability to increase the modeled surface water acidity in regions with high soil sulfur adsorption capacity (Fakhraei et al., 2016). By aggregating the amount of deposited nitrogen and sulfur, CLs for freshwater acidity and forest soil acidity have been defined as the threshold of the maximum amount of combined sulfur and nitrogen deposition that a sensitive region can tolerate without causing an acidifying effect (Lynch et al., 2017). Speciated Nr deposition fields provide detailed spatial information about the area of concern for exceedances. We focus our discussion on the comparison between deposition and the 10th percentile CL. With substantial reduction of SO_x and NO_x deposition achieved by emission control of fossil fuel combustion under the Clean Air Act (Burns 2011; Greaver et al., 2012), the prevalence of deposition exceedance has already been limited to those most sensitive regions in 2010 (Figure 3-5). The exceedance rates in 2010 over the CONUS are estimated to be 16% and 22% for surface water acidity and forest soil acidity, respectively, which are close to estimates from previous studies (McNulty et al., 2007; USEPA 2008b). The exceedance rates are expected to be halved by 2050 with the combined decline in sulfur and nitrogen deposition. For areas still having CL exceedances, the deposition level will get closer to the CL in 2050. For example, there were 18% of grid cells where Nr deposition led to the

surface water acidity CL being exceeded by over 500 eq ha^{-1} yr^{-1} in 2010, but the percentage drops to 8% in 2050. The exceedance rates in several regions are caused by high acidifying deposition, while the exceedances in some other regions are due to low base cation availability in the underlying terrain (McNulty et al., 2007). Regions with exceedances include New England, West Virginia, upper Midwest, Mid-Atlantic Appalachian Region, and part of North Carolina, and Florida, which is consistent with those summarized by EPA (USEPA 2008b).

Spatially, the transition towards low exceedance rates will mainly occur in the Northeastern U.S. where the most stringent controls are expected for emissions of SO_2 and NO_x (Val Martin et al., 2015). For the Western and Southern U.S., future emission reductions will be able to significantly reduce the areas exceeding their forest soil acidity CL. However, removing all exceedances of the surface water acidity CL in 2050 is difficult because the CL's are low. Among the areas in exceedance in 2050, 22% can be attributed to emission increases from agricultural sources leading to exceeding the forest soil acidity CL. The affected areas are mainly located in the Midwest and North Carolina (Figure 3-5 (f)), where Nr deposition from agricultural sources dominates. The proximity of the areas in exceedance to emission hotspots highlights the importance of mitigating agricultural emissions to protect ecosystem health in adjacent sensitive regions. For surface water acidity exceedances, 11% can be attributed to the same cause, mainly around CAFOs in the Southeastern U.S. Due to the rising consumption of meat, Nr emissions and discharges from animal industries is expected to pose a greater challenge to the surrounding ecosystems in the future. Mitigating Nr loss from CAFOs relies on a range of measures from implementing the best management options available to reduce Nr loss through

leaching, runoff, and diffusing to the atmosphere to optimizing feeding plans to reduce nitrogen content in the manure (Carew 2010; Kohn 2015). Alternatively, studies point to microbial protein as a food source as the ultimate solution to tackle Nr pollution while sustaining the growing population. (Pikaar et al., 2018; Pikaar et al., 2017). Results for comparison between deposition level and the average CL are provided in Figure B-13.

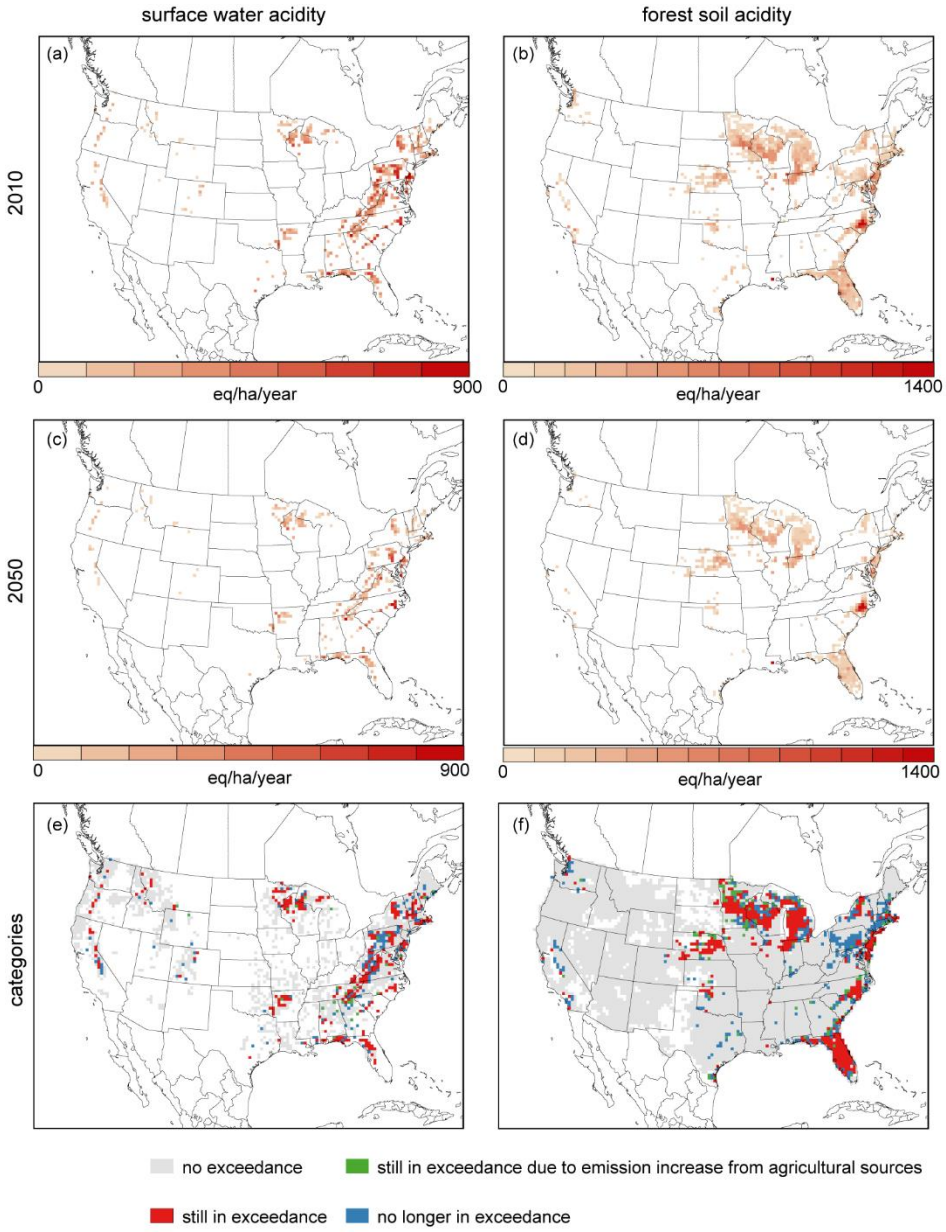

Figure 3-5 Exceedance of sulfur-nitrogen-combined (S+N) deposition for surface water acidity and forest soil acidity. (a)-(d) show the areas exceeding the 10th percentile CL values for surface water acidity and forest water acidity in 2010 and 2050, respectively. The colors represent the amount of deposition above the 10th percentile CL levels. (e) and (f) are the color-coded maps which show the status of each grid cell in 2050. Grey represents areas with deposition not exceeding the 10th percentile CL values in both 2010 and 2050. Red represents those with deposition in exceedance in both years. Blue represents those with deposition in exceedance in 2010 but below the CL values in 2050. Green represents those with deposition still in exceedance in 2050, particularly because of emission increases from agricultural sources.

Acidifying deposition in areas with exceedance can be controlled by individually or simultaneously reducing sulfur and nitrogen deposition. Over the CONUS, reducing sulfur deposition will lead to decreases in the exceedance areas of, at most, 22% and 26% for surface water acidity and forest soil acidity, respectively, in 2050 (Figure 3-6). In over half of the areas with exceedance, the amount of deposition reduction required to achieve the CL levels is twice as much as the amount of existing sulfur deposition. For areas with intense agriculture production, the required deposition reduction can be up to 30 times that of the sulfur deposition, showing the importance of decreasing Nr species. Given the decreasing trend in sulfur and oxidized-Nr deposition, strategies targeting reduced-Nr deposition from agricultural emissions will become increasingly important to reduce soil and surface water acidification. Such a finding coincides with the conclusion based on site-specific model evaluation that simultaneous reduction of sulfur and nitrogen deposition may be the most effective approach to achieve greatest overall recovery of Adirondack surface water acid neutralizing capacity (Zhou et al., 2015).

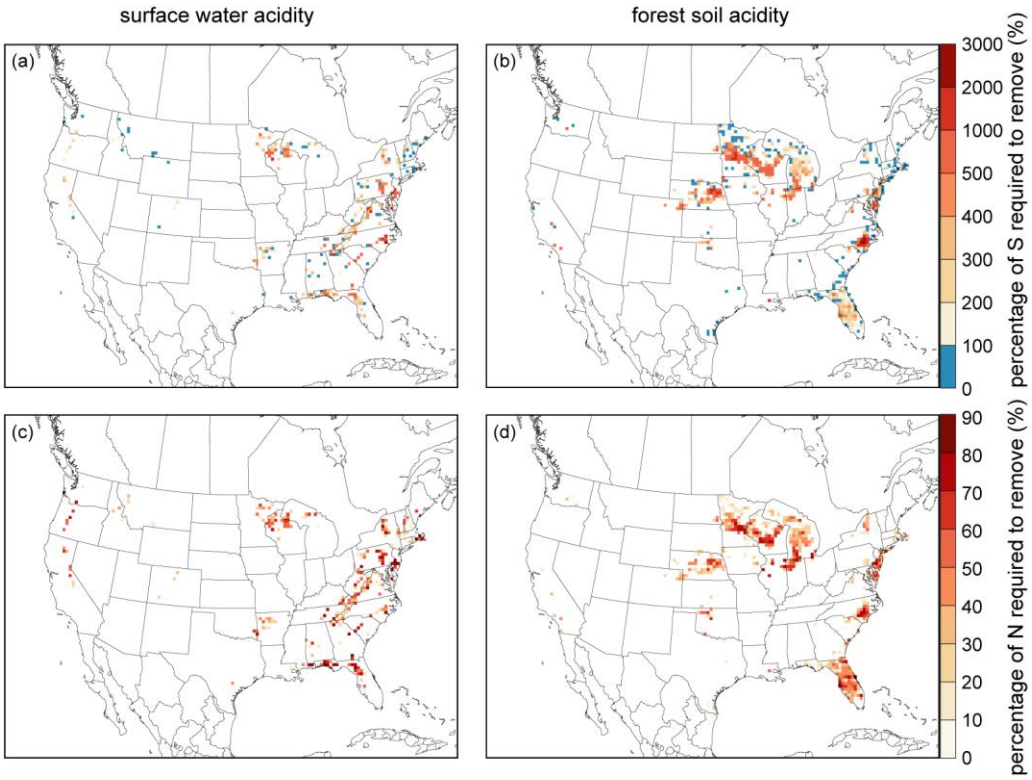

Figure 3-6 The percentage of sulfur (a and b) and Nr (c and d) deposition required to be deducted to bring sulfur-nitrogen-combined deposition down to the CL levels for surface water acidity (a and c) and forest soil acidity (b and d), respectively.

3.4.5 Impact of reactive nitrogen atmospheric deposition on total reactive nitrogen load received by watersheds

In addition to atmospheric deposition, the land and water surface also receive Nr input from other sources including Nr runoff from agriculture land, animal farms, and point sources like municipal and industrial facilities (Puckett 1994). Information about the relative importance of different sources to total Nr loading for areas with CL exceedance is useful in setting priorities of mitigation strategies. By linking the SPARROW model with the simulated Nr deposition, we located the watersheds where atmospheric deposition is the

leading Nr source. By contrasting the simulated total Nr loading based on the "Ag_projected" and "Ag_fixed" Nr deposition fields, we estimated the future changes in total Nr loading of 61117 watersheds nationwide due to the future changes in agricultural NH_3 emissions. It is found that in 2050 under the "Ag_projected" scenario, runoff from agriculture land and municipal sources remain important sources of Nr loading in populated areas. However, atmospheric deposition is the major source of Nr and key for regulation in remote areas with an absence of other significant anthropogenic contributors. 23% of the watersheds in the Great Plains region have atmospheric deposition as the major contributor (Figure 3-7). Surface waterbodies still in exceedance of their CLs within this region include lakes within the Glacier National Park in Montana and lakes within the Indian Peaks wilderness area in Colorado (Figure 3-5). Another region of concern is the area around the Superior National Forest in Minnesota where the total nitrogen loading in watersheds are sensitive to deposition changes from agricultural sources. The increases in the total Nr loading are estimated to be as high as 5–20%, indicating that Nr emission control on agricultural sources can effectively reduce Nr exceedance in this area. The changes above only address the influence through atmospheric deposition. The overall contribution from agricultural sources through atmospheric deposition, leaching, and runoff is expected to be more significant both in the magnitude and spatial coverage, which warrants further assessment. When Nr deposition changes from all emission sources are incorporated in the SPARROW simulation, the total Nr loads are expected to decrease in 2050 in most of the watersheds, except for the ones in intensive agricultural regions (Figure 3-7(c)).

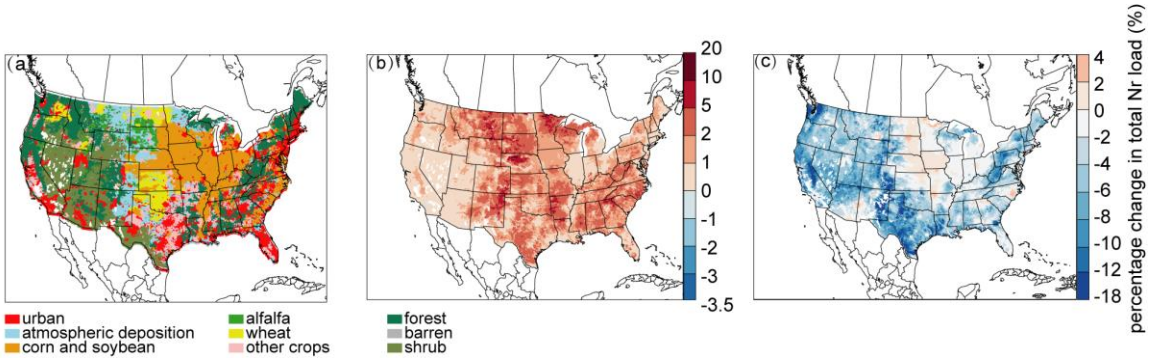

Figure 3-7 Major source of total Nr loading by watershed in "Ag_projected" scenario in 2050 (a). Percentage changes in total Nr loading by watershed across the CONUS due to Nr deposition changes related to agricultural NH_3 emission changes between 2010 and 2050 (b). Percentage changes in total Nr loading due to overall changes in Nr deposition between 2010 and 2050 (c).

3.5 Concluding Remarks

Our analysis shows that NO_x emission reductions coupled with NH_3 emission increases will lead to a transition from an Nr-ox-dominated deposition pattern in 2010 to a Nr-red-dominated pattern in 2050. While Nr deposition is estimated to decrease in most of the CONUS with further NO_x emission control, in agricultural intensive regions the decreasing trend will be offset by rising NH_3 emissions. In addition, increased NH_3 coupled with less nitrate and sulfate aerosol formation leads to more localized deposition. Adding this indirect effect upon the increasing Nr emissions from agricultural sources further increases the Nr burden in near-source regions. This analysis was based upon the $RCP_{8.5}$+SSP5 pathway, which emphasizes the impact of rising temperatures in the future with continuous dependence on fossil fuels, but still has reductions in NO_x due to controls. Total Nr deposition is expected to be lower under other RCP and SSP scenarios because of reduced fossil fuels use leading to lower NO_x emissions, especially in the eastern CONUS (Ellis et

al., 2013). Agricultural NH_3 emission will dominate the Nr deposition in such scenarios. Other future projections, such as a future scenario with a higher adoption rate of biofuels, would likely lead to an even greater proportion of future Nr deposition from agricultural sources and yield different amounts and spatial patterns of Nr deposition (Duval et al., 2015).

Total Nr deposition is projected to decline by over 20% by 2050, however, comparison between simulated Nr deposition and the empirical CLs for different ecoregions shows that Nr deposition will still exceed CLs in most sensitive areas in Northern Forest and Eastern Temperate Forest partly due to the increase in Nr-red deposition caused by NH_3 emission increase in the eastern U.S., indicating the importance to simultaneously reduce NH_3 emissions while controlling NO_x emissions in the future. Without adequate information on ecological impacts for speciated nitrogen deposition, Nr-ox and Nr-red are treated the same when assessing the CL exceedances. As greater contribution from Nr-red deposition is expected in the future, more studies on various ecosystems are need to better understand the ecological impacts of such a shift in deposition toward being Nr-red-dominated.

At present-day level, the percentage of protected areas in exceedances of surface water and forest soil acidity is 16% and 22%, respectively, much lower than that of lichen-based empirical CL (52%), similar to the findings in Europe (Hettelingh et al., 2007). Comparison between present-day and future simulations shows a significant reduction in exceedance rates nationwide between 2010 and 2050 (~50% reduction in both surface water CL exceedances and forest soil CL exceedances for acidity), mainly achieved by a reduction in Nr-ox deposition in the future when NO_x emissions are further controlled. However, increased emissions from agricultural sources contribute oppositely to deposition

reduction. We estimate that the increase in agricultural emissions between 2010 and 2050 increase the exceedance areas by 22% and 11% for forest soil acidity and freshwater acidity, respectively, which would, otherwise, return their Nr deposition to levels below CLs. The impacted regions mainly locate in areas with intense fertilizer application or hosting CAFO. We also show that atmospheric deposition is the leading contributor to total Nr load in remote watersheds where there is an absence of direct anthropogenic disturbance, including several lakes in National Parks and National Wilderness areas in Colorado, Montana, and Minnesota. Our study highlights the need to better manage diffusive Nr emissions from agricultural sources for the health of aquatic and terrestrial ecosystems under the stress of a warming climate and growing food production in the future.

3.6 Acknowledgments

This publication was made possible by funding from the US EPA under grants R83588001, the National Science Foundation (NSF SRN grant number 1444745), and China Scholarship Council (CSC) Grant #201606010393. Its contents are solely the responsibility of the grantee and do not necessarily represent the official views of the supporting agencies. Further, the US government does not endorse the purchase of any commercial products or services mentioned in the publication. All data used in this study is publicly available. Data sources are described in the "Materials and Methods" section.

CHAPTER 4. HIGH-RESOLUTION HYBRID INVERSION OF IASI AMMONIA COLUMNS TO CONSTRAIN U.S. AMMONIA EMISSIONS USING CMAQ ADJOINT MODEL

4.1 Abstract

Ammonia (NH_3) emissions have large impacts on air quality and nitrogen deposition, influencing human health and the well-being of sensitive ecosystems. Large uncertainties exist in the "bottom-up" NH_3 emission inventories due to limited source information and a historical lack of measurements, hindering the assessment of NH_3-related environmental impacts. The increasing capability of satellites to measure NH_3 abundance and the development of modeling tools enable us to better constrain NH_3 emission estimates at high spatial resolution. In this study, we constrain the NH_3 emission estimates from the widely used national emission inventory for 2011 (2011 NEI) in the U.S. using Infrared Atmospheric Sounding Interferometer NH_3 column density measurements (IASI-NH_3) gridded at a 36 km by 36 km horizontal resolution. With a hybrid inverse modeling approach, we use CMAQ and its multiphase adjoint model to optimize NH_3 emission estimates in April, July, and October. Our optimized emission estimates suggest that the total NH_3 emissions are biased low by 32% in 2011 NEI in April with overestimation in Midwest and underestimation in the Southern States. In July and October, the estimates from NEI agree well with the optimized emission estimates, despite a low bias in hotspot regions. Evaluation of the inversion performance using independent observations shows reduced underestimation in simulated ambient NH_3 concentration in all three months and reduced underestimation in NH_4^+ wet deposition in April. Implementing the optimized NH_3

emission estimates improves the model performance in simulating $PM_{2.5}$ concentration in the Midwest in April. The model results suggest that the estimated contribution of ammonium nitrate would be biased high in NEI-based assessments. The higher emission estimates in this study also imply a higher ecological impact of nitrogen deposition originating from NH_3 emissions.

4.2 Introduction

Ammonia (NH_3) emissions play a major role in ambient aerosol formation and reactive nitrogen deposition (Houlton et al., 2013; Stevens 2019). However, our understanding of NH_3 sources and sinks is limited by the large uncertainties present in the NH_3 emissions inventories (McQuilling and Adams 2015; Xu et al., 2019). In chemical transport models, uncertainties in NH_3 emissions propagate into the dynamic modeling of the atmospheric transport, chemistry, and deposition of NH_3, other reactive nitrogen species, and other key atmospheric constituents associated with NH_3 (Heald et al., 2012; Kelly et al., 2014; Paulot et al., 2013; Zhang et al., 2018b), hindering an accurate assessment of the various NH_3-related environmental impacts and the associated sources. The large uncertainties in the NH_3 emission inventories are partially due to a lack of sufficient in-situ NH_3 measurements that could be used to constrain emission estimates (Zhu et al., 2015). This work utilizes satellite observations from the Infrared Atmospheric Sounding Interferometer NH_3 column density measurements (IASI-NH_3) (Clarisse et al., 2009; Van Damme et al., 2017), to provide a high-resolution, optimized NH_3 emission inventory for the U.S. developed using an adjoint inverse modeling technique (Li et al., 2019), the robustness of which is demonstrated by evaluation against multiple independent in-situ measurements.

Emerging satellite observations of gaseous NH_3 provide a unique opportunity to better constrain the bottom-up NH_3 emission estimates for both their spatial distribution and seasonality. Bottom-up inventories calculate the NH_3 emissions based on estimated activity levels and corresponding emission factors, both of which are subject to high uncertainties, particularly for agricultural sources, the major contributor (Cooter et al., 2012; McQuilling and Adams 2015). Several studies have utilized NH_3 column density retrieved from IASI (Clarisse et al., 2009; Van Damme et al., 2015b) or the Atmospheric Infrared Sounder (AIRS; (Warner et al., 2016)) as well as the inferred surface mixing ratio of NH_3 from the Cross-track Infrared Sounder (CrIS; (Shephard et al., 2020; Shephard and Cady-Pereira 2015)) to characterize the spatiotemporal distribution of NH_3. These satellite measurements are useful for supplementing emission inventories to identify and quantify underestimated or missing emission hotspots, especially in intensive agricultural zones (Clarisse et al., 2019; Dammers et al., 2019; Van Damme et al., 2018). These studies find that the satellite-derived emission estimates are often twice as much as the bottom-up estimates on a regional scale and can be over 10 times higher over hotspots. However, the NH_3 retrievals from satellites are also subject to large uncertainties when the signal-to-noise ratio is low, which limits their ability to accurately measure NH_3 columns in low emission areas (Clarisse et al., 2010; Van Damme et al., 2015a).

Inverse modeling-based optimization combines the information from *a priori* emission inventories and observations and allows us to use the information from both. As one of the inverse modeling methods, the four-dimensional variational assimilation (4D-Var) method seeks the best emission estimate by minimizing a cost function that measures the differences between observations and model predictions, as well as the differences between

a prior and adjusted emission estimates. 4D-Var can be computationally expensive at fine model resolutions or with a large set of observations to be assimilated (Brasseur and Jacob 2017). Recent studies took advantage of the implementation of the adjoint technique in the chemical transport models to conduct 4D-Var for optimizing emissions estimation (Paulot et al., 2014; Zhang et al., 2018c; Zhu et al., 2013). The adjoint-based inversion method calculates the gradients of a cost function analytically and searches the solution using a steepest-descent optimization algorithm through iterating (Brasseur and Jacob 2017). By testing the performance of the inverse modeling method using artificial observational data, Li et al. (Li et al., 2019) proposed that a two-step optimization process, which combines the iterative mass balance (IMB) method and the 4D-Var method, can further reduce the computational cost. The IMB method assumes a linear relationship between the NH_3 column density and local NH_3 emission and searches the emission scaling factors iteratively until the simulated NH_3 column density converges to the observations. At a coarse (2°×2.5°) resolution, the IMB method is as effective as the 4D-Var method and requires 2/3 less computational time. In the second step, emission scaling factors obtained from the IMB method with a coarser resolution are used as an initial starting point for 4D-Var optimization process to reduce the overall computational time (Li et al., 2019).

In this study, the IASI-NH_3 dataset was applied to optimize NH_3 emission estimates from the 2011 National Emission Inventory (NEI 2011) using CMAQ and its adjoint model at a 36 km×36 km resolution. The multiphase adjoint model for CMAQ v5.0 was developed recently, including full adjoints for gas-phase chemistry, aerosols, cloud process, diffusion, and advection (Zhao et al., 2019). Both process-by-process and full adjoint model evaluations show reasonable accuracy based on agreements between the adjoint

sensitivities and forward sensitivities (Zhao et al., 2019). Previous inversion based NH_3 emission constraint using in-situ measures are limited by the spatial coverage and representativeness of the measurements (Gilliland et al., 2006; Henze et al., 2009; Paulot et al., 2014). Zhu et al. (2013) first attempted to optimize NH_3 emission inventory using NH_3 derived from the Tropospheric Emission Spectrometer (TES) satellite at 2°×2.5° resolution (Zhu et al., 2013). Inverse modeling at such a coarse resolution is limited to refining regional emissions. Similar to the inversion using CrIS NH3 measurements (Cao et al., 2020), inversion with the IASI-NH_3 dataset allows us to perform the optimization at a finer resolution with its daily global spatial coverage. Besides, the hybrid inversion approach adopted in this study allows us to calculate full adjoint sensitivities online instead of using approximated sensitivities from the offline-simulations (Cao et al., 2020; Zhu et al., 2013). The performance of our optimized estimates and the NEI 2011 are evaluated and compared based on in-situ observed ambient NH_3 concentrations and NH_4^+ wet deposition. Finally, by substituting the *a priori* NH_3 emissions with the optimized emissions, we assess the subsequent changes in simulated ambient $PM_{2.5}$ concentrations and nitrogen deposition exceedances.

4.3 Materials and Methods

4.3.1 IASI-NH_3 observations

NH_3 column densities retrieved from IASI onboard the Metop-A satellite are assimilated to constrain spatially-resolved NH_3 emissions using the 2011 NEI as the *a priori* inventory (Clarisse et al., 2009; USEPA 2014b; Van Damme et al., 2014). The polar sun-synchronous satellite has a 12-km diameter footprint at nadir and a bidaily global coverage. Only

observations from the morning pass around 9:30 am local standard time (LST) are used due to more favorable thermal contrast and smaller errors comparing to the ones from the night pass around 9:30 pm (LST). A comparison between the IASI-NH_3 data and ground-based Fourier transform infrared observations shows a correlation between the two with r = 0.8 and the slope = 0.73, indicating a tendency of IASI-NH_3 to underestimate the FTIR observations (Dammers et al., 2016). A comparison between IASI-NH_3 and airborne measurements also indicated an underestimation in California, while the comparison between IASI-NH_3 and ground observation from Ammonia Monitoring Network (AMoN) network indicated an overestimation (NADP 2014; Van Damme et al., 2015a). Overall, the evaluations show broad consistency between IASI-NH_3 and other independent measurements with no consistent biases identified. These evaluations were based on previous datasets. Here we use a new version that relies on another retrieval algorithm, which among other things has a better performance for measurements under unfavorable conditions (Van Damme et al., 2017; Whitburn et al., 2016).

Specifically, the NH_3 products for 2011 from ANNI-NH3-v2.2R-I datasets were used (Van Damme et al., 2017). The algorithm relies on the conversion of hyperspectral range indices to NH_3 column density using a neural network that takes into account 20 input parameters characterizing temperature, pressure, humidity, and NH_3 vertical profiles. A relative uncertainty estimate is provided along with each of the NH_3 vertical column density in the dataset. Small negative columns are possible – and these are valid observations, needed to reduce overall biases in the dataset. As the retrieval is unconstrained, no averaging kernels are calculated. We therefore directly compare the IASI-NH_3 column density with the simulated column density in CMAQ. Such comparison may be biased because the

sensitivity of retrieved NH_3 column densities to NH_3 concentrations is height-dependent (typically peaks around 700 – 850 hPa) (Dammers et al., 2017; Shephard et al., 2015). Although the CMAQ simulated NH_3 columns are also most sensitive to NH_3 concentration changes between 700 to 900 hPa (Figure C-1), we cannot quantify the relating uncertainties without knowing the averaging kernels. Without information on averaging kernels, differences between NH_3 vertical profiles in CMAQ and the ones used for retrieval may also contribute to the bias between retrieved and modeled column densities, depending on the magnitude of differences (Whitburn et al., 2016).

The NH_3 retrieved columns densities are regridded to the 36-km by 36-km CMAQ grid for 4D-Var data assimilation, and 216-km by 216-km resolution (a 6 grid by 6 grid CMAQ simulation grid matrix) for iterative mass balance (Figure 4-1). The mean column density (Ω_o) is calculated as the monthly arithmetic mean of all retrievals with their centroids falling in the same grid, following the recommendation that the unweighted mean is preferred for the updated version of IASI-NH_3 as error-weighting can lead to biases (Van Damme et al., 2017). The relative error (molec/cm^2) corresponding to mean column density in each grid is calculated following Van Damme et al. (Van Damme et al., 2014) as:

$$\bar{\sigma} = \frac{\Sigma \frac{1}{\sigma_i}}{\Sigma \frac{1}{\sigma_i^2}} \times \Omega_o \quad (1)$$

where $\bar{\sigma}$ is mean relative error (molec/cm^2), σ_i is the relative error associated with each NH_3 column density retrieval as reported, and Ω_o is the mean column density (Van Damme et al., 2014).

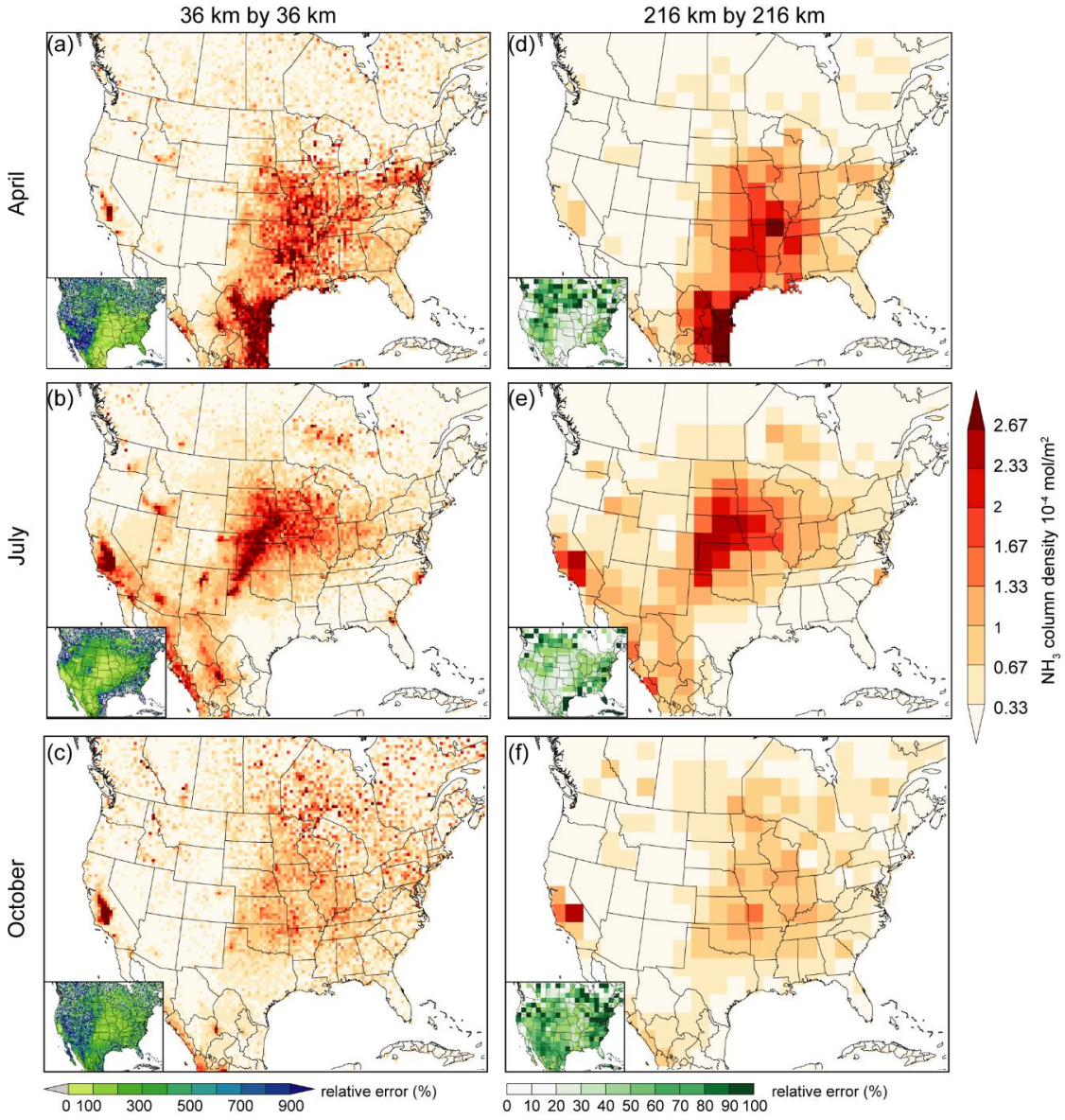

Figure 4-1 IASI monthly average NH_3 column density in April, July, and October 2011 at 36 km by 36 km (a, b, c) and 216 km by 216 km (d, e, f) resolutions within the model simulation domain of this study. The average relative error associated with the column density is shown in the corner of each plot.

The observations from April, July, and October are used to constrain the monthly NH_3 emission estimates in corresponding months from 2011 NEI. Observations from winter

months are not used because they are too noisy when the thermal contrast is low (Dammers et al., 2016).

4.3.2 NH_3 emission from 2011 NEI

The EPA 2011 NEI is used as *a priori* emission estimates. Major NH_3 sources include livestock waste management, fertilizer application, mobile sources, fire, and fuel combustion, with the majority being emitted by the first two sources. Specifically, the emissions from livestock waste management are estimated based on county-level animal population data and process-based daily emission factors. Emissions from fertilizer applications are estimated based on county-level fertilizer quantities and fixed emission factors, following the CMU ammonia Model (USEPA 2015). The NH_3 emissions over Mexico and Canada are derived from the simulation results of a fully coupled bi-directional agroecosystem and chemical-transport model (FEST_C_EPIC_CMAQ_BIDI) (Shen et al., 2019a). Emissions for other species also come from the 2011 NEI.

4.3.3 CMAQ and its adjoint

We use the Community Multiscale Air Quality Modeling System (CMAQ) v5.0 (Byun and Schere 2006; USEPA 2012) and its adjoint (Zhao et al., 2019), driven by meteorological fields produced from the Weather Research and Forecasting (WRF) Model v3.8.1 with grid nudging using the North American Regional Reanalysis (NARR) dataset (NOAA 2019). The CB05 chemical mechanism was adopted for gas-phase chemistry (Yarwood et al., 2005). The model implements ISORROPIA-II in the aerosol module (AERO06) to calculate the gas-particle partitioning of NH_3 and NH_4^+ (Fountoukis and Nenes 2007). The simulation domain covers the contiguous U.S. (CONUS) and part of Canada and Mexico

with a 36 km by 36 km horizontal resolution and 13 vertical layers extending up to 14.5 KPa (~16 km) (Figure 4-1). Monthly simulations are conducted for April, July, and October in 2011 with a 10-day spin-up for each month.

4.3.4 Hybrid inversion approach

We chose the hybrid inversion approach to combine the advantage of the faster computational speed of the mass balance method and the better optimization performance of the 4D-Var method. The first step is to apply the IMB approach to adjust the *a priori* (2011 NEI) NH_3 emission at 216 km by 216 km resolution (referred as the coarse grid hereafter) based on the ratio between the monthly-averaged observed (Ω_o) and simulated (Ω_a) NH_3 column density at the satellite overpassing time, iteratively. At each iteration, the emission in each grid is scaled by the ratio following the equation below,

$$E_t = \frac{\Omega_o}{\Omega_a} \times E_a \quad (2)$$

where E_t and E_a are the new and *a priori* emission estimates, respectively. The method has been described in detail in previous studies (Cooper et al., 2017; Li et al., 2019; Martin et al., 2003). The IMB is applied at the coarse grid so that the NH_3 column will be dominated by the local emissions instead of transport from neighboring grids (Li et al., 2019). The coarse resolution also reduces the uncertainty associated with IASI-NH_3 as the number of retrievals increases in each grid. For grids with mean relative error larger than 100%, the satellite observations are considered to be too noisy to provide useful constraints and the *a priori* emission estimates are retained. The iteration stops when the normalized mean square error either decreases by less than 10% or begins to increase. The final scaling factor

(ε_0) for each grid is the multiplication of the scaling factors derived at each iteration and downscaled to 36 km by 36 km resolution by assigning the same value to the 6 by 6 grid matrix. This scaling factor is applied to the 2011 NEI emissions to create the revised *a priori* estimate for the 4D-Var inversion.

Next, the 4D-Var inversion is performed. The solution of the optimization problem is sought iteratively by minimizing the cost function (J) defined as the combination of error-weighted, squared difference between emission scaling factor and unity and the error weighted, squared difference between IASI-NH_3 and the simulated column density, as below:

$$J = \gamma(\varepsilon - \varepsilon_0)^T S_a^{-1}(\varepsilon - \varepsilon_0) + (\Omega_o - F(\varepsilon))^T S_o^{-1}(\Omega_o - F(\varepsilon)) \quad (3)$$

ε is the monthly emission scaling factor to be optimized at each iteration where $\varepsilon = \log\left({E_t}/{E_a}\right)$ on the 36 km by 36 km CMAQ grid, consisting of 6104 elements overland grid cells in CONUS. S_a and S_o are error covariance matrices for the *a priori* emission estimates and IASI-NH_3 retrievals, respectively. The two matrices are assumed to be diagonal. For S_o, the grid average absolute error is used to represent the observational error. To reduce the influence of retrievals close to or below the detection limit, an estimated detection limit of 4.8×10^{15} molecules/cm^2 is added to the S_o (Dammers et al., 2019). Our test shows that negative Ω_o will lead to a continuous decrease in the adjusted emission for the grid cell because modeled column density cannot become negative. To limit the influence of these negative Ω_o, their original weights are multiplied by 0.01. For S_a, the uncertainty in each grid is assumed to be 100% of the *a priori* emissions. F(ε) is CMAQ

simulated NH_3 column density sampled at the satellite passing time if there is at least one IASI-NH_3 retrieval in that grid; γ is the regularization factor balancing the relative contribution of the *a priori* emission inventory and IASI-NH_3 retrievals to the J value. γ is chosen to be 30 for all 3 months based on the L-curve criteria (Hansen 1999) (Figure C-2).

The gradients of the cost function to NH_3 emissions are calculated by the CMAQ adjoint model. In each iteration, the emission-weighted monthly averaged sensitivities in each grid are supplied to the L-BFGS-B optimization routine contained in the "optimr" package in R to find the scaling factors that will achieve the minimum of the cost function (Byrd et al., 1995; Zhu et al., 1997). NH_3 column density is re-simulated using adjusted emissions by the new set of scaling factors. The iteration process is terminated when the decrease in J is less than 2% or the local minimum is reached.

4.3.5 Posterior evaluation

The posterior emissions are evaluated by comparing the model simulation from optimized emissions with observations. Simulated results are compared with ambient NH_3 concentrations from the AMoN (NADP 2014), and the NH_4^+ wet deposition from the National Atmospheric Deposition Program (NADP 2019). The simulated NH_3 concentration in ppmV is converted to $\mu g/m^3$ using local temperature and pressure from the model meteorological inputs. For evaluation against the NH_4^+ wet deposition, the simulated deposition is scaled by the ratio between measured and simulated precipitation to eliminate the bias introduced by precipitation fields (Appel et al., 2011).

4.4 Results

4.4.1 Optimization performance evaluation

The optimized NH_3 emissions reduce the bias in the NH_3 columns between the satellite observation and the model prediction as shown by the decrease in the values of normalized root mean square error (NRMSE) and normalized mean biases (NMBs) in Figure 4-2. There are negative biases using 2011 NEI in all three months, especially in areas with high emission rates. Although the IMB inversion can lower the NRMSE, it tends to over-adjust and introduce a positive bias likely because of the coarse resolution and neglect of the impact of transport. The 4D-Var inversion effectively decreases the positive bias and further reduces the NRMSE. The cost function value reduces by 50%, 57%, and 34% with the 4D-Var inversion in April, July, and October, respectively. We find that it is more challenging to adjust the emissions in April than in the other two months because of the greater differences in the magnitude and the spatial distribution of the emissions. The optimized NH_3 emission successfully captures the high NH_3 column density in the Southern States, reducing the NRMSE by 98%. Despite the general improvement in the model performance, negative biases in July increase in California's San Joaquin Valley. Scaling up the emission in the San Joaquin Valley will result in high NH_3 concentrations downwind even when the local NH_3 emissions downwind are zeroed, whereas the IASI-NH_3 observed concentrations downwind are low. The transported hotspot downwind of the San Joaquin Valley in CMAQ only occurs in July, suggesting near field removal may not be captured at the current resolution, and warrants further investigation. Grid by grid comparison between model-simulated NH_3 column density using the *a priori* and optimized estimates with IASI-NH_3 shows improved agreement in both high and low emission grids after optimization (Figure C-3). It shows that the hybrid inversion approach

can alleviate the weakness of direct 4D-Var inversion which tends to over-adjust high emission regions and under-adjust low emission regions, mainly because the IMB inversion provides a better initial state.

The IMB inversion took three iterations to achieve the convergence condition for each month, and subsequently, the 4D-Var inversion took five, four, and three iterations for April, July, and October, respectively. Fewer iterations are needed with the hybrid approach than the direct 4D-Var inversion which typically takes up to 15 to 20 iterations of adjoint simulation (Paulot et al., 2014; Zhang et al., 2018a). The CPU time of a forward simulation is only 1/5 of an adjoint simulation. In total, the CPU time required by the hybrid approach is expected to be 60% lower than the direct 4D-Var inversion approach.

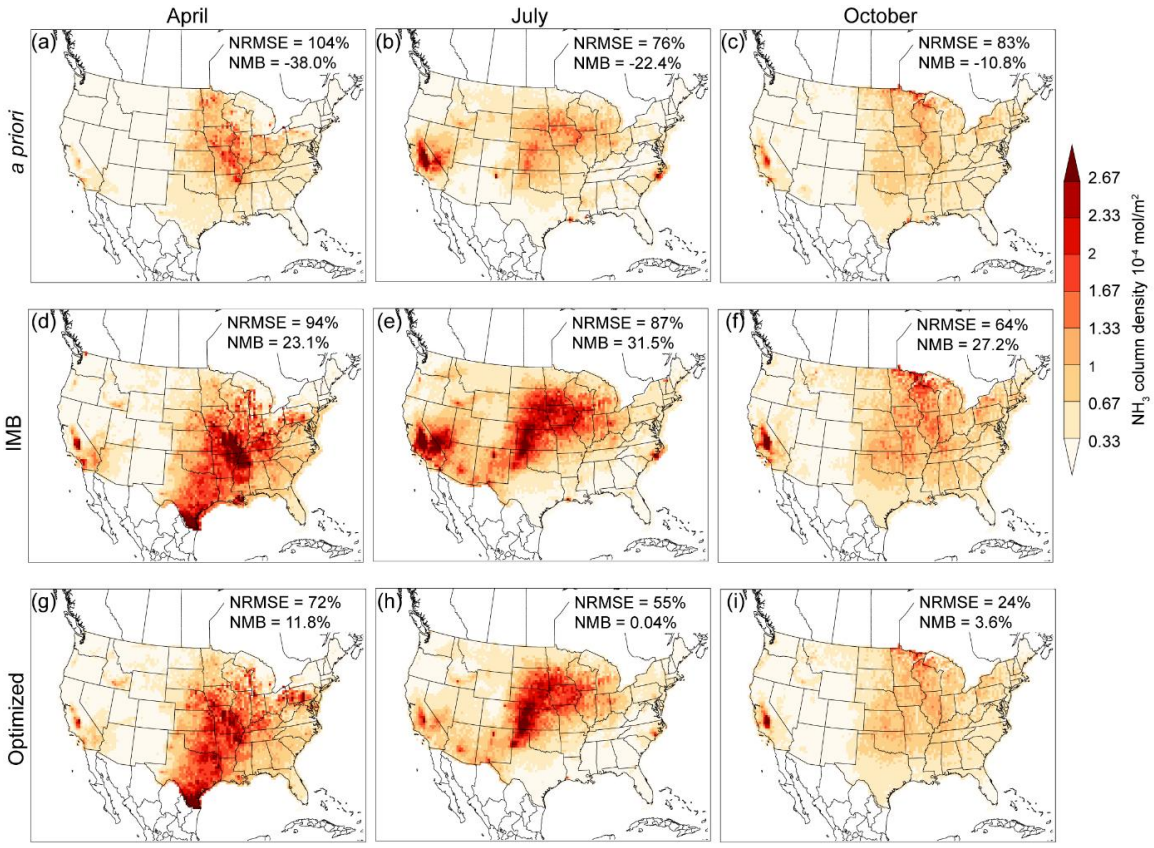

Figure 4-2 CMAQ simulated monthly average NH_3 column density for April, July, and October 2011 using the *a priori* emissions (a, b, c), the emissions adjusted by IMB (d,e,f), and the final optimized emissions using the hybrid approach (g,h,i). For comparison with the IASI-NH_3 retrievals, simulated NH_3 columns at the passing time were derived when there are observations in that grid. Normalized root mean square error (NRMSE) and normalized mean bias (NMB) between the simulated values and IASI-NH_3 are provided.

4.4.2 Optimized estimate of NH_3 emissions

The monthly total NH_3 emission in CONUS increases by 46% in April, 6.6% in July, and 6.9% in October for the optimized estimates, respectively. Spatially, the distribution for high emission regions shifts from Midwest in the 2011 NEI to the Southern States in the optimized estimates in April, whereas the hot spot regions remain consistent in July and

October (Figure 4-3). Regional total emissions are summarized according to the USDA Farm Production regions, which defines the areas with similar crop production activities (Cooter et al., 2012). In general, the regional variation of NH_3 emissions in April is dominated by fertilizer application. The optimized estimates in regions with high contributions from fertilizer applications in 2011 NEI, including the Corn Belt, Lake States, and Northern Plains, are lower than the 2011 NEI. In contrast, the optimized estimates are 2 – 3 times higher than the 2011 NEI estimates in the Delta States and Southern States where the *a priori* estimates for NH_3 emission from fertilizer application are low. The optimized NH_3 emission pattern in April is more consistent with the spatial pattern of inorganic nitrogen fertilizer estimated based on plant demand (Cooter et al., 2012) as well as the livestock population distribution (USDA 2012), suggesting the potential bias in the agricultural practices used in 2011 NEI. In July, regional differences are smaller except for the Northern Plain and Southeast. In the Northern Plain, the NH_3 emission is 66% higher in the optimized estimates, driven by the emission increase in hotspot areas with concentrated animal feeding operations (CAFO) (Clarisse et al., 2019; USDA 2012; Van Damme et al., 2017). The potential bias in different sectors suggests the need for sectoral inversion when a larger observational dataset becomes available in the future. In the Southeast, the IASI-NH_3 column densities are very low, even over known CAFO sites, and had high errors associated with the retrievals because of the low thermal contrast and a smaller number of retrievals (Schiferl et al., 2014). The negative increment in the Pacific region is due to the disagreement between modeled high NH_3 columns and observed low values from IASI-NH_3 downwind of the San Joaquin Valley of California, as discussed previously. In October, the relative difference is less than 10% in most of the regions,

indicating that the 2011 NEI appropriately reflects the NH_3 emission pattern. There is a significant increase in the NH_3 emissions in Mexico during all three months. Such an emission increment is crucial to improving the model performance in both Mexico and the southwestern U.S. However, it was not a goal of this study to determine emissions biases in Mexico given the limited information on NH_3 emissions.

The total NH_3 emissions in the optimized estimates are 671 Gg, 500 Gg, and 320 Gg per month in April, July, and October, respectively. Similar to a bottom-up agricultural NH_3 emission inventory (MASAGE_NH_3) and two inverse model optimized estimates based on NH_4^+ wet deposition, we find a higher emission in the spring season (Gilliland et al., 2006; Paulot et al., 2014), while others, including the NEI, estimates a summertime peak (Cooter et al., 2012; USEPA 2015; Zhu et al., 2013). The large variation between different inventories warrants both improved information on bottom-up inventories and more observations to support inverse model optimization in the spring season. Better knowledge about agricultural activities and more independent ground and space observations are needed. It should also be noted that there are interannual variations in emission inventories developed for different years. The total emission estimates in July and October are closer to the 2011 NEI estimates than those estimates from other emission inventories and inverse analysis. The good agreement with IASI-NH_3 indicates that the 2011 NEI captures the NH_3 emission pattern in general in these two months.

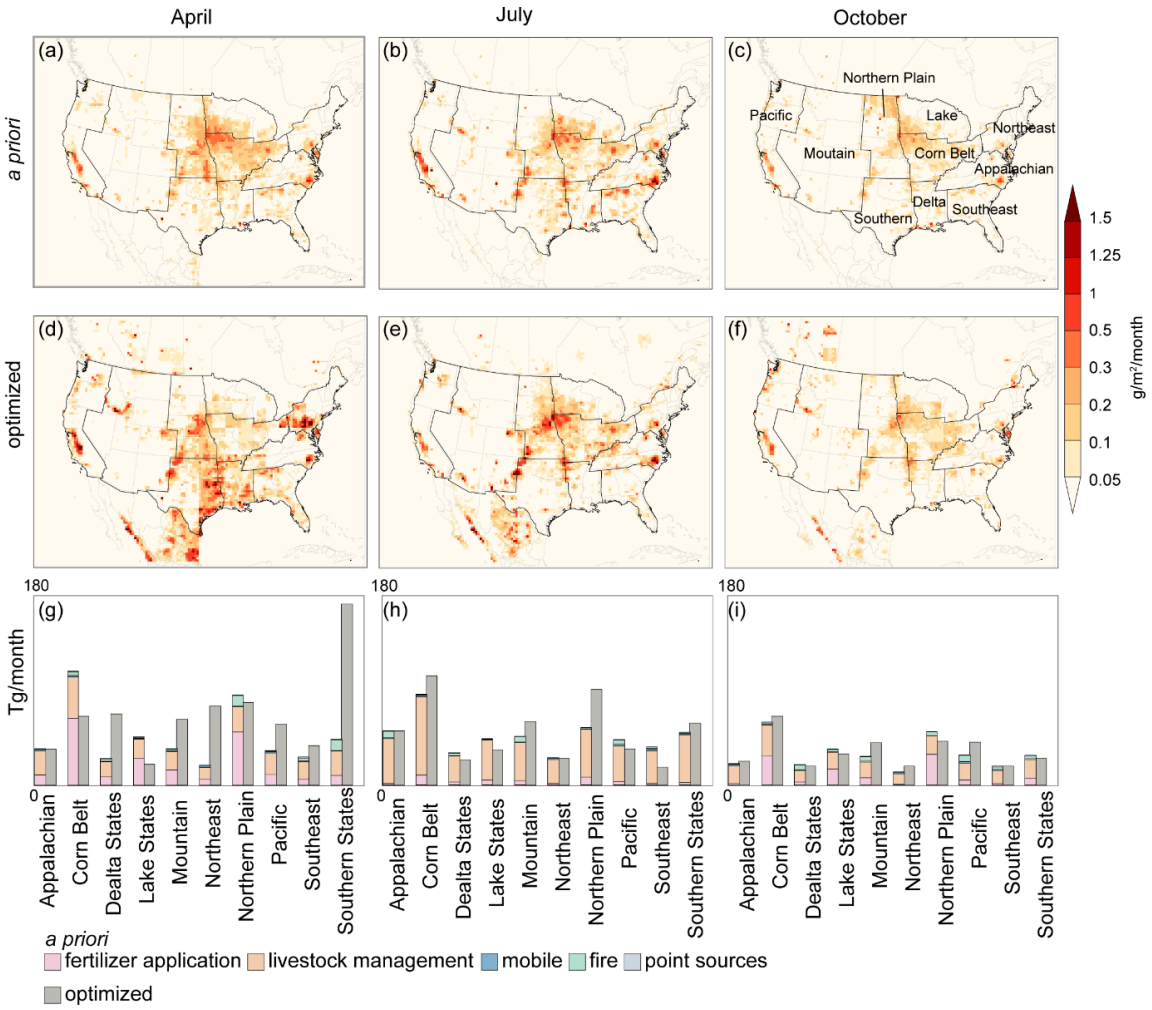

Figure 4-3 The spatial distribution of monthly total NH3 emission from the *a priori* (a, b, c) and optimized (d, e, f) estimates in April, July, and October. The total emission based on the a priori and optimized estimates are summarized for each USDA Farm Production region (g, h, i). The source contributions to total emission are shown for the *a priori* estimates.

4.4.3 Evaluation of the optimized emission estimates against independent datasets

The robustness of the NH_3 emission optimization is evaluated by comparing the model outputs using both the *a priori* and optimized emission estimates with independent observations. The bias and uncertainties inherited in the CMAQ forward model and its adjoint, as well as the assumptions made about the uncertainties of the *a priori* emission

inventory and IASI-NH_3 observations, will all influence the robustness. Here, we choose to evaluate the outputs against 1) biweekly average ambient NH_3 concentrations measured by AMoN; 2) weekly average NH_4^+ wet deposition measured by NADP (Figure 4-4).

In general, the optimized NH_3 emission reduces the negative NMB when comparing the CMAQ outputs with AMoN NH_3 concentration for all three months. Yet, the NRMSE gets higher and R^2 gets lower, indicating a higher spatial variation in the residuals. This is likely due to the tendency of satellite-based inversion to over-adjust emissions in high concentration areas (Zhu et al., 2013). There is a greater improvement at the high concentration end than the low concentration end because both IASI satellite and the passive samplers at the AMoN sites have higher uncertainties in areas with low NH_3 abundance (Puchalski et al., 2011; Van Damme et al., 2015a). There is an over-adjustment for sites in Pennsylvania in April where there is a hotspot observed by IASI. The hotspot in monthly average is dominated by high NH_3 column densities observed in April 14th and 15th, possibly from a large transported plume from the central U.S. to Pennsylvania (Figure C-4). The fact that it is transported at higher altitude in 2 days could explain that it is not measured by ground observations at AMoN sites at biweekly resolution. The long-range transport at higher altitude may lead to an overestimation in IASI retrieved NH_3 column densities which assume a vertical profile with highest concentrations near the surface (Whitburn et al., 2016). Such transport is also not well represented in the hybrid inverse modeling approach where the transport effect is not included in the IMB inversion at 216 km by 216 km resolution.

For evaluation against NADP observations, there is a noticeably improved agreement in April with reduced negative NMB and reduced discrepancies for most of the data pairs.

For July, the emission optimization only slightly improved the model performance. For October, the optimization increased the NMB from -1.8% to 10%. It indicates that NH_3 emission is not the dominant explanatory factor for bias in simulated NH_4^+ wet deposition that is commonly observed in chemical transport models (Appel et al., 2011; Paulot et al., 2014). Overall, the improved model operational performance for ambient NH_3 suggests that the inverse model optimization applied in this study provides improvements in the NH_3 emission estimates during all three months in most of the CONUS.

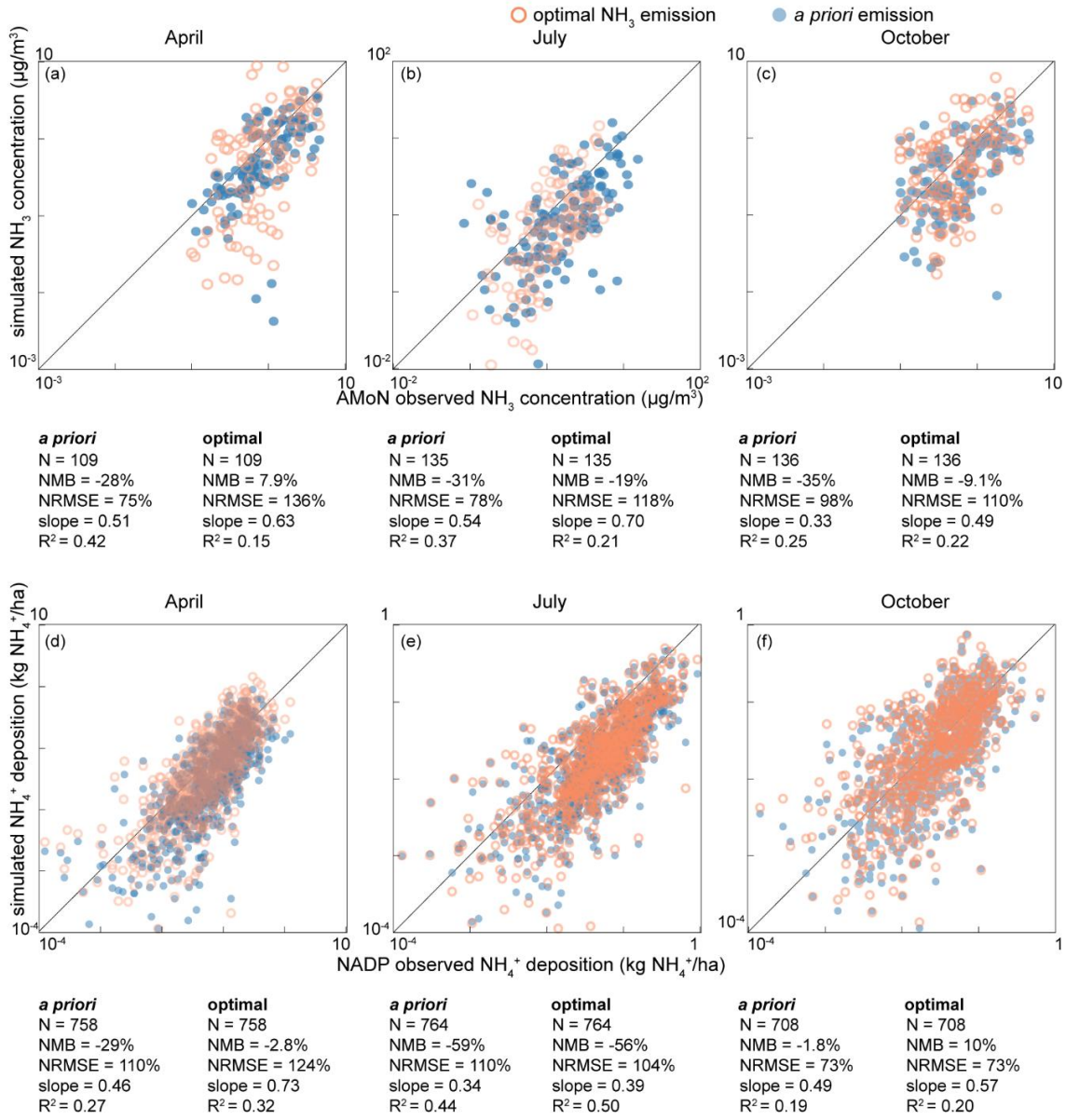

Figure 4-4 Evaluation of the simulated NH_3 surface concentration (a, b, c) and NH_4^+ wet deposition (d, e, f) against biweekly NH_3 concentration observations from AMoN and weekly NH_4^+ wet deposition observations from NADP, respectively. The orange circles and blue dots represent comparison using the *a priori* and optimized NH_3 emission estimates, respectively. Summary statistics including sample size (N), normalized mean bias (NMB), normalized root mean square error (NRMSE), least square error regression slope and intercept, and R square (R^2) for all comparisons are listed below the plots.

4.5 Implications

4.5.1 Ambient aerosol concentration

As a major precursor of ambient aerosol formation, the NH_3 emission inventory is believed to be a major source of uncertainty in $PM_{2.5}$ assessment in several parts of the CONUS (Heald et al., 2012; Henze et al., 2009; Schiferl et al., 2014), which can further bias the source contribution assessments on $PM_{2.5}$-related health impacts (Lee et al., 2015; Zhao et al., 2019). Comparison of the simulated $PM_{2.5}$ mass concentration using the *a priori* and optimized NH_3 emission estimates shows that the NH_3 emission bias in April is a major factor for bias in the modeled $PM_{2.5}$ concentration leading to high or low bias in ammonium nitrate (NH_4NO_3) formation (Figure 4-5). The relative change of the monthly average $PM_{2.5}$ concentration is over 10% in one-fifth of the CONUS, including an increase in the Northeastern, Pacific West, and Rocky Mountains regions, and a decrease in the Midwest. For most of these regions, over 90% of the change is driven by the change in concentration of NH_4^+ and NO_3^-.

Comparison of the simulated monthly average NH_4^+ and NO_3^- concentration using the *a priori* estimates against ambient monitoring network data (USEPA 2018) shows that there is a high bias in the Midwest region and Pennsylvania state, and underestimation low bias for the rest of the sites (Table 4-1). Simulations using the optimized NH_3 emission estimates reduce the high bias in the Midwest region but exacerbate the high bias in the Pennsylvania state and surrounding areas. For the other sites, the impact of optimization is mixed but minor in general.

For the Midwest, our optimized NH_3 emission is 31% lower than the 2011 NEI, leading to a 20 - 30% decrease in NH_4^+ and NO_3^- concentration. Overestimation of NO_3^- in the Midwest has been recognized in previous model evaluations. Previous studies attempted to moderate the high bias by lowering the nitric acid (HNO_3) concentration through either lowering both daytime and nighttime HNO_3 formation rate or raising deposition removal rate. It was found that such modification in the model parameterization cannot fully account for the overestimation (Heald et al., 2012; Walker et al., 2012; Zhang et al., 2012). Our study implies that the springtime overestimation can partly be explained by the overestimation in NH_3 emissions which drives the high bias in NH_4NO_3 formation.

The large increase of the NH_4NO_3 concentration in Pennsylvania state and surrounding areas is due to the over-amplified local NH_3 emissions in the optimized estimates to match the high NH_3 column density in IASI-NH_3 2011, as discussed earlier. It adds to the existing overestimation in NH_4^+ and NO_3^- concentration as compared to ground measurements. The fact that the simulated ambient NH_3 concentration, NH_4^+ concentration, and NH_4^+ wet deposition using the optimized NH_3 estimates is biased high in comparison with independent ground measurements suggests the enhanced NH_3 abundance observed from IASI is driven by long-range transport at higher altitudes instead of local surface emissions.

For the rest of the CONUS, there is only a slight impact of the optimization on simulated NH_4NO_3 formation. For example, although the NH_3 emission is doubled in the San Joaquin Valley in California, the modeled NH_4^+ and NO_3^- concentrations are still biased low using the optimized estimates. A sensitivity test using GEOS-Chem shows that the San Joaquin Valley region is nitric acid-limited instead of ammonia-limited (Walker et al., 2012), suggesting that there is an underestimation in HNO_3 formation. A comparison of the

simulated and measured speciated $PM_{2.5}$ shows that there is a low bias in non-volatile cation concentrations in the sites in the San Joaquin Valley, limiting the formation of NH_4NO_3 through gas-particle partitioning (Chen et al., 2019). Thus, attempts to close the gap between the simulated and monitored NH_4^+ and NO_3^- concentrations by scaling NH_3 emission alone are ineffective and might lead to an overestimation in local NH_3 emissions.

For July and October, there is a very limited difference between the simulated $PM_{2.5}$ concentration using the optimized and *a priori* NH_3 emission estimates, as expected, because the change in NH_3 emission is small. There are only 1% and 4% of the CONUS with a relative change in $PM_{2.5}$ concentration over 10%. This result shows that the uncertainty in NH_3 emission estimates is moderate and is not a major contributor to biases in modeled $PM_{2.5}$ in July and October.

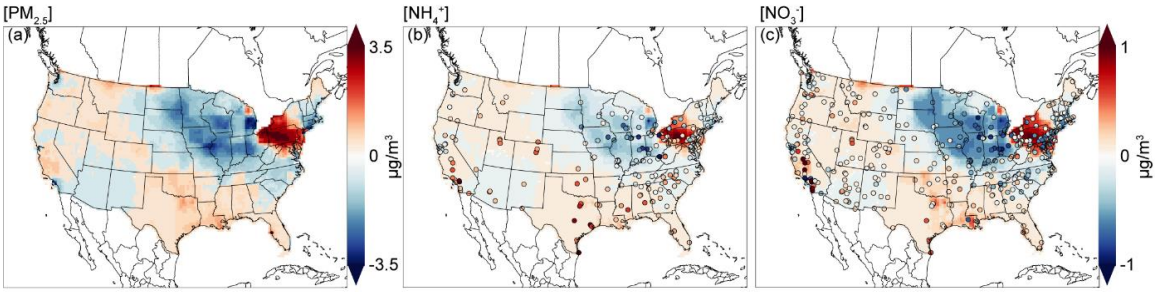

Figure 4-5 The changes in monthly average $PM_{2.5}$, NH_4^+, and NO_3^- mass concentration in April due to the NH_3 emission adjustment in the optimized estimates. The change is defined as $conc_{optimized} - conc_{a\ priori}$, where $conc_{optimized}$ and $conc_{a\ priori}$ represents the simulated monthly average mass concentration using the optimized and *a priori* NH_3 emission estimates, respectively. The difference between the observed NH_4^+, and NO_3^- mass concentration and simulated concentrations using the *a priori* NH_3 emission ($conc_{obs} - conc_{a\ priori}$, where $conc_{obs}$ represents the observed monthly average mass concentration) are overlaid using colored dots with the same color scheme.

Table 4-1 Statistical summary of the correlation between simulated monthly average NH_4^+ and NO_3^- concentrations and observations in April[a]

NH_4^+	Midwest		Penn		Other	
	a priori	optimized	*a priori*	optimized	*a priori*	optimized
N	47		37		115	
NMB	0.18	0.03	0.03	0.33	-0.24	-0.2
NRMSE	0.39	0.29	0.33	0.59	0.45	0.49
slope	0.52	0.60	0.47	0.33	0.74	0.28
R^2	0.60	0.65	0.34	0.49	0.22	0.08
NO_3^-	Midwest		Penn		Other	
	a priori	optimized	*a priori*	optimized	*a priori*	optimized
N	69		38		240	
NMB	0.50	0.22	0.10	0.58	-0.66	-0.69
NRMSE	0.75	0.51	0.27	0.72	0.82	1.03
slope	0.44	0.50	0.18	0.48	0.33	0.48
R^2	0.76	0.72	0.31	0.67	0.13	0.67

[a] The correlation between observed concentrations and simulated ones based on *a priori* and optimized NH_3 emission estimates are compared. The sites are grouped as the Midwest region, Pennsylvania state and surrounding areas, and other areas.

4.5.2 Reactive nitrogen (Nr) deposition

The uncertainties in NH_3 emission inventory also impact the reactive nitrogen (Nr) deposition assessment, which informs the ecosystem impacts evaluation and effective mitigation actions (Ellis et al., 2013). To evaluate the impact of the NH_3 emission optimization on simulated Nr deposition, the Nr deposition amount simulated using optimized and *a priori* emission estimates is analyzed in all biodiversity-protected areas designated by the USGS (Figure C-5) within CONUS (USGS 2018). In total, the Nr deposition increased by 39%, 2%, and 9% on average in these protected areas in April, July, and October, respectively. A regional comparison based on the Level I ecoregions (Pardo et al., 2015) shows that the deposition increment is the highest in the Great Plain region (+73%), followed by the Eastern Temperate Forest (+41%) (Figure 4-6). Although the overall increase is small in July and October, the increment can be high in individual ecoregions, including Southern Semiarid Highlands (+109% in July), Temperate Sierras (+66% in July), and Marine West Coast (+64% in October). In addition to the increment in deposition amount, higher NH_3 emission, especially in intensive agriculture regions, may indicate higher source contribution from agricultural NH_3 than previous estimates (Lee et al., 2016a).

Driven by the increase in the reduced form of Nr (NH_3 and NH_4^+) deposition, a higher share of reduced form of Nr to the total Nr deposition is found in most of the ecoregions for all three months than the NEI-based estimates. More detrimental impacts on sensitive species and biodiversity are expected when this change in dominant Nr form are considered in addition to the increase in magnitude because the growth of many sensitive plant species will be inhibited by a high NH_4^+ to NO_3^- ratio in soil and water (Bobbink and Hicks 2014).

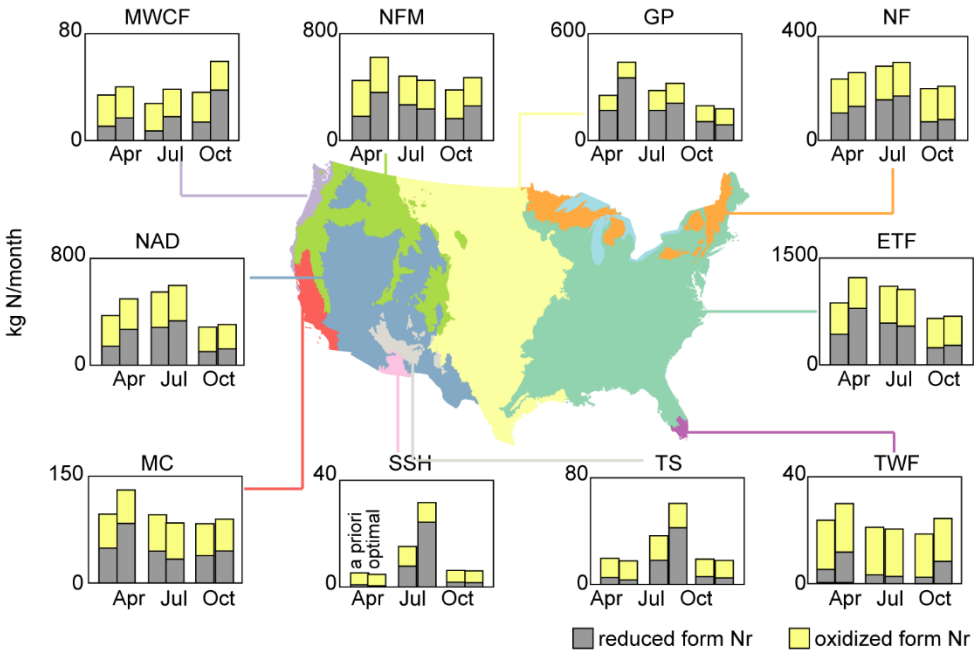

Figure 4-6 The changes in the simulated monthly reactive nitrogen (Nr) deposition amount in protected areas for biodiversity conservation caused by the emission adjustment in April, July, and October. The deposition is grouped for 10 level I ecoregions defined by the Commission for Environmental Cooperation, including Northern Forests (NF), Great Plains (GP), Northwestern Forested Mountains (NFM), Marine West Coast Forest (MWCF), North American Deserts (NAD), Mediterranean California (MC), Southern Semiarid Highlands (SSH), Temperate Sierras (TS), and Tropical Wet Forests (TWF).

4.6 Conclusions

We apply the newly developed multiphase adjoint of the CMAQ v5.0 chemical transport model and NH_3 column observations from the satellite-borne IASI to optimize NH_3

emissions estimates in the CONUS using a hybrid inversion modeling approach. The approach consists of a coarse-resolution iterative mass balance inversion (216 km by 216 km) and a fine-resolution 4D-VAR inversion (36 km by 36 km) and is performed using IASI-NH_3 observations in April, July, and October. The hybrid approach overcomes the over-adjusting problem for high emission areas in the direct 4D-Var method and reduces the computational cost.

We use the NH_3 emission from 2011 NEI commonly used in regional and national simulations and assessments as the *a priori* emission. We find that the optimized NH_3 emission inventory differs greatly with the 2011 NEI in April. The emission in Midwest is overestimated and the emission in Southern states is underestimated in the 2011 NEI. Overall, the optimized emission is 46% higher. The optimized emission estimates in July and October are slightly higher (6.6% and 6.9%) than the 2011 NEI estimates and the spatial distribution agrees well. The IASI-NH_3 observations indicate a consistent underestimation of NH_3 emissions in California's San Joaquin Valley in all three months, however, the inverse modeling fails to properly scale up the emissions in July. The evaluation of simulation outputs against ground measurements including ambient NH_3 concentrations from AMoN and NH_4^+ wet deposition from NADP shows that the optimized NH_3 emission estimates improve the agreement between model outputs and independent observations, especially in April.

Application of the optimized NH_3 emission estimates also yields a better agreement between the simulated and observed $PM_{2.5}$ concentration in April in the Midwest region by improving the model performance on simulated NH_4^+ and NO_3^-. It is consistent with previous findings that the uncertainty in NH_3 emission is a key factor limiting the model

performance of $PM_{2.5}$. The optimized NH_3 emission estimates in general increase the Nr deposition amount and the relative importance of reduced form Nr, highlighting the importance of constraining NH_3 emission estimates for accurately assessing nitrogen deposition and ecosystem health over sensitive regions.

Data availability. The IASI/Metop-B NH3 total column Level 2 data is available at the IASI portal provided by the AERIS data infrastructure (ULB 2018). Independent observations for evaluation including surface NH_3 concentrations, NH_4^+ wet depositions, and speciated $PM_{2.5}$ concentrations are available from the NADP website and Air Quality System (NADP 2014; 2019; USEPA 2018).

4.7 Acknowledgments

This publication was made possible by funding from the US EPA under grants R83588001, NASA under grant NNX16AQ29G, and China Scholarship Council (CSC) Grant #201606010393. The authors acknowledge the AERIS data infrastructure for providing access to the IASI data in this study and ULB-LATMOS for the development of the retrieval algorithms. Contents of this publication are solely the responsibility of the grantee and do not necessarily represent the official views of the supporting agencies. Further, the US government does not endorse the purchase of any commercial products or services mentioned in the publication.

CHAPTER 5. SUMMARY AND FUTURE WORK

This thesis has presented the development, evaluation, and application of an integrated modeling framework to estimate the environmental impacts of agricultural NH_3 emission in the United States when other conventional pollutants are being further regulated. The three main chapters presented here are published or in submission. The conclusions from previous chapters and suggestions for future works are summarized here.

5.1 Summary

Future simulations and sensitivity tests with different emission levels and boundary conditions show that the aerosol will remain acidic in the future even with an aggressive reduction of anthropogenic SO_2 emissions and increase in NH_3 emissions in the US. This results from the buffering effect of NH_3-NH_4^+ partition and rapid NH_3 deposition, as well as the increasing relative contribution from background SO_4^{2-}. Rising agricultural NH_3 emissions and SO_2 reduction will not cause a significant increase in ammonia nitrate concentration in most areas. However, the nitrate substitution will undermine the $PM_{2.5}$ reduction efforts through traditional emission regulations in the central regions if NH_3 and NO_x emissions are not further controlled.

Comparison between future baseline and counterfactual scenarios in which agricultural NH_3 emissions are projected to rise or stay constant at present-day level, respectively, shows that the decline in nitrogen deposition achieved by NO_x emission control for power and transport sectors would be offset or even reversed by NH_3 emission increase from the agricultural sector. The impact of Nr deposition on sensitive ecosystems

is evaluated by comparing the simulated Nr deposition with multiple critical loads. The evaluation identifies that areas with intensive NH_3 emission from agricultural practices will continue to exceed CLs despite effective NO_x emission control. To bring the nitrogen deposition level below the critical loads requires simultaneous control of NH_3 emissions from agriculture activities and NO_x emissions from fossil fuel combustion. The impact on Nr loading received by watersheds is quantified by linking CMAQ simulated Nr deposition with a water quality model. Watersheds in remote areas with an absence of other significant anthropogenic contributors are identified as vulnerable areas to agricultural NH_3 emission increase, and include the Glacier National Park in Montana, lakes within the Indian Peaks wilderness area in Colorado, and the Superior National Forest in Minnesota.

The potential of constraining the NEI NH_3 emissions using satellite observations and hybrid inverse modeling was examined in response to the evidence suggesting that current NH_3 inventories may be biased. The newly developed multiphase adjoint model of CMAQ v5.0 is applied to emission optimization using satellite observations from IASI-NH_3. The hybrid inverse modeling consists of a coarse-resolution iterative mass balance inversion and a fine-resolution 4D-Var inversion. This approach overcomes the over-adjusting problem for high emission areas in the direct 4D-Var method and reduces the computational cost. The optimized NH_3 emission in April is 46% higher than the NEI estimates. Emissions in Midwest were found to be overestimated in the NEI and largely underestimated in the Southern States. To prove the robustness of the optimization, evaluation against independent ground observations including NH_3 concentration, NH_4^+ wet deposition, and particulate NH_4^+ concentration are performed. In general, the optimized NH_3 emissions reduce model bias although the variations get larger in some

cases. For April, re-evaluation of $PM_{2.5}$ concentration and Nr deposition with the optimized NH_3 emissions shows the optimization lead to over a 10% change in $PM_{2.5}$ mass concentrations in over 1/5 of the CONUS, mainly because of the change in NH_4NO_3 concentrations. The Nr deposition in sensitive ecosystems might be underestimated by 40% due to the low bias in NEI NH_3 emission. For July and October, the optimized NH_3 emission and NEI estimates are in good agreement.

5.2 Future Work

5.2.1 Environmental impacts analysis at global and local scales

The analysis in this thesis focuses on the CONUS at 36 km by 36 km resolution. The results suggest the need for both more global and more local scale analyses. Global simulation is needed to better understand the impact of transboundary transport when domestic anthropogenic emissions in the U.S. are further controlled. When designing future standards, it is important to recognize the background concentration which may be dominated by emissions from countries upwind. Local-scale analysis at a finer resolution provides more detailed information, particularly when more local measurements are taken into consideration. For Nr deposition analysis, the national scale model does not fully capture spatial gradients because of the sharp change in topographical and meteorological parameters like precipitation, soil condition, and elevation. A local-scale analysis can improve the results by including site-specific precipitation measurements and fine resolution land cover data. Besides, the Nr exceedances calculated using site-specific dynamic critical loads in the future would better help planners. Model simulation at finer resolution may be computationally expensive but is becoming increasingly feasible. The

regions adversely affected by agriculture NH_3 emission identified in this study would be particularly ripe for future research when refining study domains.

5.2.2 Ground and space observations for further constrain NH_3 emission inventory

As demonstrated in this thesis, inverse modeling can effectively reduce the bias in NH_3 emission estimates. The inverse modeling approach relies on high-quality observations. Future development in both ground and space NH_3 abundance observations will provide further improvements in NH_3 emission inventory optimization.

Currently, the AMoN network is too sparse to fully characterize the spatial distribution of NH_3 concentration over CONUS because NH_3 is highly reactive, leading to a relatively short transport distance and potentially high concentration gradients. More ground monitoring sites are desired in the future, especially in hot-spot NH_3 emission regions identified by satellite-based inversion where the current AMoN network does not cover. The dataset will provide a great constrain for NH_3 emission inventories as NH_3 in concentrated near the surface. In particular, inverse modeling using ground observation in winter can help fill the gap for satellite-based optimization, that result when the thermal contrast and NH_3 concentration are low and satellite retrievals become very noisy.

For satellite observations, additional information associated with the NH_3 column density retrieval will be useful for improving satellite-based inverse modeling. The vertical profile information is not provided in IASI-NH_3, introducing unknown bias in the optimization process by assuming the vertical profile is identical to the simulated profiles in CMAQ. Recently published satellite products from CrIS contains vertical information. Applying the inverse modeling approach developed in Chapter 4 using NH_3 column density from

CrIS can be used to evaluate the importance of vertical distribution assumption, and the general uncertainty in different satellite observations.

The NH_3 emission and concentration exhibit great diel variation. However, little is known about the diel temporal profile due to a lack of observation. Sun-synchronous satellites including IASI, CrIS, and AIRS only provide semi-daily information, and routine monitoring from AMoN network only has bi-weekly sampling. Future research involving continuous ground monitoring and geostationary-orbit sounders will provide valuable datasets to constrain the diel emission cycle of NH_3, which is important to understand its contribution to $PM_{2.5}$ formation.

5.2.3 Accounting for Bias in CMAQ Model in 4D-Var inversion

The 4D-Var inversion assumes that the bias in CMAQ model processes are neglectable comparing to the bias in NH_3 emission estimates. The emission estimates optimization can be complicated by bias in important model processes influencing the budget and spatial-temporal distribution of atmospheric NH_3. Future works refining the pertinent processes, including gas-particle partitioning of NH_3, cloud and precipitation, and dry and wet deposition of NH_3 and NH_4^+, will help improve the 4D-Var inversion emission optimization.

Moreover, previous efforts have also been made to improve NH_3 emission and ambient concentration estimation by characterizing the bi-directional flux of NH_3 in chemical transport models. The surface exchange flux is found to be important to estimate NH_3 abundance and spatial distribution. When the bi-directional NH_3 flux model is incorporated

into the adjoint model of CMAQ, reapplying the optimization framework developed in this thesis may further improve the NH_3 emission estimates.

5.2.4 Process-based Bottom-up NH_3 emission inventory

While the inverse modeling optimization can help identify the time and location of the emissions bias, it cannot distinguish which sources are contributing to the bias. This thesis found that the largest uncertainty exists in springtime emission estimates. Due to the varying timing for fertilizer application, a comparison for March and May can help us better identify the specific source(s) of the bias in springtime NH_3 emission estimates. For regional and national scale bottom-up NH_3 emission inventory development, a combination of empirical and process-based approaches utilizing both new ground measurements at various conditions and conceptual first-principle processes would be the most promising. An improved emission inventory with detailed source information would best guide regulation strategy design for NH_3 emission control in the future.

5.2.5 Advancing modeling and measurement techniques to better understand the Nr deposition

In addition to the improvements in knowledge of the NH_3 sources, a better understanding of the sinks of NH_3 is essential to improve our estimates for the abundance, as well as the spatial and temporal distribution of NH_3 and its environmental impacts. The high uncertainties associated with Nr deposition estimates from simulations in this dissertation suggest there is much work to be done refining model simulations for processing affecting the Nr deposition. A range of model features contribute to the uncertainty and can be improved in the future in the support of new field and chamber studies. For one thing, the

speciated model evaluation of dry and wet Nr deposition presented in the thesis show that higher uncertainties exist in both dry and wet deposition than total deposition because they are partially cancelled out when adding up. The uncertainty can be improved with more detailed model treatment including deposition parameterization, advection and cloud processes, and sub-grid land-use related feature characterization. Such improvement can be better informed using a wide range of measurements at different meteorological conditions and over various vegetation and terrain surfaces. A better representation of cloud in the weather models, including cloud types, cloud properties, and spatial and temporal distribution of cloud, and a better representation of the scavenging process can also improve the estimation of wet deposition. For dry deposition, more measurements of throughfall and bulk deposition will also improve estimates, though this is hard to measure directly.

Another complication is that neither models nor existing monitoring networks well capture the atmospheric organic Nr deposition. Studies have found a significant contribution of organic Nr to total Nr deposition (Cape et al., 2011; Jickells et al., 2013). Future studies should update the chemical mechanisms to better represent organic Nr formations, reactions and depositions. A more complete atmospheric Nr budget estimate will benefit both CL estimation and CL exceedances assessment.

5.2.6 Model simulation of cloud acidity

This dissertation shows that a good estimate of the response of aerosol acidity to emission changes is the key factor to understand the response of aerosol mass concentration and chemical composition. In addition to aerosol acidity, cloud acidity warrants further studies

in the future because it is found to play a more important role in determining the SO_4^{2-} production rate in cloud (Paulot et al., 2017; Pye et al., 2020). As a result of increased NH_3 emissions and reduced SO_2 emissions, the cloud acidity decreases and facilitates the SO_4^{2-} production through the O_3 oxidation pathway, which in turn will influence the gas-particle partitioning and atmospheric life-time of NH_3 and HNO_3, and deposition of Nr (amount, speciation, and deposition). Further studies refining the representation of cloud acidity in models and sampling cloud acidity at different locations and conditions will improve our ability to understand the interaction between emission regulations and cloud acidity, and its impact on air quality and ecosystem protection.

In summary, the first section (chapter 2 and 3) of the thesis evaluates the environmental impacts of rising agricultural NH_3 emissions among co-occurring emissions and climatological changes, through model simulations. By identifying regions where the agricultural NH_3 emission increase would raise aerosol formation and/or ecosystem Nr burden, this thesis provides valuable information to help guide regulation priorities for NH_3 emission regulation in the U.S. Recognizing the high uncertainty in inventoried NH_3 emission, the second section of the thesis (chapter 4) optimizes the NH_3 emission estimates in NEI with satellite observations. The results demonstrate the influence of NH_3 emission uncertainties and bias on model-based environmental impact assessments and the capability of inverse modeling to constrain bottom-up NH_3 emission inventories. The research presented in this thesis is only preliminary but helps guide priorities for future mitigations and studies, and the importance to regulate NH_3 emissions together with other conventional pollutants is evident.

APPENDIX A. SUPPLEMENTAL MATERIAL FOR CHAPTER 2

Table A-1 Sectoral adjustment factors for each species from 2011 to 2050 based on the RCP4.5 pathway

	international shipping	mobile sources	residential and commercial use	power plants	industry	solvents
NO_x	1.1	0.20	0.69	0.26	0.50	1.0
SO_2	0.64	0.50	0.62	0.08	0.44	1.0
NH_3	1.0	0.60	0.67	0.47	0.77	1.0
CO	1.1	0.12	0.32	0.80	0.39	0.39
CH_4	1.7	0.52	0.72	1.1	0.93	1.0
VOC	1.3	0.31	0.52	1.8	0.59	0.62
EC	1.3	0.67	0.41	0.50	0.32	1.0
OC	1.3	0.53	0.57	0.42	0.45	1.0
other PM	1.3	0.62	0.54	0.42	0.38	1.0

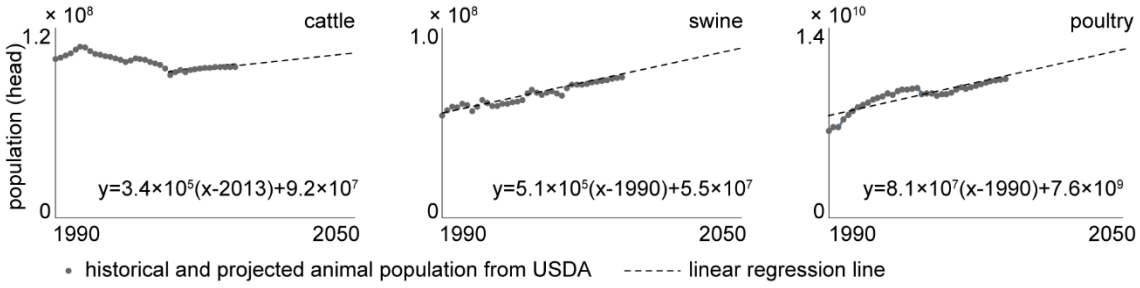

Figure A-1 Animal-specific population regressions for cattle, swine, and poultry production. Statistics data points from USDA (grey dots) (USDA 2018b) and the linear regression line (dashed line) were plotted in the figure with the regression equations shown.

For swine and poultry, historical statistics and projection from 1990 to 2027 were used for regression. For cattle, the regression only included data from 2013 to 2027. Least squares regression was applied, and the results were used for extrapolation to 2050. The NH_3 emission from livestock waste management was projected based on the animal population grow, and emission factors for all related processes were assumed to be constant. The total NH_3 emission was estimated to be 2.06 (1.96 – 2.16 as 95% CI) million ton N per year in 2050, when the uncertainties of animal population projections are considered. The linear extrapolation into the future represent a conservative scenario in which the NH_3 emission will be continuously pushed up by an increase in meat consumption and no further regulations are implemented to lower the NH_3 emission factors.

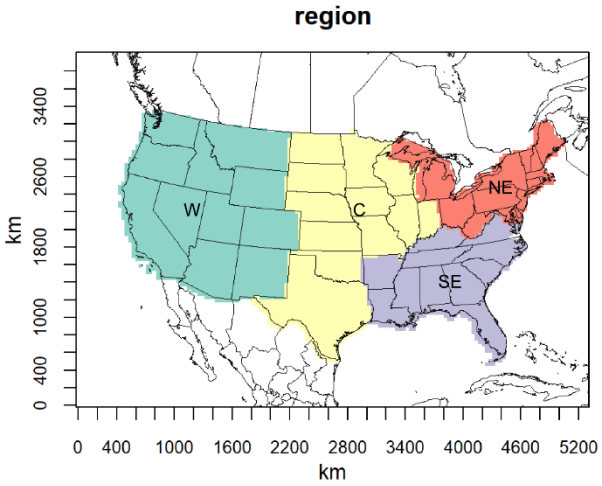

Figure A-2 Definition of the four regions in the CONUS. The northeastern (NE), southeastern (SE), central (C) and western (W) US are color-coded by red, purple, yellow, and green, respectively.

The difference in temporal average pHs using different ways of averaging

We compared the annual average aerosol pH results using two averaging approaches. The first approach (adopted in this study) averages the hourly H^+ activities and LWCs and then calculates the daily aerosol pH from daily average H^+ activities and LWCs; the second approach calculates pH from hourly H^+ activities and LWCs directly. The pH values calculated by the first approach are lower than the second approach because the first approach gives more weight to hours with high H^+ activities while the second approach will give more weight to the hours with high pH (low acidity). For most areas, the absolute difference in annual average pH values calculated using the two approaches is less than 0.4 unit. However, the difference will yield one above when the diel change of aerosol acidity is very large. Although there is no right or wrong between the two, the first approach is more compatible to the calculation using gases and speciated particle concentrations from filter-based measurements which report concentration values averaged over one or several days. In addition, averaging H^+ activities and LWCs reduces the occurrence of extreme cases when H^+ activities or LWCs approach zero.

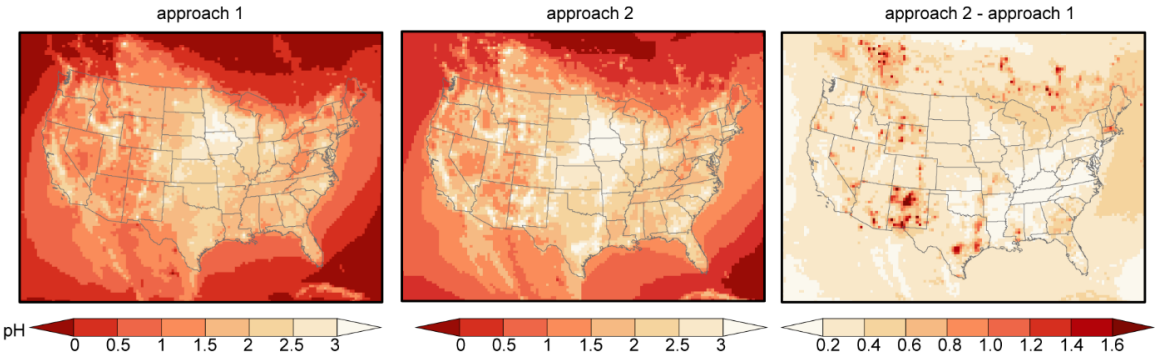

Figure A-3 Spatial distribution of annual average aerosol pH in the future baseline scenario using two averaging approaches. The first approach calculates pH based on daily average H^+ activities in the particle water (left). The second approach averages hourly pH values (middle). The absolute difference (pH calculated using the second approach minus the first approach) is shown on the right.

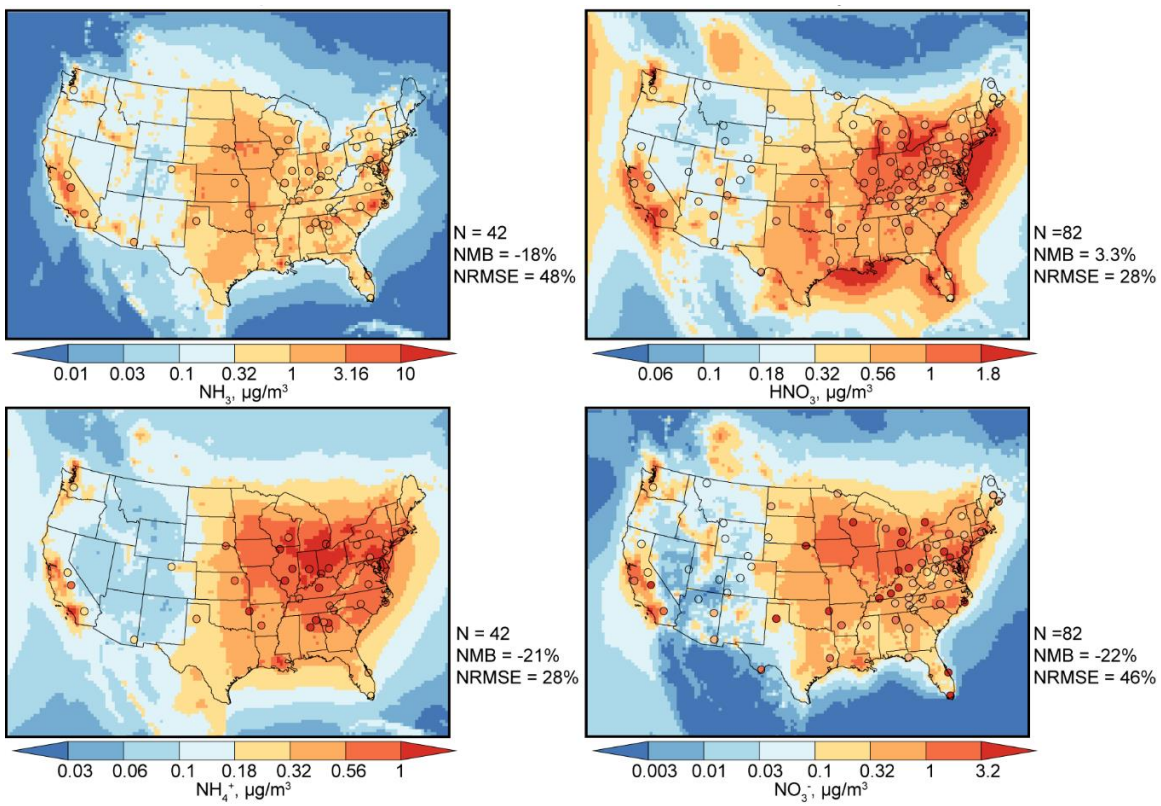

Figure A-4 Overlay of simulated (color map) and observed (colored dots) annual mean surface concentrations of NH_3, NH_4^+, HNO_3, and NO_3^-. The number of monitoring sites (N), NBM and NRMSE are provided along the figures.

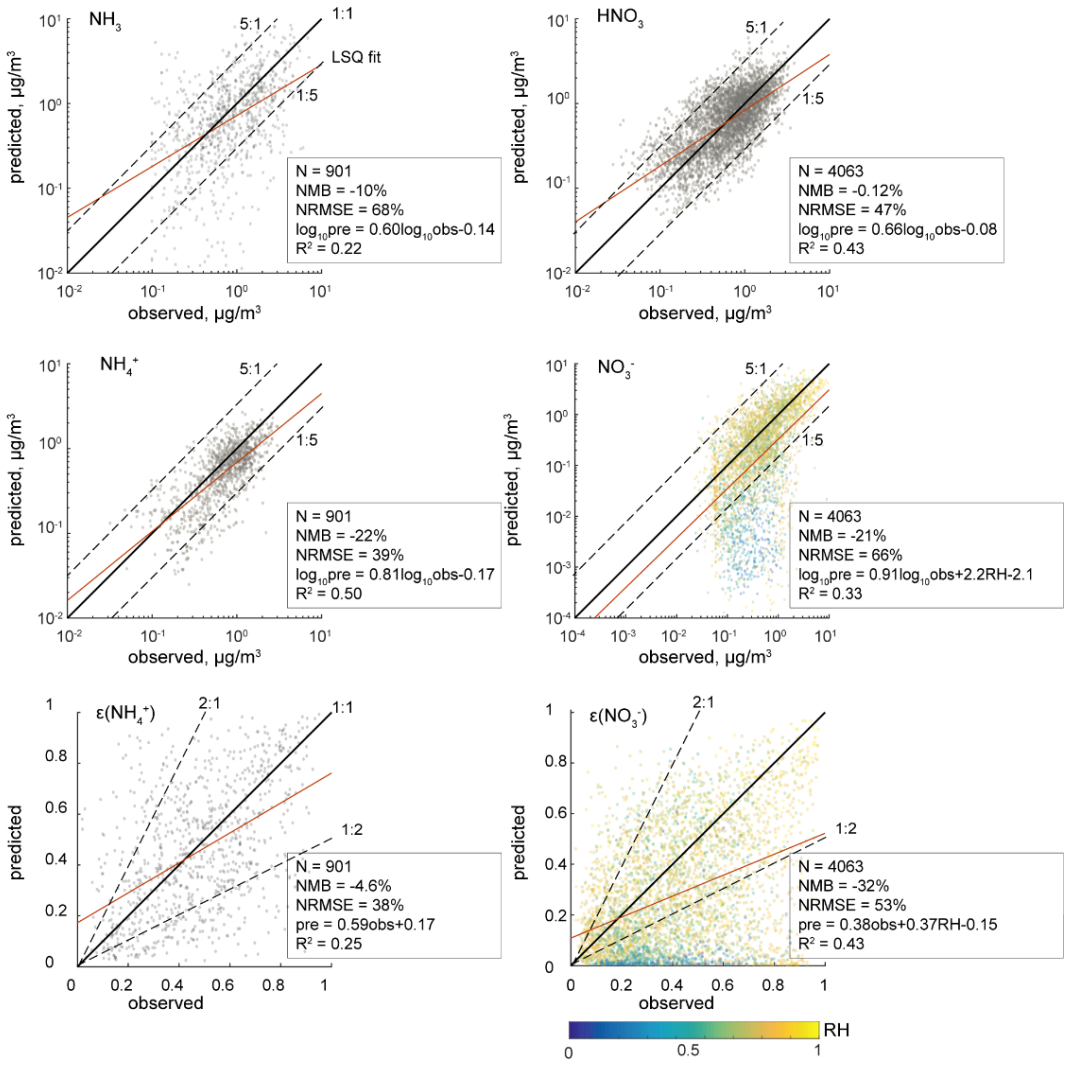

Figure A-5 Simulated and observed average surface concentrations of NH_3, NH_4^+, HNO_3 and NO_3^-, as well as the gas-particle partitioning ratios, $\varepsilon(NH_4^+)$ and $\varepsilon(NO_3^-)$. Biweekly averages and weekly averages were compared for NH_3 - NH_4^+ and HNO_3 - NO_3^-, respectively. The 1:1 line (solid black line), data range line (dashed back line with ratio labeled) and regression line (red) is also plotted. Number of data points (N), NMB, NRMSE, regression equation and adjusted R square are provided along each plot. Dots in NO_3^- and $\varepsilon(NO_3^-)$ plot are colored based on the RH (fractional scale used) calculated from WRF reanalysis meteorology fields for each grid.

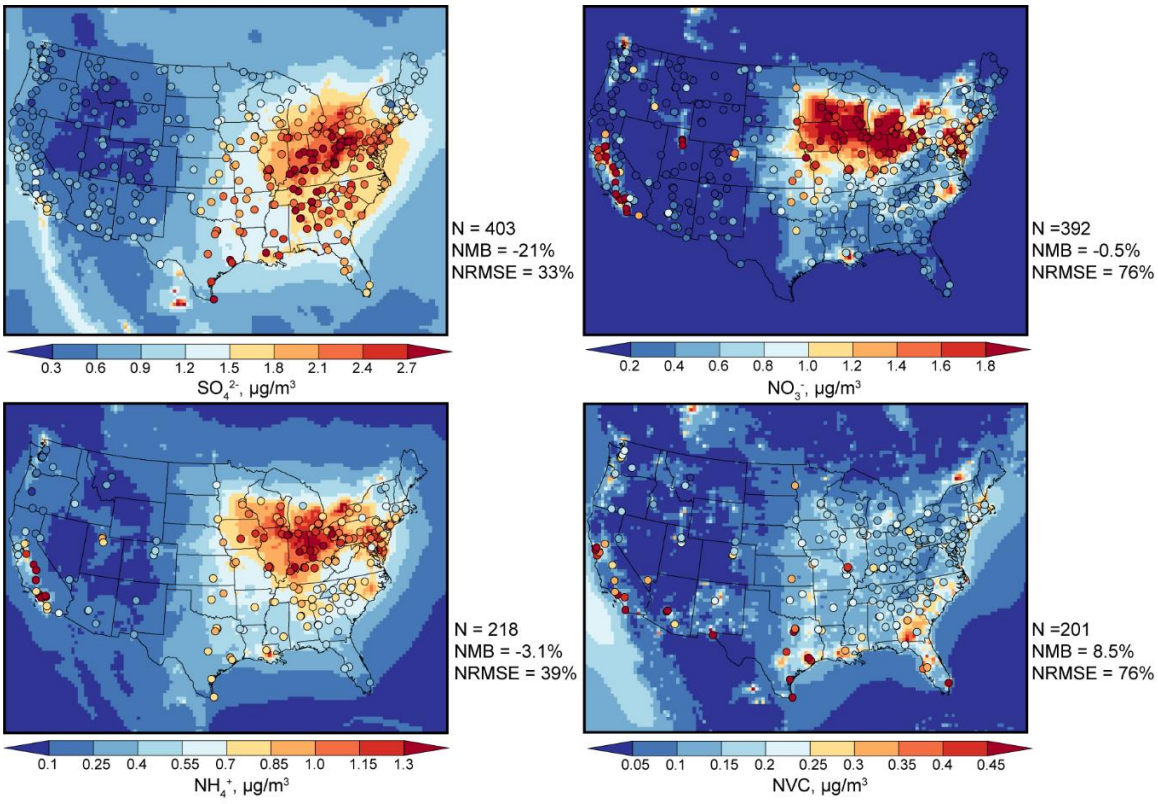

Figure A-6 Overlay of simulated (color map) and observed (colored dots) annual mean surface concentrations of SO_4^{2-}, NO_3^-, NH_4^+, and NVC over the study domain. The number of monitoring sites (N), NBM and NRMSE are provided along the figures.

Model evaluation using daily simulated and observed speciated fine PM

The scatter plots show a general agreement between simulated and observed daily average concentrations of NH_4^+ and SO_4^{2-}, with better agreement at the high concentration end and more variation at the low concentration end. Similar to the comparison of simulated values to the Clean Air Status and Trends Network (CASTNET) measurements, the simulated concentrations of NO_3^- is biased low when the relative humidity (RH) is low. For non-volatile cations, the CMAQ simulated values are biased low for most of the data with a normalized mean bias of -88%. The comparison results again show that predicting aerosol pH with CMAQ is more challenging in areas with high impact from NVCs and/or low RH and pollutant concentrations.

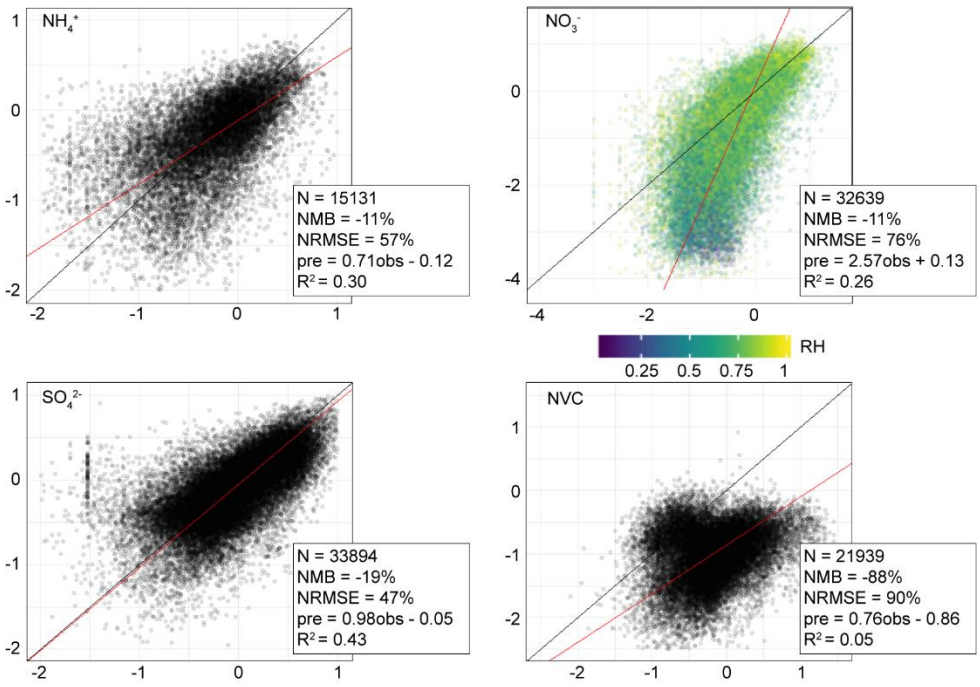

Figure A-7 Simulated and observed daily average surface concentrations of NH_4^+, NO_3^-, SO_4^{2-}, and non-volatile cations (NVC). The 1:1 line (black) and regression line (red) is also plotted. Number of data points (N), NMB, NRMSE, regression equation and adjusted R square are provided along each plot. Dots in the NO_3^- plot are colored based on the RH (fractional scale used) calculated from WRF reanalysis meteorology fields for each grid.

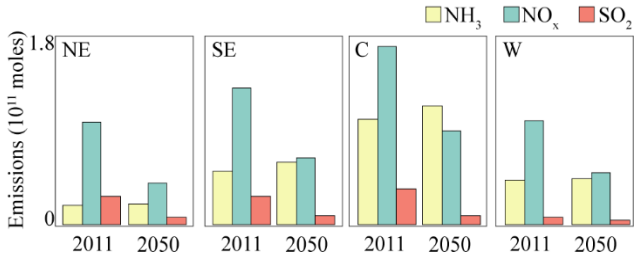

Figure A-8 Comparison of NH_3, SO_2, NO_x emission equivalents (in mole units) in the northeastern (NE), southeastern (SE), central (C), and the western US between the year 2011 and year 2050.

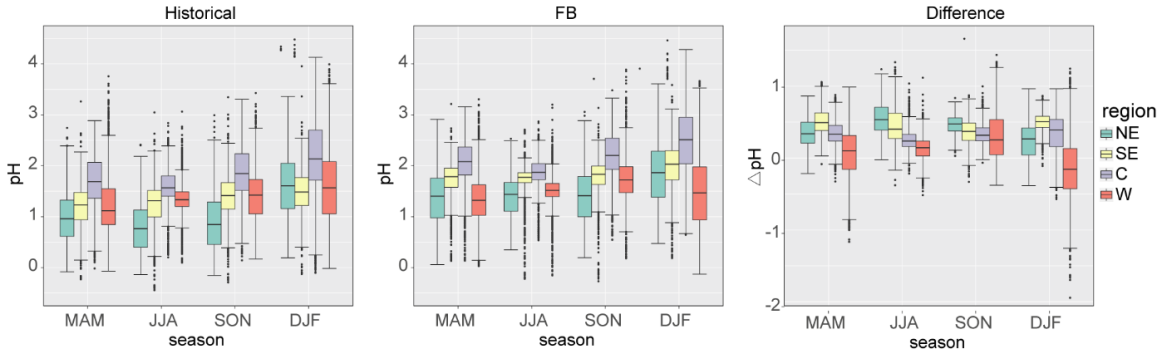

Figure A-9 Comparison between change of seasonal average aerosol pH for northeastern (NE), southeastern (SE), central (C) and western (W) US in 2011 (left) and 2050 (middle), as well as their differences (right). March, April, and May (MAM) are defined as spring. June, July, and August (JJA) are defined as summer. September, October, and November (SON) are defined as autumn. December, January, and February (DJF) are defined as winter.

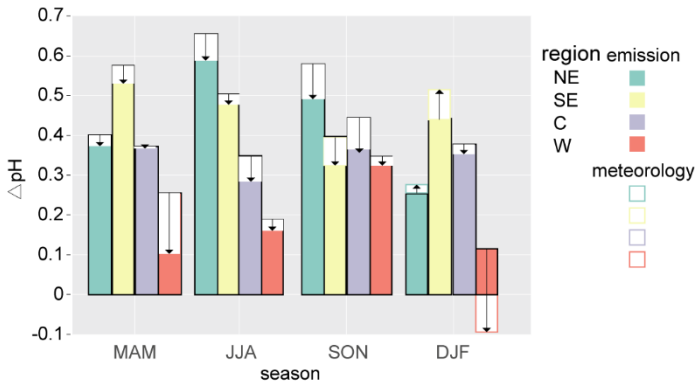

Figure A-10 The impact of emission and meteorology changes on aerosol pH by region and season. The arrow indicates the direction of pH change in response to meteorology changes.

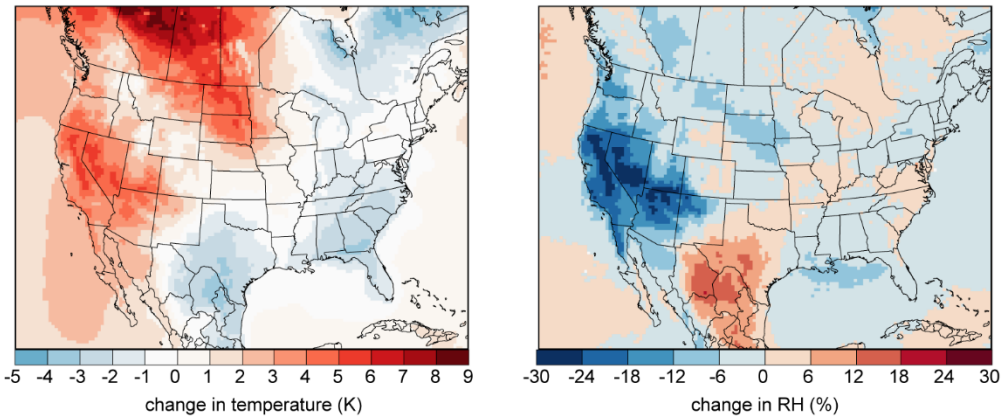

Figure A-11 Changes in the winter (January, February, and December) average daily surface air temperature (left) and relative humidity (right) between the historical and future scenarios.

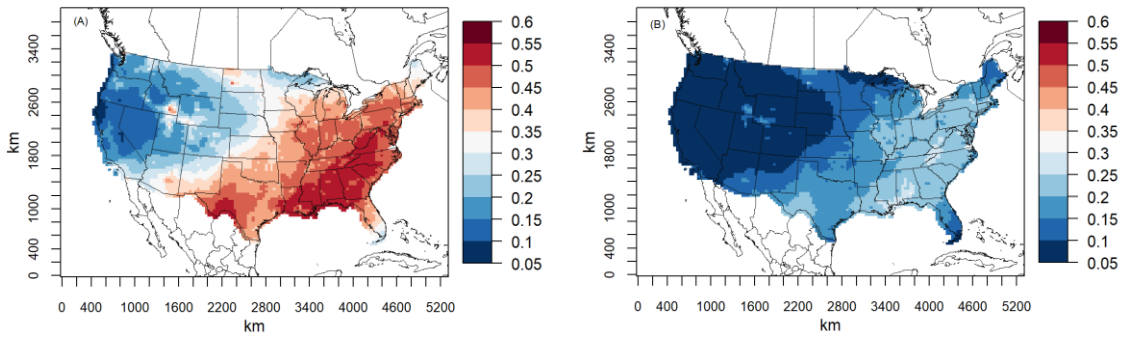

Figure A-12 The sensitivity of SO_4^{2-} concentration to SO_2 emission reduction. The sensitivity is defined as the normalized SO_4^{2-} concentration change in response to SO_2 emission reduction. Figure (A) and (B) are defined as $\frac{([SO_4^{2-}]_{FS1}-[SO_4^{2-}]_{FB})/[SO_4^{2-}]_{FB}}{(E_{SO_2\,FS1}-E_{SO_2\,FB})/E_{SO_2\,FB}}$ and $\frac{([SO_4^{2-}]_{FS2}-[SO_4^{2-}]_{FS1})/[SO_4^{2-}]_{FS1}}{(E_{SO_2\,FS2}-E_{SO_2\,FS1})/E_{SO_2\,FS1}}$, respectively.

Sensitivity test for boundary conditions

Six one-month simulations with 10-day spin-ups were conducted by cutting the SO_2 and SO_4^{2-} concentrations in the boundary condition by 50%. All other inputs were kept identical with the base cases, including historical, future baseline (FB), and future sensitivity scenario 2 (FS2), in June and December, respectively. The differences in the monthly average aerosol pH were taken by subtracting the pH values from the corresponding base cases from the pH values from the sensitivity simulations. The pH changes depicted in **Figure A-13** indicate the magnitudes of contributions from the boundary conditions.

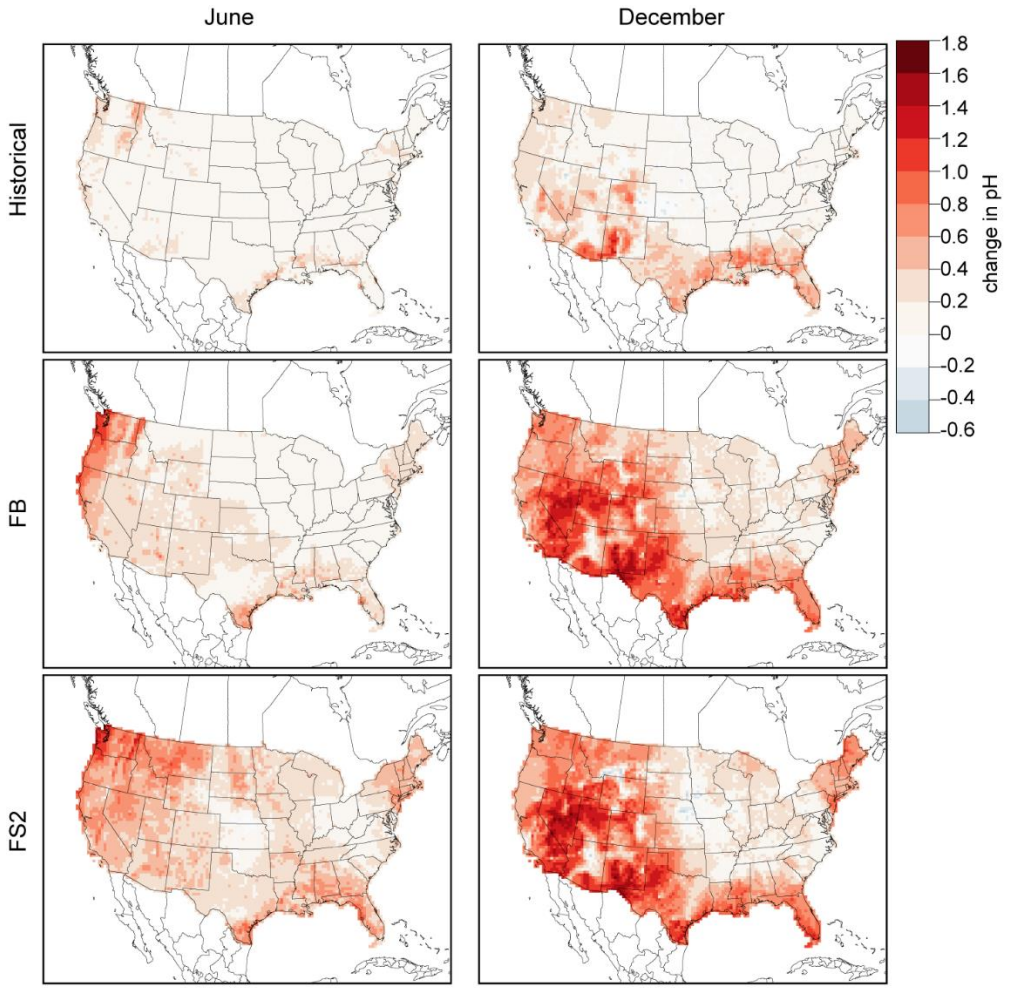

Figure A-13 Sensitivity of aerosol pH to the SO2 and SO42- concentrations from the boundary condition. The maps show the difference in monthly average aerosol pH in June (left column) and December (right column) between the sensitivity tests and the corresponding reference cases, including the historical, FB, and FS2 scenarios. Changes are calculated as the values in the sensitivity test minus the values in the reference case.

A one-month simulations with 10-day spin-ups was conducted assuming only ammonium sulfate exist at the boundary and the molar concentration is the twice as much as sulfate concentration in the CMAQ default boundary condition. All other inputs were kept identical with the future baseline scenario (FB)in June. The differences in the monthly average aerosol pH between the sensitivity test case and FB are shown in **Figure A-14**. Although the difference in the monthly average aerosol pH is over 1 unit around the boundary, the difference within the CONUS is generally under 0.2 unit.

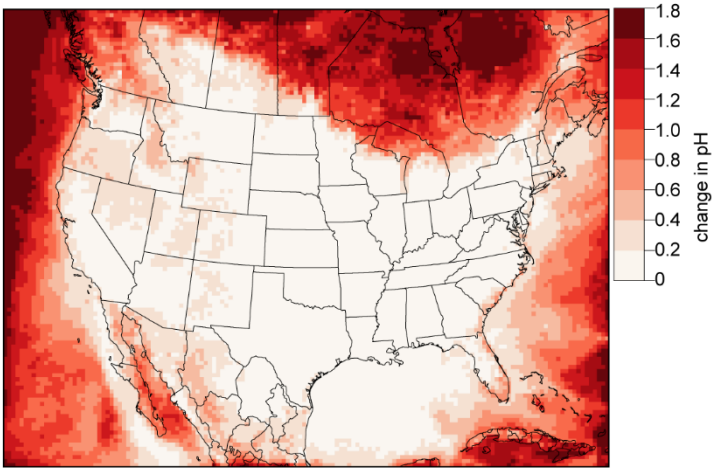

Figure A-14 Sensitivity test of aerosol pH to the cations from the boundary condition. The maps show the difference in monthly average aerosol pH in June between the sensitivity test cases and the future baseline scenario.

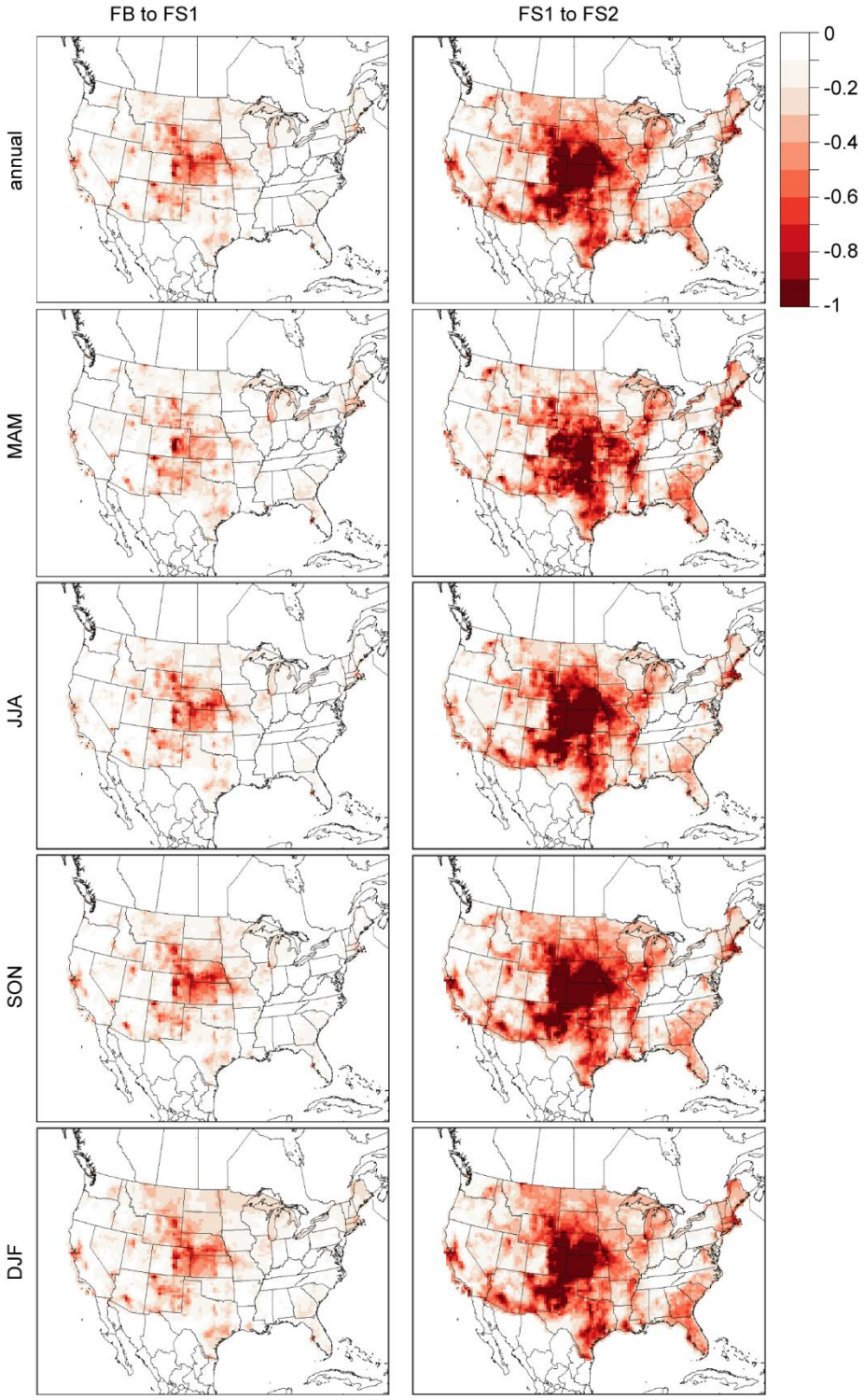

Figure A-15 The yearly and seasonal sensitivity of NO_3^- mass concentration change to SO_4^{2-} mass concentration change. Sensitivities in the left column and right column are defined as $\frac{([NO_3^-]_{FS1}-[NO_3^-]_{FB})/[NO_3^-]_{FB}}{([SO_4^{2-}]_{FS1}-[SO_4^{2-}]_{FB})/[SO_4^{2-}]_{FB}}$ and $\frac{([NO_3^-]_{FS1}-[NO_3^-]_{FB})/[NO_3^-]_{FB}}{([SO_4^{2-}]_{FS1}-[SO_4^{2-}]_{FB})/[SO_4^{2-}]_{FB}}$, respectively.

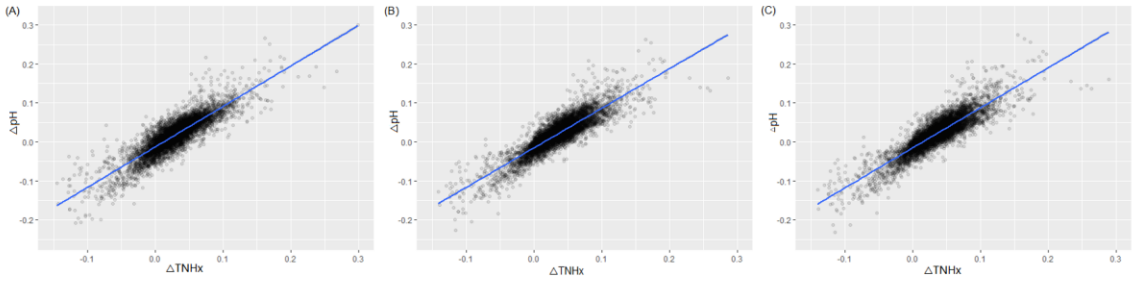

Figure A-16 The linear regression of annual averaged pH difference (ΔpH) and TNHx concentration difference(ΔTNHx, in log scale) between current and future NH3 emission scenarios. Figure (A), (B), and (C) shows the relationship based on FB (A), FS1 (B), and FS2 (C).

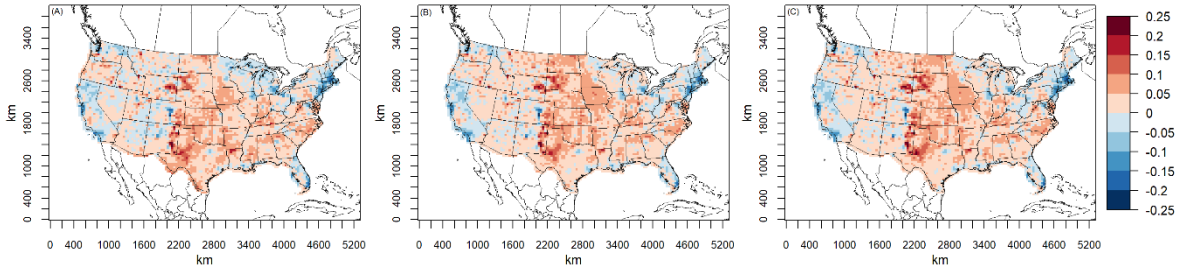

Figure A-17 The annual averaged particle pH difference attributable to NH_3 emission change between current and future levels. Figure (A), (B), and (C) shows the difference based on FB, FS1, and FS2 scenarios.

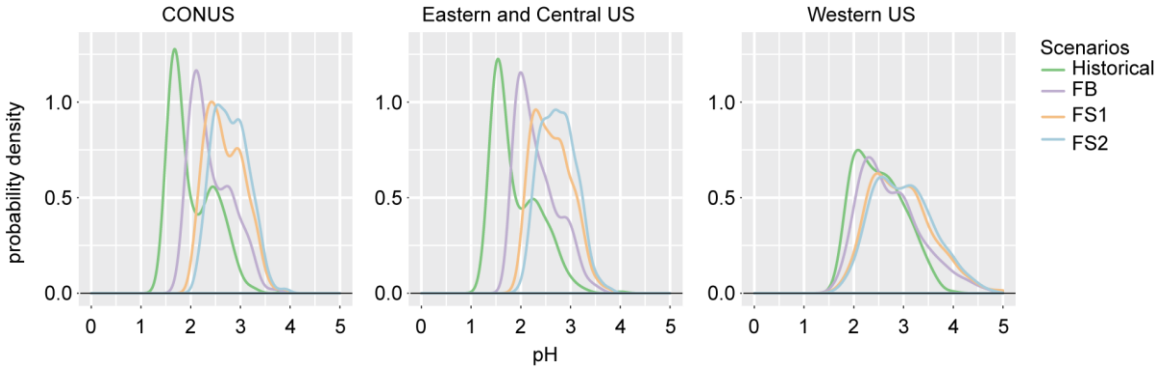

Figure A-18 The distribution of daily averaged particle pH under historical, FB, FS1 and FS2 scenarios for densely populated areas (grids with population over 0.1 million) over the CONUS, eastern and central US, and western US.

APPENDIX B. SUPPLEMENTAL MATERIAL FOR CHAPTER 3

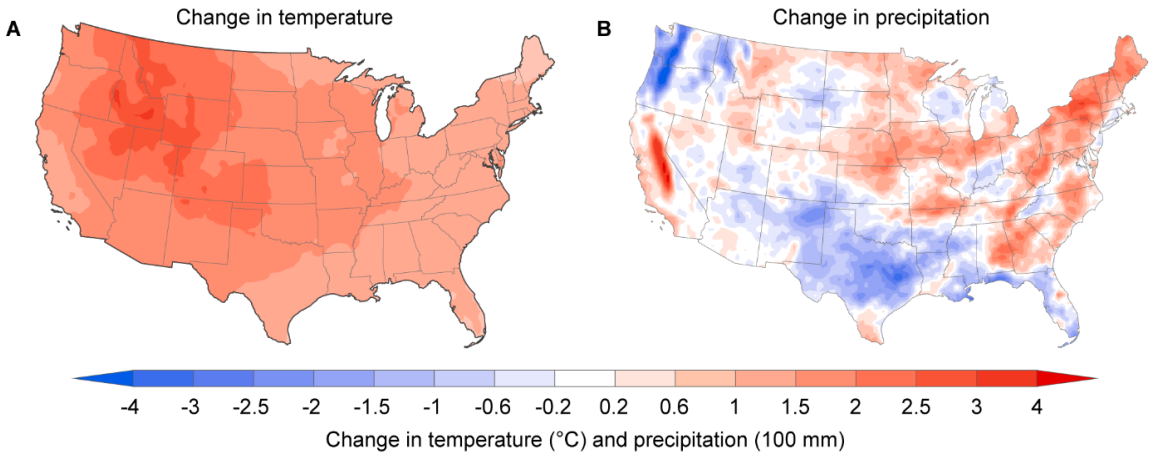

Figure B-1 The projected change in annual averaged temperature (A) and precipitation (B) between 2010 and 2050 under RCP $_{8.5}$.

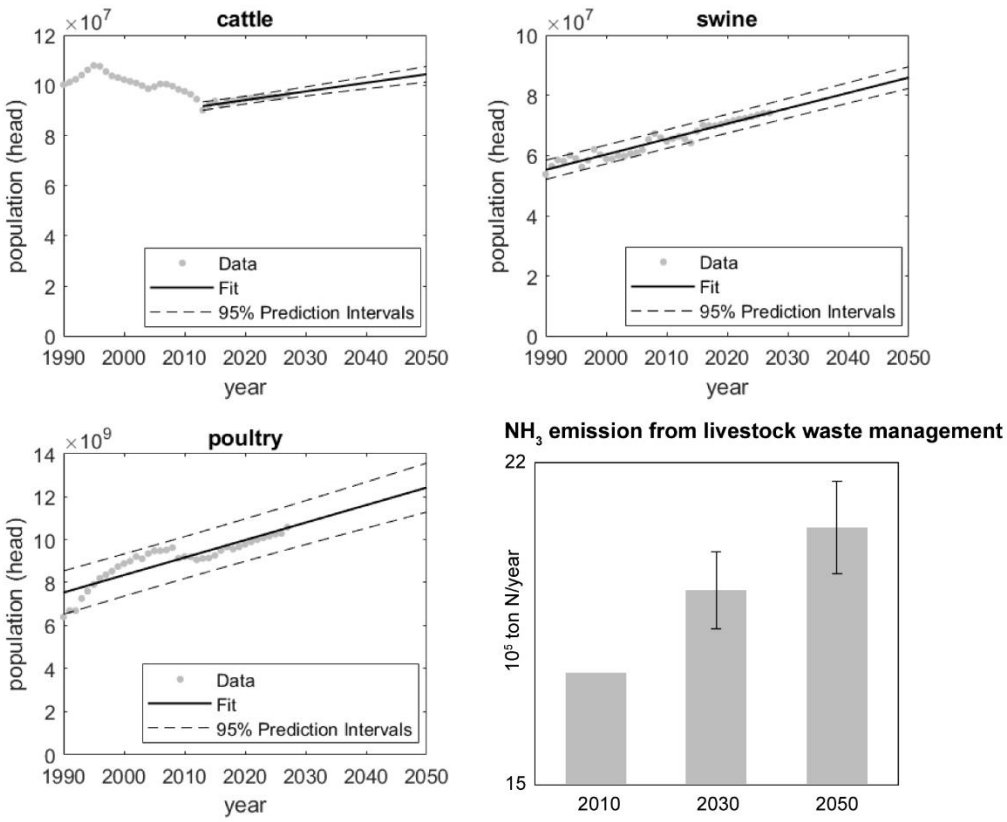

Figure B-2 Animal-specific population regressions for cattle, swine, and poultry production and projected NH_3 emissions from livestock waste management. The projected 95% confidence interval of NH_3 emission due to the uncertainty of animal population projections is shown as error bars.

Animal-specific population regressions were performed for cattle, swine, and poultry production using historical and future livestock projection statistics from U.S. Department of Agriculture (*USDA*, 2018a; b). For swine and poultry, historical statistics and projection from 1990 to 2027 were used for regression. For cattle, the regression only included data from 2013 to 2027. Least squares regression was applied, and the results were used for extrapolation to 2030 and 2050. The NH_3 emission from livestock waste management was projected based on the animal population grow, and emission factors for all related processes were assumed to be constant. The total NH_3 emission was estimated to be 1.92

(1.84 – 2.00 as 95% CI) and 2.06 (1.96 – 2.16) million ton N per year in 2030 and 2050, respectively, when the uncertainties of animal population projections are considered.

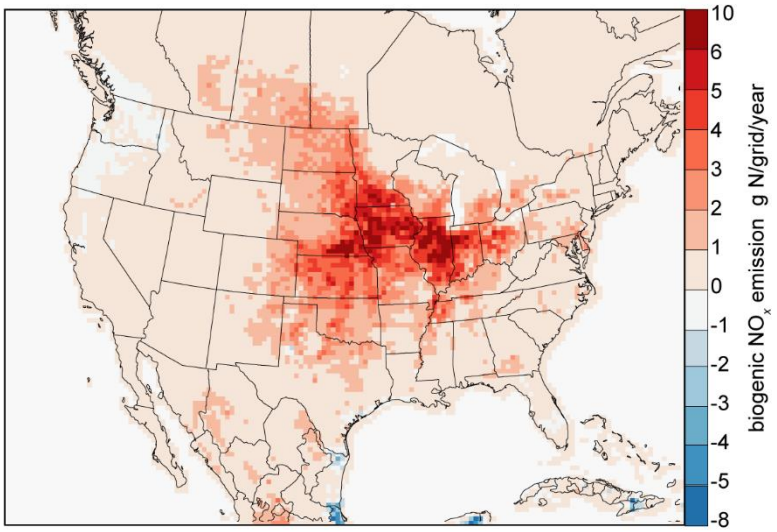

Figure B-3 Changes in biogenic NO_x emissions between 2010 and 2050.

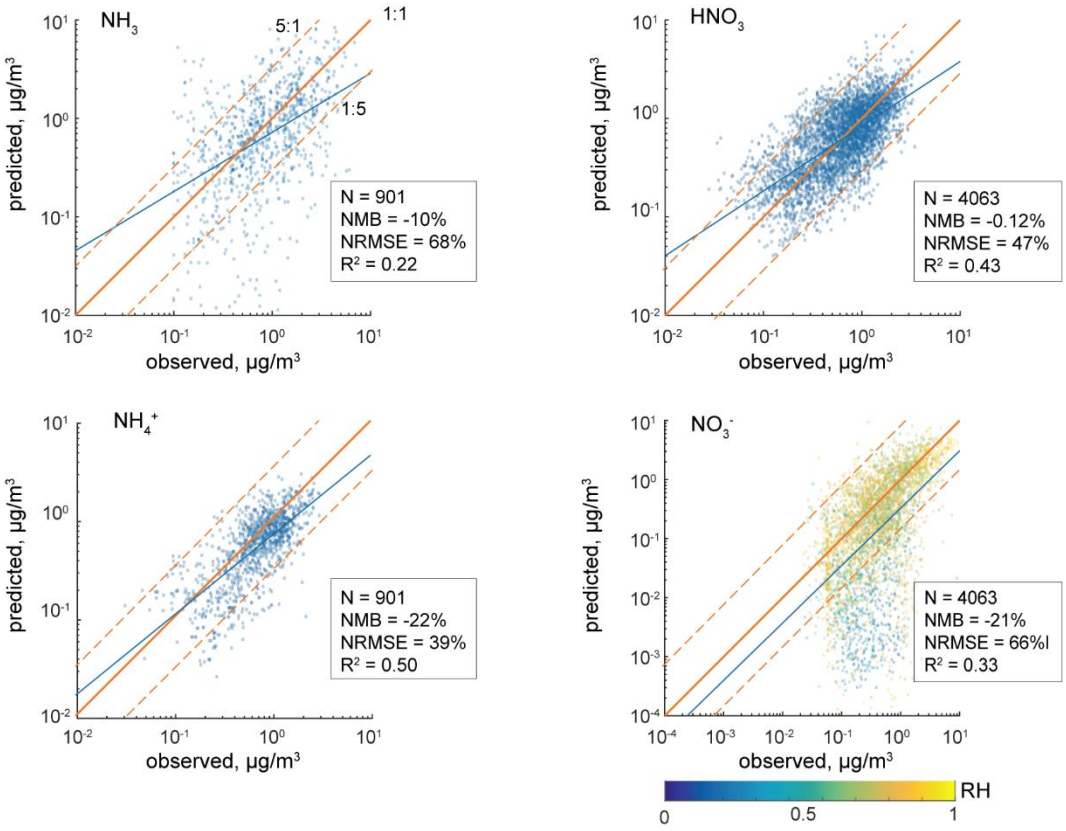

Figure B-4 Model evaluation for CMAQ simulated HNO_3, NH_3, NO_3^- and NH_4^+ concentrations against observations from the Clean Air Status and Trends Network (CASTNET). The scatter plots show the comparison between CMAQ predicted and observed biweekly means, with the blue line showing the linear regression line. A solid orange line represents the 1:1 ratio line. 500% ranges are shown in dashed lines in each plot. Normalized mean bias (NMB) and normalized residue mean square error (NRMSE) of the predicted depositions against the observed values is also provided for each plot.

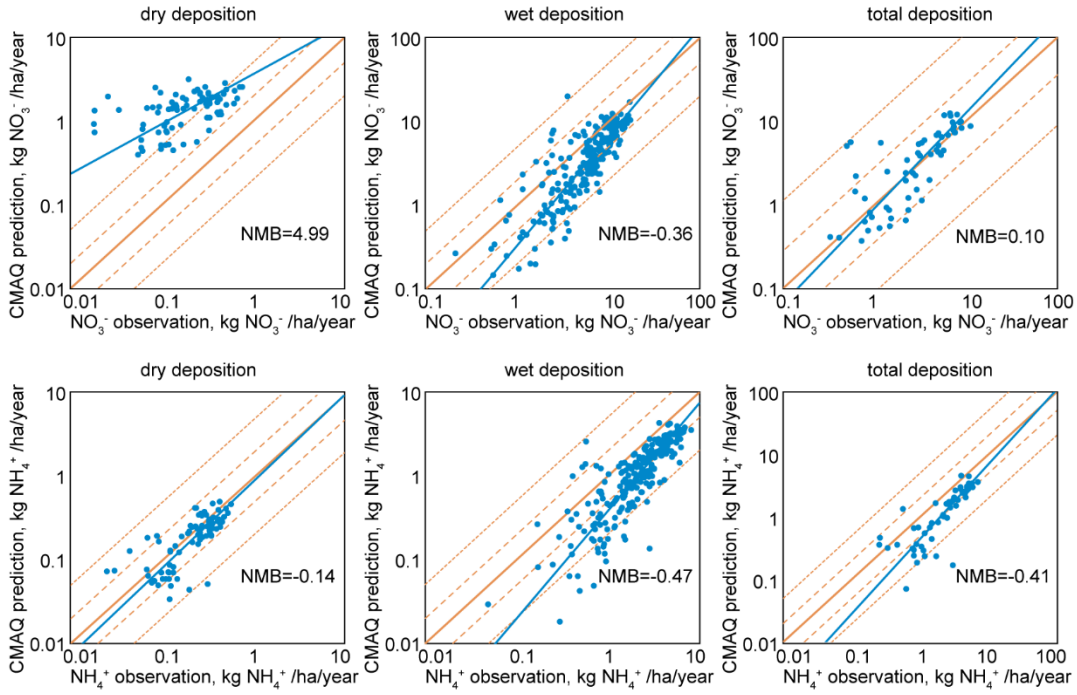

Figure B-5 Model evaluation for CMAQ simulated NO_3^- and NH_4^+ deposition against observations from the National Atmospheric Deposition Program (NADP) and the Clean Air Status and Trends Network (CASTNET). The scatter plots show the comparison between CMAQ predicted and observed annual dry, wet, and total deposition amounts, with the blue line showing the linear regression line. A solid orange line represents the 1:1 ratio line. 200% and 500% ranges are shown in dashed lines in each plot. Normalized mean bias (NMB) of the predicted depositions against the observed values is also provided for each plot.

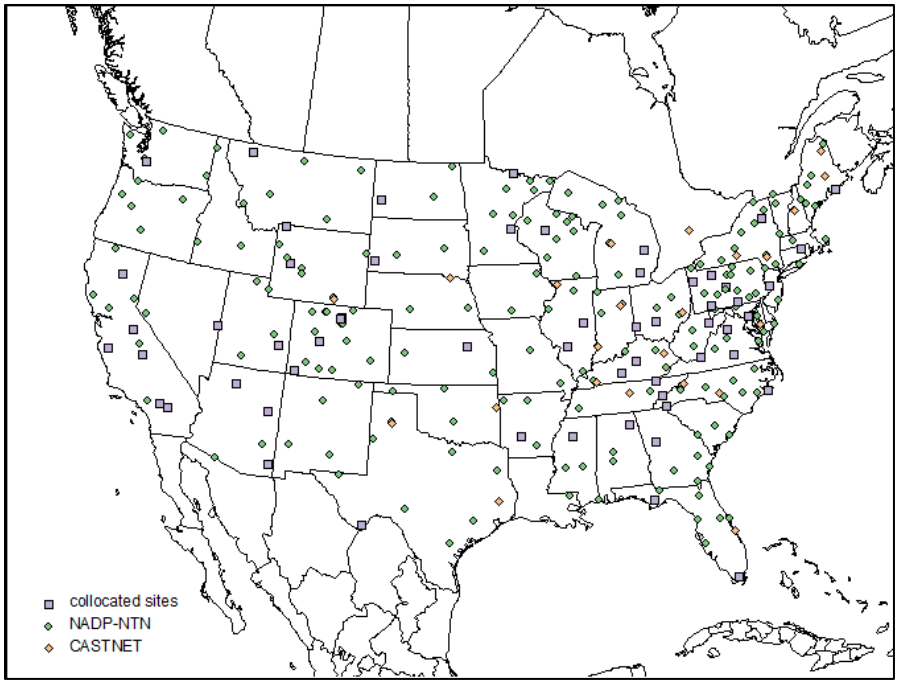

Figure B-6 The location of the sites in National Atmospheric Deposition Program-National Trends Network (NADP-NTN in green circles), Clean Air Status and Trends Network (CASTNET in yellow diamonds), and their collocated sites (in purple squares).

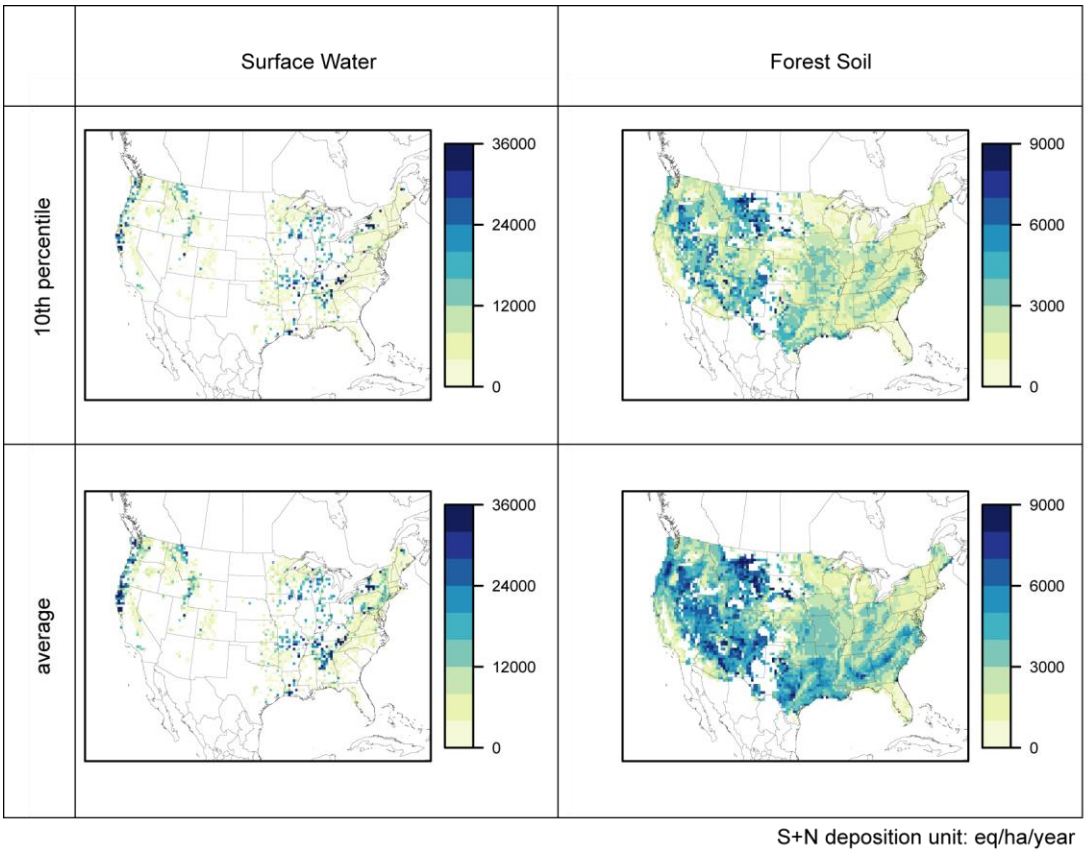

Figure B-7 The surface water and forest soil critical load for acidity. 10th percentile and average aggregation for 36 km by 36 km grids with sulfur and nitrogen depositions are shown in the top and bottom panels, respectively.

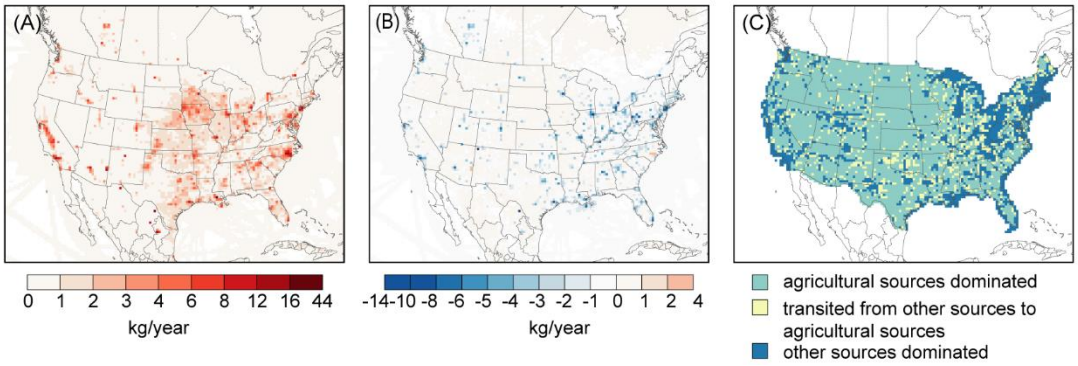

Figure B-8 The spatial distribution of total Nr emissions in 2050 (A) and the emissions change between 2010 and 2050 (B). The transition of dominating emission sources category in each grid between 2010 and 2050 (C) is color coded with green representing grids by agricultural sources in both 2010 and 2050, blue representing grids dominated by other sources, and yellow representing grids that will transit from other sources dominated to agricultural sources dominated.

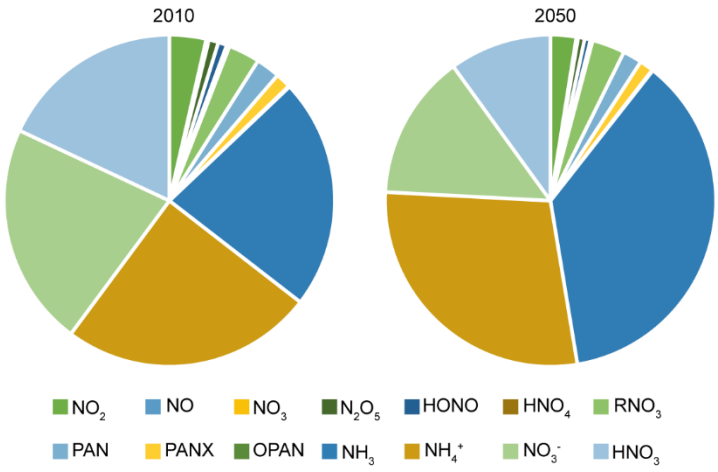

Figure B-9 Changes in the speciation profile of Nr deposition between "present-day" and "Ag_projected" scenarios.

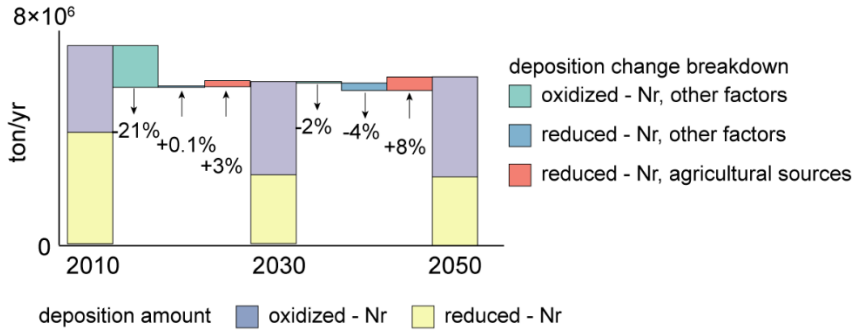

Figure B-10 Projected changes in total deposition of Nr over the CONUS from 2010 to 2050 (stacked bars). The changes attributed to agricultural sources and other factors including emission changes in other sources and meteorological conditions are also displayed.

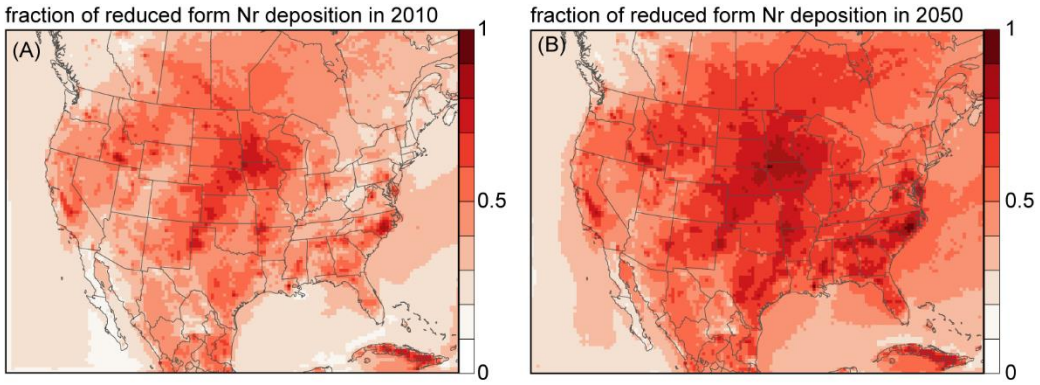

Figure B-11 Changes in the fraction of reduced form Nr deposition between "present-day" and "Ag_projected" scenarios.

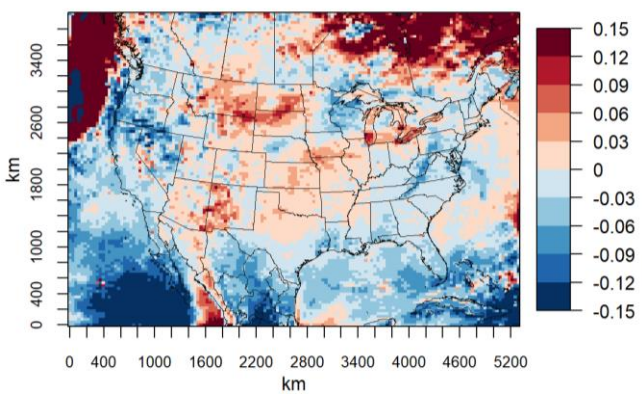

Figure B-12 The sensitivity of total Nr deposition (dep_{Nr}) change to sulfate mass concentration ($[SO_4^{2-}]$) change. The normalized brute-force sensitivity is defined as $\frac{(dep_{Nr_{FS}} - dep_{Nr_{FB}})/dep_{Nr_{FB}}}{([SO_4^{2-}]_{FS} - [SO_4^{2-}]_{FS})/[SO_4^{2-}]_{FB}}$, where FS and FB are future sensitivity and future baseline scenarios, respectively.

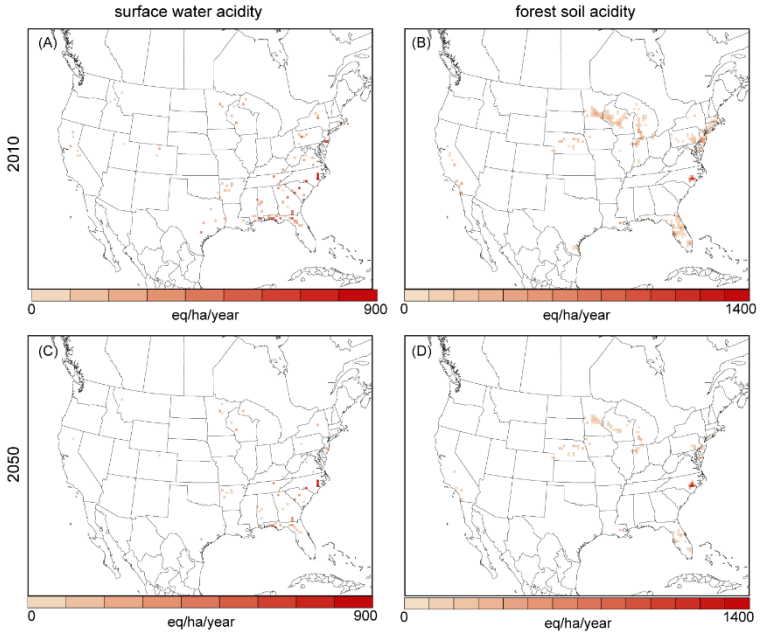

Figure B-13 Sulfur and nitrogen (S+N) deposition exceedance for surface water acidity and forest soil acidity. Map A to D shows the grids and amount of exceedance above the average CL values in "present-day" and "Ag_projected" scenarios.

APPENDIX C. SUPPLEMENTAL MATERIAL FOR CHAPTER 4

Correlation between CMAQ simulated NH_3 column density to NH_3 concentrations at different vertical layers is evaluated to test the sensitivity of modeled NH_3 column densities to surface NH_3 and NH_3 at lower free troposphere. The results show that the modeled NH3 column densities are most sensitive to NH3 concentrations at around 700 to 850 hPa and the sensitivity drops rapidly beyond 585 hPa. For satellite instruments including TES and CrIS, the vertical sensitivities are also highest around 700-800 hPa and drops beyond ~600 hPa. Therefore, direct comparison between IASI observed and CMAQ simulated NH_3 column densities will not introduce significant errors due to differences in vertical sensitivities.

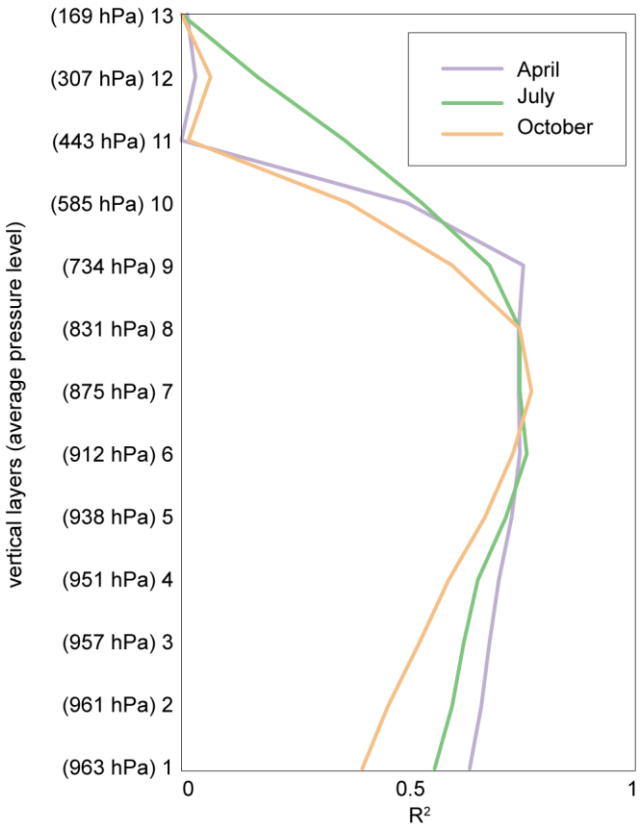

Figure C-1 The correlation between monthly average CMAQ simulated NH_3 column densities and NH_3 concentration at all 13 layers in April, July, and October. The grid cells with satellite observations are sampled at the IASI overpassing time. Monthly average NH_3 column densities and concentrations are calculated for each grid cell. R^2 for all data pairs in each month are calculated.

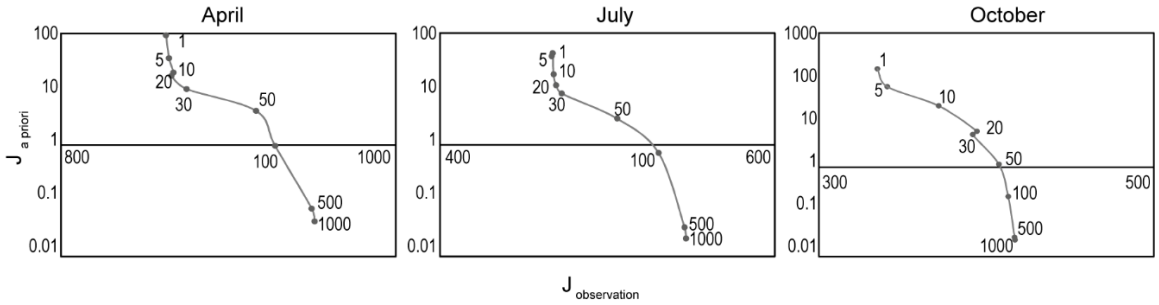

Figure C-2 The L-curve for regularization factor (γ) value selection for April, July, and October. The error weighted squared difference between emission scaling factor and the a priori values ($J_{a\ priori}$) is plotted against error weighted squared difference between IASI-NH_3 and simulated column density ($J_{observation}$) with different choices of γ values as denoted along the curve.

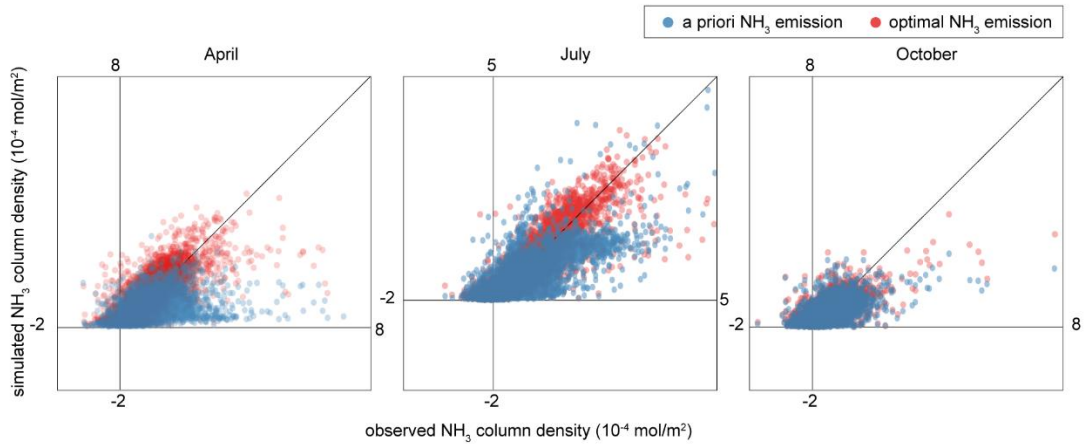

Figure C-3 Comparison between simulated NH_3 column density against the IASI-NH_3 observations in April, July, and October using a priori (blue dots) and optimized NH_3 emission estimates (red dots).

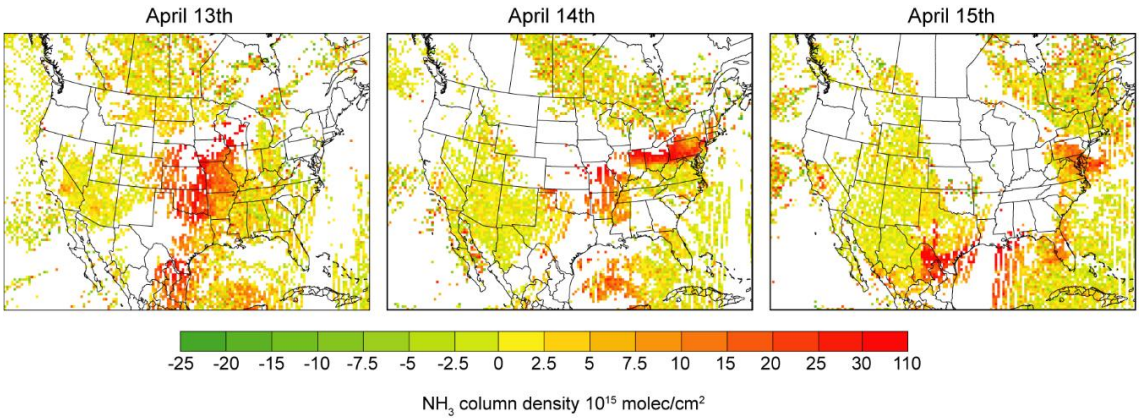

Figure C-4 IASI NH_3 column density in April 13th, 14th, and 15th at 36 m by 36 km resolution within the model simulation domain of this study.

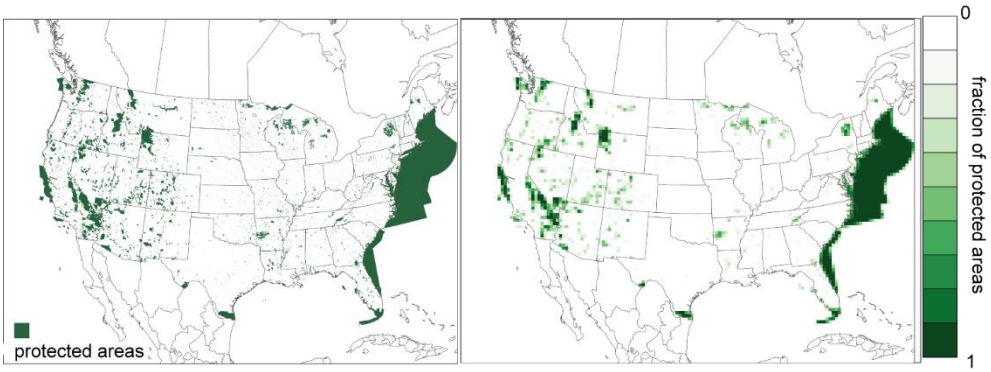

Figure C-5 Protected areas for biodiversity conservation defined by the U.S. Geological Survey (USGS) Gap Analysis Project (A). And fraction of protected areas in each 36 km by 36 km simulated grids in this study (B).

REFERENCES

Alexander, R.B., Smith, R.A., Schwarz, G.E., Boyer, E.W., Nolan, J.V., Brakebill, J.W., 2008. Differences in phosphorus and nitrogen delivery to the gulf of Mexico from the Mississippi river basin. Environ. Sci. Technol. 42, 822-830.

Almaraz, M., E. Bai, C. Wang, J. Trousdell, S. Conley, I. Faloona, and B. Z. Houlton, 2018. Agriculture is a major source of NO_x pollution in California, Sci. Adv., 4(1), doi: 10.1126/sciadv.aao3477

Appel, K.W., Chemel, C., Roselle, S.J., Francis, X.V., Hu, R.M., Sokhi, R.S., et al., 2012. Examination of the Community Multiscale Air Quality (CMAQ) model performance over the North American and European domains. Atmos. Environ. 53, 142-155.

Appel, K.W., Foley, K.M., Bash, J.O., Pinder, R.W., Dennis, R.L., Allen, D.J., et al., 2011. A multi-resolution assessment of the Community Multiscale Air Quality (CMAQ) model v4.7 wet deposition estimates for 2002-2006. Geosci. Model Dev. 4, 357-371.

Appel, K.W., Pouliot, G.A., Simon, H., Sarwar, G., Pye, H.O.T., Napelenok, S.L., et al., 2013. Evaluation of dust and trace metal estimates from the Community Multiscale Air Quality (CMAQ) model version 5.0. Geosci. Model Dev. 6, 883-899.

Baron, J.S., Driscoll, C.T., Stoddard, J.L., Richer, E.E., 2011. Empirical Critical Loads of Atmospheric Nitrogen Deposition for Nutrient Enrichment and Acidification of Sensitive US Lakes. Bioscience. 61, 602-613.

Bash, J.O., Cooter, E.J., Dennis, R.L., Walker, J.T., Pleim, J.E., 2013. Evaluation of a regional air-quality model with bidirectional NH_3 exchange coupled to an agroecosystem model. Biogeosciences. 10, 1635-1645.

Battaglia, M.A., Douglas, S., Hennigan, C.J., 2017. Effect of the Urban Heat Island on Aerosol pH. Environ. Sci. Technol. 51, 13095-13103.

Battye, W., Aneja, V.P., Roelle, P.A., 2003. Evaluation and improvement of ammonia emissions inventories. Atmos. Environ. 37, 3873-3883.

Battye, W., Aneja, V.P., Schlesinger, W.H., 2017. Is nitrogen the next carbon? Earth's Future. 5, 894-904.

Bettez, N.D., Groffman, P.M., 2013. Nitrogen deposition in and near an urban ecosystem. Environ. Sci. Technol. 47, 6047-6051.

Bobbink, R., Hicks, W.K. Factors Affecting Nitrogen Deposition Impacts on Biodiversity: An Overview. in: Sutton M.A., Mason K.E., Sheppard L.J., Sverdrup H., Haeuber

R., Hicks W.K., eds. Nitrogen Deposition, Critical Loads and Biodiversity. Dordrecht: Springer Netherlands; 2014

Brasseur, G.P., Jacob, D.J. Modeling of atmospheric chemistry: Cambridge University Press; 2017

Bruyere, C.L., Done, J.M., Holland, G.J., Fredrick, S., 2014. Bias corrections of global models for regional climate simulations of high-impact weather. Clim. Dyn. 43, 1847-1856.

Buck, R.P., Rondinini, S., Covington, A.K., Baucke, F.G.K., Brett, C.M.A., Camoes, M.F., et al., 2002. Measurement of pH. Definition, standards, and procedures. Pure Appl. Chem. 74, 2169-2200.

Burnett, R.T., Pope, C.A., III, Ezzati, M., Olives, C., Lim, S.S., Mehta, S., et al., 2014. An Integrated Risk Function for Estimating the Global Burden of Disease Attributable to Ambient Fine Particulate Matter Exposure. Environ. Health Perspect. 122, 397-403.

Burns, D., Lynch, J., Cosby, B., Fenn, M., Baron, J., 2011. National Acid Precipitation Assessment Program Report to Congress 2011: An Integrated Assessment. Washington, DC.: Office of Science and Technology Policy, National Science and Technology Council, Executive Office of the President;

Burns, D.A., Blett, T., Haeuber, R., Pardo, L.H., 2008. Critical loads as a policy tool for protecting ecosystems from the effects of air pollutants. Front. Ecol. Environ. 6, 156-159.

Byrd, R.H., Lu, P., Nocedal, J., Zhu, C., 1995. A limited memory algorithm for bound constrained optimization. SIAM J. Sci. Comput. 16, 1190-1208.

Byun, D., Schere, K.L., 2006. Review of the governing equations, computational algorithms, and other components of the models-3 Community Multiscale Air Quality (CMAQ) modeling system. Appl. Mech. Rev. 59, 51-77.

Campbell, P., Zhang, Y., Yan, F., Lu, Z., Streets, D., 2018. Impacts of transportation sector emissions on future U.S. air quality in a changing climate. Part I: Projected emissions, simulation design, and model evaluation. Environ. Pollut. 238, 903-917.

Cao, H., Henze, D.K., Shephard, M.W., Dammers, E., Cady-Pereira, K., Alvarado, M., et al., 2020. Inverse modeling of NH3 sources using CrIS remote sensing measurements, (under review).

Cape, J.N., Cornell, S.E., Jickells, T.D., Nemitz, E., 2011. Organic nitrogen in the atmosphere - Where does it come from? A review of sources and methods. Atmos. Res. 102, 30-48.

Carew, R., 2010. Ammonia emissions from livestock industries in Canada: feasibility of abatement strategies. Environ. Pollut. 158, 2618-2626.

Cayan, D.R., Das, T., Pierce, D.W., Barnett, T.P., Tyree, M., Gershunov, A., 2010. Future dryness in the southwest US and the hydrology of the early 21st century drought. Proc. Natl. Acad. Sci. U.S.A. 107, 21271-21276.

Chen, Y., Shen, H., Russell, A.G., 2019. Current and Future Responses of Aerosol pH and Composition in the U.S. to Declining SO_2 Emissions and Increasing NH_3 Emissions. Environ. Sci. Technol. 53, 9646-9655.

Chen, Y., Shen, H., Shih, J., Russell, A. G., Shao, S., Hu, Y., et al., 2020. Greater contribution from agricultural sources to future reactive nitrogen deposition in the United States. Earths Future (under review).

Chen, Y., Shen, H., Kaiser, J., Hu, Y., Capps, S. L., Zhao, S., et al., 2020. High-resolution Hybrid Inversion of IASI Ammonia Columns to Constrain U.S. Ammonia Emissions Using the CMAQ Adjoint Model. Atmos. Chem. Phys. Discuss. 1-25.

Cheng, Y.F., Zheng, G.J., Wei, C., Mu, Q., Zheng, B., Wang, Z.B., et al., 2016. Reactive nitrogen chemistry in aerosol water as a source of sulfate during haze events in China. Sci. Adv. 2, e1601530.

Church, M.R., Van Sickle, J., 1999. Potential relative future effects of sulfur and nitrogen deposition on lake chemistry in the Adirondack Mountains, United States. Water Resour. Res. 35, 2199-2211.

Clarisse, L., Clerbaux, C., Dentener, F., Hurtmans, D., Coheur, P.F., 2009. Global ammonia distribution derived from infrared satellite observations. Nat. Geosci. 2, 479-483.

Clarisse, L., Shephard, M.W., Dentener, F., Hurtmans, D., Cady-Pereira, K., Karagulian, F., et al., 2010. Satellite monitoring of ammonia: A case study of the San Joaquin Valley. J. Geophys. Res. Atmos. 115,

Clarisse, L., Van Damme, M., Clerbaux, C., Coheur, P.F., 2019. Tracking down global NH3 point sources with wind-adjusted superresolution. Atmos. Meas. Tech. 12, 5457-5473.

Clegg, S.L., Brimblecombe, P., Wexler, A.S., 1998. Thermodynamic model of the system H^+-NH_4^+-Na^+-SO_4^{2-}-NH_3-Cl^--H_2O at 298.15 K. J. Phys. Chem. A. 102, 2155-2171.

Clegg, S.L., Pitzer, K.S., 1992. Thermodynamics of Multicomponent, Miscible, Ionic-Solutions - Generalized Equations for Symmetrical Electrolytes. J. Phys. Chem. 96, 3513-3520.

Cohen, A.J., Brauer, M., Burnett, R., Anderson, H.R., Frostad, J., Estep, K., et al., 2017. Estimates and 25-year trends of the global burden of disease attributable to ambient

air pollution: an analysis of data from the Global Burden of Diseases Study 2015. Lancet. 389, 1907-1918.

Conant, R.T., Berdanier, A.B., Grace, P.R., 2013. Patterns and trends in nitrogen use and nitrogen recovery efficiency in world agriculture. Global Biogeochem. Cy. 27, 558-566.

Cooper, M., Martin, R.V., Padmanabhan, A., Henze, D.K., 2017. Comparing mass balance and adjoint methods for inverse modeling of nitrogen dioxide columns for global nitrogen oxide emissions. J. Geophys. Res. Atmos. 122, 4718-4734.

Cooter, E.J., Bash, J.O., Benson, V., Ran, L., 2012. Linking agricultural crop management and air quality models for regional to national-scale nitrogen assessments. Biogeosciences. 9, 4023-4035.

Craig, R.L., Peterson, P.K., Nandy, L., Lei, Z., Hossain, M.A., Camarena, S., et al., 2018. Direct Determination of Aerosol pH: Size-Resolved Measurements of Submicrometer and Supermicrometer Aqueous Particles. Anal. Chem. 90, 11232-11239.

Dallmann, T.R., Harley, R.A., 2010. Evaluation of mobile source emission trends in the United States. J. Geophys. Res. Atmos. 115,

Dammers, E., McLinden, C.A., Griffin, D., Shephard, M.W., Van der Graaf, S., Lutsch, E., et al., 2019. NH_3 emissions from large point sources derived from CrIS and IASI satellite observations. Atmos. Chem. Phys. 19, 12261-12293.

Dammers, E., Palm, M., Van Damme, M., Vigouroux, C., Smale, D., Conway, S., et al., 2016. An evaluation of IASI-NH_3 with ground-based Fourier transform infrared spectroscopy measurements. Atmos. Chem. Phys. 16, 10351-10368.

Dammers, E., Shephard, M.W., Palm, M., Cady-Pereira, K., Capps, S., Lutsch, E., et al., 2017. Validation of the CrIS fast physical NH3 retrieval with ground-based FTIR. Atmos. Meas. Tech. 10, 2645-2667.

Davis, K.F., Gephart, J.A., Emery, K.A., Leach, A.M., Galloway, J.N., D'Odorico, P., 2016. Meeting future food demand with current agricultural resources. Global Environ. Chang. 39, 125-132.

Dockery, D.W., Cunningham, J., Damokosh, A.I., Neas, L.M., Spengler, J.D., Koutrakis, P., et al., 1996. Health effects of acid aerosols on North American children: Respiratory symptoms. Environ. Health Perspect. 104, 500-505.

Du, E.Z., 2016. Rise and fall of nitrogen deposition in the United States. Proc. Natl. Acad. Sci. U.S.A. 113, E3594-E3595.

Duval, B.D., Hartman, M., Marx, E., Parton, W.J., Long, S.P., DeLucia, E.H., 2015. Biogeochemical consequences of regional land use change to a biofuel crop in the

southeastern United States. Ecosphere. 6 (12), 265. http://dx.doi.org/10.1890/ES15-00546.1

Ellis, R.A., Jacob, D.J., Sulprizio, M.P., Zhang, L., Holmes, C.D., Schichtel, B.A., et al., 2013. Present and future nitrogen deposition to national parks in the United States: critical load exceedances. Atmos. Chem. Phys. 13, 9083-9095.

Fakhraei, H., Driscoll, C.T., Renfro, J.R., Kulp, M.A., Blett, T.F., Brewer, P.F., et al., 2016. Critical loads and exceedances for nitrogen and sulfur atmospheric deposition in Great Smoky Mountains National Park, United States. Ecosphere. 7 (10), https://doi.org/10.1002/ecs2.1466

Fang, T., Guo, H., Verma, V., Peltier, R.E., Weber, R.J., 2015. $PM_{2.5}$ water-soluble elements in the southeastern United States: automated analytical method development, spatiotemporal distributions, source apportionment, and implications for heath studies. Atmos. Chem. Phys. 15, 11667-11682.

Fang, T., Guo, H., Zeng, L., Verma, V., Nenes, A., Weber, R.J., 2017. Highly Acidic Ambient Particles, Soluble Metals, and Oxidative Potential: A Link between Sulfate and Aerosol Toxicity. Environ. Sci. Technol. 51, 2611-2620.

Fenn, M.E., Bytnerowicz, A., Schilling, S.L., Vallano, D.M., Zavaleta, E.S., Weiss, S.B., et al., 2018. On-road emissions of ammonia: An underappreciated source of atmospheric nitrogen deposition. Sci. Total Environ. 625, 909-919.

Fenn, M.E., Sickman, J.O., Bytnerowicz, A., Clow, D.W., Molotch, N.P., Pleim, J.E., et al. Methods for measuring atmospheric nitrogen deposition inputs in arid and montane ecosystems of western North America. Amsterdam: Elsevier; 2009

Fountoukis, C., Nenes, A., 2007. ISORROPIA II: a computationally efficient thermodynamic equilibrium model for K^+-Ca^{2+}-Mg^{2+}-$NH4^+$-Na^+-SO_4^{2-}-NO_3^--Cl^--H_2O aerosols. Atmos. Chem. Phys. 7, 4639-4659.

Fowler, D., Coyle, M., Skiba, U., Sutton, M.A., Cape, J.N., Reis, S., et al., 2013. The global nitrogen cycle in the twenty-first century. Philos T R Soc B. 368,: 20130164. http://dx.doi.org/10.1098/rstb.2013.0164

Friese, E., Ebel, A., 2010. Temperature Dependent Thermodynamic Model of the System H^+-NH_4^+-Na^+-SO_4^{2-}-NO_3^--Cl^--H_2O. J. Phys. Chem. A. 114, 11595-11631.

Galloway, J.N., Aber, J.D., Erisman, J.W., Seitzinger, S.P., Howarth, R.W., Cowling, E.B., et al., 2003. The nitrogen cascade. Bioscience. 53, 341-356.

Galloway, J.N., Burke, M., Bradford, G.E., Naylor, R., Falcon, W., Chapagain, A.K., et al., 2007. International trade in meat: The tip of the pork chop. Ambio. 36, 622-629.

Galloway, J.N., Townsend, A.R., Erisman, J.W., Bekunda, M., Cai, Z.C., Freney, J.R., et al., 2008. Transformation of the nitrogen cycle: Recent trends, questions, and potential solutions. Science. 320, 889-892.

Galloway, J.N., Winiwarter, W., Leip, A., Leach, A.M., Bleeker, A., Erisman, J.W., 2014. Nitrogen footprints: past, present and future. Environ Res Lett. 9 115003.

Gantt, B., Kelly, J.T., Bash, J.O., 2015. Updating sea spray aerosol emissions in the Community Multiscale Air Quality (CMAQ) model version 5.0.2. Geosci. Model Dev. 8, 3733-3746.

Gilliland, A.B., Wyat Appel, K., Pinder, R.W., Dennis, R.L., 2006. Seasonal NH_3 emissions for the continental united states: Inverse model estimation and evaluation. Atmos. Environ. 40, 4986-4998.

Gipson, G.L., 1999. Science Algorithms of the EPA Models-3 Community Multiscale Air Quality (CMAQ) Modeling System. Research Triangle Park, NC 27711, USA;

Greaver, T.L., Sullivan, T.J., Herrick, J.D., Barber, M.C., Baron, J.S., Cosby, B.J., et al., 2012. Ecological effects of nitrogen and sulfur air pollution in the US: what do we know? Front. Ecol. Environ. 10, 365-372.

Guo, H., Liu, J., Froyd, K.D., Roberts, J.M., Veres, P.R., Hayes, P.L., et al., 2017a. Fine particle pH and gas–particle phase partitioning of inorganic species in Pasadena, California, during the 2010 CalNex campaign. Atmos. Chem. Phys. 17, 5703-5719.

Guo, H., Sullivan, A.P., Campuzano-Jost, P., Schroder, J.C., Lopez-Hilfiker, F.D., Dibb, J.E., et al., 2016. Fine particle pH and the partitioning of nitric acid during winter in the northeastern United States. J. Geophys. Res. Atmos. 121, 10,355-310,376.

Guo, H., Weber, R.J., Nenes, A., 2017b. High levels of ammonia do not raise fine particle pH sufficiently to yield nitrogen oxide-dominated sulfate production. Sci Rep. 7, 12109.

Guo, H., Xu, L., Bougiatioti, A., Cerully, K.M., Capps, S.L., Hite, J.R., et al., 2015. Fine-particle water and pH in the southeastern United States. Atmos. Chem. Phys. 15, 5211-5228.

Hansen, P. C., 1999. The L-curve and its use in the numerical treatment of inverse problems, in: Computational Inverse Problems in Electrocardiology, ed. P. Johnston, Advances in Computational Bioengineering, 119-142.

Heald, C.L., Collett, J.L., Lee, T., Benedict, K.B., Schwandner, F.M., Li, Y., et al., 2012. Atmospheric ammonia and particulate inorganic nitrogen over the United States. Atmos. Chem. Phys. 12, 10295-10312.

Hennigan, C.J., Izumi, J., Sullivan, A.P., Weber, R.J., Nenes, A., 2015. A critical evaluation of proxy methods used to estimate the acidity of atmospheric particles. Atmos. Chem. Phys. 15, 2775-2790.

Henze, D.K., Seinfeld, J.H., Shindell, D.T., 2009. Inverse modeling and mapping US air quality influences of inorganic $PM_{2.5}$ precursor emissions using the adjoint of GEOS-Chem. Atmos. Chem. Phys. 9, 5877-5903.

Hettelingh, J.P., Posch, M., Slootweg, J., Reinds, G.J., Spranger, T., Tarrason, L. Critical Loads and Dynamic Modelling to Assess European Areas at Risk of Acidification and Eutrophication. in: Brimblecombe P., Hara H., Houle D., Novak M., eds. Acid Rain - Deposition to Recovery. Dordrecht: Springer Netherlands; 2007

Houlton, B.Z., Boyer, E., Finzi, A.C., Galloway, J., Leach, A., Liptzin, D., et al., 2013. Intentional versus unintentional nitrogen use in the United States: trends, efficiency and implications. Biogeochemistry. 114, 11-23.

Jacobson, M.Z., Tabazadeh, A., Turco, R.P., 1996. Simulating equilibrium within aerosols and nonequilibrium between gases and aerosols. J. Geophys. Res. Atmos. 101, 9079-9091.

Jickells, T., Baker, A.R., Cape, J.N., Cornell, S.E., Nemitz, E., 2013. The cycling of organic nitrogen through the atmosphere. Philos T R Soc B. 368, Article 20130115.

Kelly, J.T., Baker, K.R., Nowak, J.B., Murphy, J.G., Markovic, M.Z., VandenBoer, T.C., et al., 2014. Fine-scale simulation of ammonium and nitrate over the South Coast Air Basin and San Joaquin Valley of California during CalNex-2010. J. Geophys. Res. Atmos. 119, 3600-3614.

Kim, S.W., Heckel, A., McKeen, S.A., Frost, G.J., Hsie, E.Y., Trainer, M.K., et al., 2006. Satellite-observed U.S. power plant NO*x* emission reductions and their impact on air quality. Geophys. Res. Lett. 33, https://doi.org/10.1029/2006GL027749.

Kim, Y.P., Seinfeld, J.H., Saxena, P., 1993. Atmospheric Gas Aerosol Equilibrium .1. Thermodynamic Model. Aerosol Sci. Technol. 19, 157-181.

Kohn, R.A., 2015. Nitrogen Emissions from Animal Agricultural Systems and Strategies to Protect the Environment. CABI Clim. Change Ser. 6, 61-73.

Kriegler, E., Bauer, N., Popp, A., Humpenoder, F., Leimbach, M., Strefler, J., et al., 2017. Fossil-fueled development (SSP5): An energy and resource intensive scenario for the 21st century. Global Environ. Chang. 42, 297-315.

Lamarque, J.F., Kyle, G.P., Meinshausen, M., Riahi, K., Smith, S.J., van Vuuren, D.P., et al., 2011. Global and regional evolution of short-lived radiatively-active gases and aerosols in the Representative Concentration Pathways. Climatic Change. 109, 191-212.

Lawal, A.S., Guan, X.B., Liu, C., Henneman, L.R.F., Vasilakos, P., Bhogineni, V., et al., 2018. Linked Response of Aerosol Acidity and Ammonia to SO_2 and NO_x Emissions Reductions in the United States. Environ. Sci. Technol. 52, 9861-9873.

Lee, C.J., Martin, R.V., Henze, D.K., Brauer, M., Cohen, A., van Donkelaar, A., 2015. Response of Global Particulate-Matter-Related Mortality to Changes in Local Precursor Emissions. Environ. Sci. Technol. 49, 4335-4344.

Lee, H.M., Paulot, F., Henze, D.K., Travis, K., Jacob, D.J., Pardo, L.H., et al., 2016a. Sources of nitrogen deposition in Federal Class I areas in the US. Atmos. Chem. Phys. 16, 525-540.

Lee, Y., Shindell, D.T., Faluvegi, G., Pinder, R.W., 2016b. Potential impact of a US climate policy and air quality regulations on future air quality and climate change. Atmos. Chem. Phys. 16, 5323-5342.

Li, C., Martin, R.V., Shephard, M.W., Cady‐Pereira, K., Cooper, M.J., Kaiser, J., et al., 2019. Assessing the Iterative Finite Difference Mass Balance and 4D‐Var Methods to Derive Ammonia Emissions Over North America Using Synthetic Observations. J. Geophys. Res. Atmos. 124, 4222-4236.

Li, H., McNulty, S.G., 2007. Uncertainty analysis on simple mass balance model to calculate critical loads for soil acidity. Environmental Pollution. 149, 315-326.

Li, Y., Schichtel, B.A., Walker, J.T., Schwede, D.B., Chen, X., Lehmann, C.M.B., et al., 2016. Increasing importance of deposition of reduced nitrogen in the United States. Proc. Natl. Acad. Sci. U.S.A. 113, 5874-5879.

Lynch, J.A., Phelan, J., Pardo, L.H., McDonnell, T.C., Clark, C.M., 2017. Detailed Documentation of the National Critical Load Database (NCLD) for U.S. Critical Loads of Sulfur and Nitrogen, version 3.0. Champaign, IL.

Marais, E.A., Jacob, D.J., Jimenez, J.L., Campuzano-Jost, P., Day, D.A., Hu, W., et al., 2016. Aqueous-phase mechanism for secondary organic aerosol formation from isoprene: application to the southeast United States and co-benefit of SO_2; emission controls. Atmos. Chem. Phys. 16, 1603-1618.

Martin, R.V., Jacob, D.J., Chance, K., Kurosu, T.P., Palmer, P.I., Evans, M.J., 2003. Global inventory of nitrogen oxide emissions constrained by space-based observations of NO_2 columns. J. Geophys. Res. Atmos. 108, https://doi.org/10.1029/2003JD003453.

Massad, R.S., Nemitz, E., Sutton, M.A., 2010. Review and parameterisation of bi-directional ammonia exchange between vegetation and the atmosphere. Atmos. Chem. Phys. 10, 10359-10386.

McNulty, S.G., Cohen, E.C., Myers, J.A.M., Sullivan, T.J., Li, H., 2007. Estimates of critical acid loads and exceedances for forest soils across the conterminous United States. Environ. Pollut. 149, 281-292.

McQuilling, A.M., Adams, P.J., 2015. Semi-empirical process-based models for ammonia emissions from beef, swine, and poultry operations in the United States. Atmos. Environ. 120, 127-136.

Moise, T., Flores, J.M., Rudich, Y., 2015. Optical Properties of Secondary Organic Aerosols and Their Changes by Chemical Processes. Chem. Rev. 115, 4400-4439.

Monaghan, A., Steinhoff, D., Bruyere, C., Yates, D., 2014. NCAR CESM global bias-corrected CMIP5 output to support WRF/MPAS research. Research Data Archive at the National Center for Atmospheric Research, Computational and Information Systems Laboratory. Boulder, CO.

NADP, 2014. Ambient Ammonia Monitoring Network (AMoN). Wisconsin State Laboratory of Hygiene, 465 Henry Mall, Madison, WI 53706., NADP Program Office. http://nadp.slh.wisc.edu/data/AMoN/ last access: 22 April 2020.

NADP, 2019. National Atmospheric Deposition Program (NRSP-3). . Wisconsin State Laboratory of Hygiene, 465 Henry Mall, Madison, WI 53706., NADP Program Office. http://nadp.slh.wisc.edu/data/NTN/ last access: 22 April 2020.

NCAR, 2011. community earth system model (CESM) 1.0 experiments, data and diagnostics, National Center for Atmospheric Research (NCAR), Boulder, CO. http://www.cesm.ucar.edu/experiments/cesm1.0/. Accessed on 12/08/2019.

Nel, A., 2005. Air pollution-related illness: Effects of particles. Science. 308, 804-806.

Nenes, A., Pandis, S.N., Weber, R.J., Russell, A., 2020. Aerosol pH and liquid water content determine when particulate matter is sensitive to ammonia and nitrate availability. Atmos. Chem. Phys. 20(5), 3249-3258.

Nilsson, J.G., P 1988. Critical loads for sulphur and nitrogen: Report from a workshop held at Skokloster, Sweden, 19-24 March 1988, Skokloster, Sweden.

NOAA (2019), North American Regional Reanalysis. National Oceanic and Atmospheric Administration (NOAA), Asheville, NC. https://www.ncdc.noaa.gov/data-access/model-data/model-datasets/north-american-regional-reanalysis-narr. Accessed on 12/07/2019.

Nolte, C.G., Appel, K.W., Kelly, J.T., Bhave, P.V., Fahey, K.M., Collett, J.L., et al., 2015. Evaluation of the Community Multiscale Air Quality (CMAQ) model v5.0 against size-resolved measurements of inorganic particle composition across sites in North America. Geosci. Model Dev. 8, 2877-2892.

Nowak, J.B., Neuman, J.A., Bahreini, R., Middlebrook, A.M., Holloway, J.S., McKeen, S.A., et al., 2012. Ammonia sources in the California South Coast Air Basin and their impact on ammonium nitrate formation. Geophys. Res Lett. 39,

NRC, (National Research Council), 2008. Water Implications of Biofuels Production in the United States. Washington, DC: The National Academies Press. https://doi.org/10.17226/12039.

Oakes, M., Ingall, E.D., Lai, B., Shafer, M.M., Hays, M.D., Liu, Z.G., et al., 2012. Iron Solubility Related to Particle Sulfur Content in Source Emission and Ambient Fine Particles. Environ. Sci. Technol. 46, 6637-6644.

Overpeck, J., Udall, B., 2010. Dry Times Ahead. Science. 328, 1642-1643.

Paltsev, S., Jacoby, H.D., Reilly, J.M., Ejaz, Q.J., Morris, J., O'Sullivan, F., et al., 2011. The future of U.S. natural gas production, use, and trade. Energy Policy. 39, 5309-5321.

Pardo, L.H., Fenn, M.E., Goodale, C.L., Geiser, L.H., Driscoll, C.T., Allen, E.B., et al., 2011a. Effects of nitrogen deposition and empirical nitrogen critical loads for ecoregions of the United States. Ecol. Appl. 21, 3049-3082.

Pardo, L.H., Robin-Abbott, M.J., Driscoll, C.T.e., 2011b. Assessment of Nitrogen deposition effects and empirical critical loads of Nitrogen for ecoregions of the United States., Gen. Tech. Rep. NRS-80. Newtown Square, PA: U.S. Department of Agriculture, Forest Service, Northern Research Station. 291 p. https://doi.org/10.2737/NRS-GTR-80.

Pardo, L.H., Robin-Abbott, M.J., Fenn, M.E., Goodale, C.L., Geiser, L.H., Driscoll, C.T., et al., 2015. Effects and Empirical Critical Loads of Nitrogen for Ecoregions of the United States. Environ. Pollut. Ser. 25, 129-169.

Paulot, F., Fan, S., Horowitz, L.W., 2017. Contrasting seasonal responses of sulfate aerosols to declining SO_2 emissions in the Eastern U.S.: Implications for the efficacy of SO_2 emission controls. Geophys. Res. Lett. 44, 455-464.

Paulot, F., Jacob, D.J., Henze, D.K., 2013. Sources and Processes Contributing to Nitrogen Deposition: An Adjoint Model Analysis Applied to Biodiversity Hotspots Worldwide. Environ. Sci. Technol. 47, 3226-3233.

Paulot, F., Jacob, D.J., Pinder, R.W., Bash, J.O., Travis, K., Henze, D.K., 2014. Ammonia emissions in the United States, European Union, and China derived by high-resolution inversion of ammonium wet deposition data: Interpretation with a new agricultural emissions inventory (MASAGE_NH_3). J. Geophys. Res. Atmos. 119, 4343-4364.

Pierce, T., C. Geron, G. Pouliot, E. Kinnee, J. Vukovich, 2002. Integration of the Biogenic Emissions Inventory System (BEIS3) into the Community Multiscale Air Quality

(CMAQ) Modeling System. Presented at 25th Conference on Agricultural and Forest Meteorology, Norfolk, VA, May 20-24.

Pikaar, I., Matassa, S., Bodirsky, B.L., Weindl, I., Humpenoder, F., Rabaey, K., et al., 2018. Decoupling Livestock from Land Use through Industrial Feed Production Pathways. Environ. Sci. Technol. 52, 7351-7359.

Pikaar, I., Matassa, S., Rabaey, K., Bodirsky, B.L., Popp, A., Herrero, M., et al., 2017. Microbes and the Next Nitrogen Revolution. Environ. Sci. Technol. 51, 7297-7303.

Pinder, R.W., Adams, P.J., Pandis, S.N., 2007. Ammonia emission controls as a cost-effective strategy for reducing atmospheric particulate matter in the eastern United States. Environ. Sci. Technol. 41, 380-386.

Porter, E.M., Bowman, W.D., Clark, C.M., Compton, J.E., Pardo, L.H., Soong, J.L., 2013. Interactive effects of anthropogenic nitrogen enrichment and climate change on terrestrial and aquatic biodiversity. Biogeochemistry. 114, 93-120.

Pozzer, A., Tsimpidi, A.P., Karydis, V.A., de Meij, A., Lelieveld, J., 2017. Impact of agricultural emission reductions on fine-particulate matter and public health. Atmos. Chem. Phys. 17, 12813-12826.

Puchalski, M.A., Sather, M.E., Walker, J.T., Lehmann, C.M., Gay, D.A., Mathew, J., et al., 2011. Passive ammonia monitoring in the United States: comparing three different sampling devices. J. Environ. Monit. 13, 3156-3167.

Puckett, L.J., 1994. Nonpoint and point sources of nitrogen in major watersheds of the United States., U.S. Geological Survey, Water-Resources Investigations Report 94-4001.

Pye, H.O.T., Liao, H., Wu, S., Mickley, L.J., Jacob, D.J., Henze, D.K., et al., 2009. Effect of changes in climate and emissions on future sulfate-nitrate-ammonium aerosol levels in the United States. J. Geophys. Res. Atmos.. 114, D01205.

Pye, H.O.T., Nenes, A., Alexander, B., Ault, A.P., Barth, M.C., Clegg, S.L., et al., 2020. The acidity of atmospheric particles and clouds. Atmos. Chem. Phys. 20, 4809-4888.

Pye, H.O.T., Zuend, A., Fry, J.L., Isaacman-VanWertz, G., Capps, S.L., Appel, K.W., et al., 2018. Coupling of organic and inorganic aerosol systems and the effect on gas-particle partitioning in the southeastern US. Atmos. Chem. Phys. 18, 357-370.

Ramanathan, V., Crutzen, P.J., Kiehl, J.T., Rosenfeld, D., 2001. Atmosphere - Aerosols, climate, and the hydrological cycle. Science. 294, 2119-2124.

Rao, S., Klimont, Z., Smith, S.J., Van Dingenen, R., Dentener, F., Bouwman, L., et al., 2017. Future air pollution in the Shared Socio-economic Pathways. Global Environ. Chang. 42, 346-358.

Scheffe, R.D., Lynch, J.A., Reff, A., Kelly, J.T., Hubbell, B., Greaver, T.L., et al., 2014. The Aquatic Acidification Index: A New Regulatory Metric Linking Atmospheric and Biogeochemical Models to Assess Potential Aquatic Ecosystem Recovery. Water Air Soil Poll., 225(2), 1838.

Schiferl, L.D., Heald, C.L., Nowak, J.B., Holloway, J.S., Neuman, J.A., Bahreini, R., et al., 2014. An investigation of ammonia and inorganic particulate matter in California during the CalNex campaign. J. Geophys. Res. Atmos. 119, 1883-1902.

Schwarz, G., A. Hoos, R. Alexander, and R. Smith, 2006. The SPARROW surface water-quality model: theory, application and user documentation, US geological survey techniques and methods report, 6-B3, 248, U.S. Geological Survey, Reston, VA.

Sehmel, G.A., 1980. Particle and Gas Dry Deposition - a Review. Atmos. Environ. 14, 983-1011.

Seinfeld, J.H., Pandis., S.N., 2016. Atmospheric chemistry and physics : from air pollution to climate change. John Wiley & Sons, Inc.: New Jersey.

Shen, H., Chen, Y., Hu, Y., Ran, L., Lam, S.K., Pavur, G.K., et al., 2019a. Increased agricultural nitrogen loss via cropland ammonia volatilization under warming. (under review).

Shen, H., Chen, Y., Li, Y., Russell, A.G., Hu, Y., Henneman, L.R.F., et al., 2019b. Relaxing Energy Policies Coupled with Climate Change Will Significantly Undermine Efforts to Attain US Ozone Standards. One Earth. 1, 229-239.

Shephard, M., Dammers, E., Cady-Pereira, K.E., Kharol, S.K., Thompson, J., Gainariu-Matz, Y., et al., 2020. Ammonia measurements from space with the Cross-track Infrared Sounder (CrIS): characteristics and applications. Atmos. Chem. Phys. 20, 2277-2302.

Shephard, M.W., Cady-Pereira, K.E., 2015. Cross-track Infrared Sounder (CrIS) satellite observations of tropospheric ammonia. Atmos. Meas. Tech. 8, 1323-1336.

Shephard, M.W., McLinden, C.A., Cady-Pereira, K.E., Luo, M., Moussa, S.G., Leithead, A., et al., 2015. Tropospheric Emission Spectrometer (TES) satellite observations of ammonia, methanol, formic acid, and carbon monoxide over the Canadian oil sands: validation and model evaluation. Atmos. Meas. Tech. 8, 5189-5211.

Shimadera, H., Hayami, H., Chatani, S., Morino, Y., Mori, Y., Morikawa, T., et al., 2014. Sensitivity analyses of factors influencing CMAQ performance for fine particulate nitrate. J. Air Waste Manage. 64, 374-387.

Solomon, P.A., Crumpler, D., Flanagan, J.B., Jayanty, R.K.M., Rickman, E.E., McDade, C.E., 2014. U.S. National $PM_{2.5}$ Chemical Speciation Monitoring Networks—CSN and IMPROVE: Description of networks. J. Air Waste Manage. 64, 1410-1438.

Song, C., Gyawali, M., Zaveri, R.A., Shilling, J.E., Arnott, W.P., 2013. Light absorption by secondary organic aerosol from alpha-pinene: Effects of oxidants, seed aerosol acidity, and relative humidity. J. Geophys. Res. Atmos. 118, 11741-11749.

Song, S., Gao, M., Xu, W., Shao, J., Shi, G., Wang, S., et al., 2018. Fine-particle pH for Beijing winter haze as inferred from different thermodynamic equilibrium models. Atmos. Chem. Phys. 18, 7423-7438.

Spengler, J.D., Keeler, G.J., Koutrakis, P., Ryan, P.B., Raizenne, M., Franklin, C.A., 1989. Exposures to Acidic Aerosols. Environ. Health Perspect. 79, 43-51.

Steffen, W., Richardson, K., Rockstrom, J., Cornell, S.E., Fetzer, I., Bennett, E.M., et al., 2015. Planetary boundaries: Guiding human development on a changing planet. Science. 347, 10.1126/science.1259855.

Stevens, C.J., 2019. Nitrogen in the environment. Science. 363, 578-580.

Struthers, H., Ekman, A.M.L., Glantz, P., Iversen, T., Kirkevag, A., Seland, O., et al., 2013. Climate-induced changes in sea salt aerosol number emissions: 1870 to 2100. J. Geophys. Res. Atmos. 118, 670-682.

Sun, K., Tao, L., Miller, D.J., Pan, D., Golston, L.M., Zondlo, M.A., et al., 2017. Vehicle Emissions as an Important Urban Ammonia Source in the United States and China. Environ. Sci. Technol. 51, 2472-2481.

Surratt, J.D., Kroll, J.H., Kleindienst, T.E., Edney, E.O., Claeys, M., Sorooshian, A., et al., 2007. Evidence for organosulfates in secondary organic aerosol. Environ. Sci. Technol. 41, 517-527.

Sutton, M.A., Reis, S., Riddick, S.N., Dragosits, U., Nemitz, E., Theobald, M.R., et al., 2013. Towards a climate-dependent paradigm of ammonia emission and deposition. Philos. Trans. R. Soc. London, Ser. B, 368(1621), 20130166.

Tagaris, E., Liao, K.J., Manomaiphiboon, K., Woo, J.H., He, S., Amar, P., et al., 2008. Impacts of future climate change and emissions reductions on nitrogen and sulfur deposition over the United States. Geophys. Res Lett. 35(8), doi: 10.1029/2008GL033477.

Tegen, I., Werner, M., Harrison, S.P., Kohfeld, K.E., 2004. Relative importance of climate and land use in determining present and future global soil dust emission. Geophys. Res Lett. 31, L05105.

Thomson, A.M., Calvin, K.V., Smith, S.J., Kyle, G.P., Volke, A., Patel, P., et al., 2011. RCP4.5: a pathway for stabilization of radiative forcing by 2100. Climatic Change. 109, 77-94.

Trail, M., Tsimpidi, A.P., Liu, P., Tsigaridis, K., Hu, Y., Nenes, A., et al., 2013. Downscaling a global climate model to simulate climate change over the US and the implication on regional and urban air quality. Geosci. Model Dev. 6, 1429-1445.

Trail, M., Tsimpidi, A.P., Liu, P., Tsigaridis, K., Rudokas, J., Miller, P., et al., 2014. Sensitivity of air quality to potential future climate change and emissions in the United States and major cities. Atmos. Environ. 94, 552-563.

ULB, 2018. Ammonia total columns retrieved from IASI measurements from the ANNI-NH3-v2.2 retrieval algorithm, Universite Libre de Bruxelles (ULB)/Laboratoire atmosphères, milieux et observations spatiales (LATMOS). https://iasi.aeris-data.fr/NH3_IASI_A_data.

USDA, 2012. 2012 Census Ag Atlas Maps - Livestock and Animals. United States Department of Agriculture, National Agricultural Statistics Service, https://www.nass.usda.gov/Publications/AgCensus/2012/Online_Resources/Ag_Atlas_Maps/Livestock_and_Animals.

USDA, 2018a. Quick Stats, National Agricultural Statistics Service; United States Department of Agriculture (USDA): Washington, DC. Accessed on 08/02/2018.

USDA, 2018b. USDA Agricultural Projections to 2027; United States Department of Agriculture (USDA): Washington, DC, 2018. https://www.ers.usda.gov/webdocs/publications/87459/oce-2018-1.pdf?v=0

USEPA, 2008a. Integrated Science Assessment (ISA) for Oxides of Nitrogen and Sulfur - Ecological Criteria. EPA/600/R-08/082F, United States Environmental Protection Agency (USEPA): Washington, DC.

USEPA, 2008b. Integrated science assessment for oxides of nitrogen and sulfur: Ecological criteria. U.S. Environmental Protection Agency, Office of Research and Development, National Center for Environmental Assessment- RTP Division: Research Triangle Park, NC.

USEPA, 2011. The Benefits and Costs of the Clean Air Act from 1990 to 2020 Final Report. U.S. Environmental Protection Agency Office of Air and Radiation: United States Environmental Protection Agency (USEPA): Washington, DC.

USEPA, 2012. CMAQ v5.0, US Environmental Protection Agency, http://doi.org/10.5281/zenodo.1079888.

USEPA, 2014. Preparation of Emissions Inventories for the Version 6.1, 2011 Emissions Modeling Platform, US Environmental Protection Agency, https://www.epa.gov/air-emissions-modeling/2011-version-61-technical-support-document.

USEPA, 2015. 2011 National Emissions Inventory Data & Documentation, https://www.epa.gov/air-emissions-inventories/2011-national-emissions-

inventory-nei-data, US Environmental Protection Agency Office of Air Quality Planning and Standards.

USEPA, 2018. Air Quality System Data Mart, US Environmental Protection Agency, https://aqs.epa.gov/aqsweb/documents/data_api.html, last access: 06 July 2018.

USEPA, 2019a. Agricultural Management Practices for Water Quality Protection. United States Environmental Protection Agency (USEPA): Washington, DC. https://cfpub.epa.gov/watertrain/moduleFrame.cfm?parent_object_id=1362. Accessed on 12/08/2019.

USEPA, 2019b. Clean Air Status and Trends Network (CASTNET). United States Environmental Protection Agency (USEPA): Washington, DC. https://www.epa.gov/castnet. Accessed on 12/08/2019.

USEPA, 2019c. Integrated Science Assessment (ISA) for Particulate Matter (Final Report, 2019), United States Environmental Protection Agency (USEPA): Washington, DC.

USGS, 2018. Protected Areas Database of the United States (PAD-US) 2.0. U.S. Geological Survey (USGS) Gap Analysis Project (GAP), https://gapanalysis.usgs.gov/padus/, doi:10.5066/P955KPLE. Assessed on 12/08/2019.

Val Martin, M., Heald, C.L., Lamarque, J.F., Tilmes, S., Emmons, L.K., Schichtel, B.A., 2015. How emissions, climate, and land use change will impact mid-century air quality over the United States: a focus on effects at national parks. Atmos. Chem. Phys. 15, 2805-2823.

Van Damme, M., Clarisse, L., Dammers, E., Liu, X., Nowak, J.B., Clerbaux, C., et al., 2015a. Towards validation of ammonia (NH_3) measurements from the IASI satellite. Atmos. Meas. Tech. 8, 1575-1591.

Van Damme, M., Clarisse, L., Heald, C.L., Hurtmans, D., Ngadi, Y., Clerbaux, C., et al., 2014. Global distributions, time series and error characterization of atmospheric ammonia (NH_3) from IASI satellite observations. Atmos. Chem. Phys. 14, 2905-2922.

Van Damme, M., Clarisse, L., Whitburn, S., Hadji-Lazaro, J., Hurtmans, D., Clerbaux, C., et al., 2018. Industrial and agricultural ammonia point sources exposed. Nature. 564, 99-103.

Van Damme, M., Erisman, J.W., Clarisse, L., Dammers, E., Whitburn, S., Clerbaux, C., et al., 2015b. Worldwide spatiotemporal atmospheric ammonia (NH_3) columns variability revealed by satellite. Geophys. Res Lett. 42, 8660-8668.

Van Damme, M., Whitburn, S., Clarisse, L., Clerbaux, C., Hurtmans, D., Coheur, P.F., 2017. Version 2 of the IASI NH_3 neural network retrieval algorithm: near-real-time and reanalysed datasets. Atmos. Meas. Tech. 10, 4905-4914.

van Vuuren, D.P., Bouwman, L.F., Smith, S.J., Dentener, F., 2011. Global projections for anthropogenic reactive nitrogen emissions to the atmosphere: an assessment of scenarios in the scientific literature. Curr. Opin. Env. Sust. 3, 359-369.

Vanbreemen, N., Burrough, P.A., Velthorst, E.J., Vandobben, H.F., Dewit, T., Ridder, T.B., et al., 1982. Soil Acidification from Atmospheric Ammonium-Sulfate in Forest Canopy Throughfall. Nature. 299, 548-550.

Vasilakos, P., Russell, A., Weber, R., Nenes, A., 2018. Understanding nitrate formation in a world with less sulfate. Atmos. Chem. Phys. 18, 12765-12775.

Vayenas, D.V., Takahama, S., Davidson, C.I., Pandis, S.N., 2005. Simulation of the thermodynamics and removal processes in the sulfate-ammonia-nitric acid system during winter: Implications for $PM_{2.5}$ control strategies. J. Geophys. Res. Atmos. 110,

Walker, J.M., Philip, S., Martin, R.V., Seinfeld, J.H., 2012. Simulation of nitrate, sulfate, and ammonium aerosols over the United States. Atmos. Chem. Phys. 12, 11213-11227.

Wang, G., Zhang, R., Gomez, M.E., Yang, L., Levy Zamora, M., Hu, M., et al., 2016a. Persistent sulfate formation from London Fog to Chinese haze. Proc. Natl. Acad. Sci. U. S. A. 113, 13630-13635.

Wang, G.H., Zhang, R.Y., Gomez, M.E., Yang, L.X., Zamora, M.L., Hu, M., et al., 2016b. Persistent sulfate formation from London Fog to Chinese haze. Proc. Natl. Acad. Sci. U.S.A. 113, 13630-13635.

Warner, J.X., Wei, Z.G., Strow, L.L., Dickerson, R.R., Nowak, J.B., 2016. The global tropospheric ammonia distribution as seen in the 13-year AIRS measurement record. Atmos. Chem. Phys. 16, 5467-5479.

Weathers, K.C.L., J.A. Deposition, Chapter 3. in: Pardo L.H., Robin-Abbott M.J., Driscoll C.T., eds. Assessment of Nitrogen deposition effects and empirical critical loads of Nitrogen for ecoregions of the United States. Gen. Tech. Rep. NRS-80. Newtown Square, PA: U.S. Department of Agriculture, Forest Service, Northern Research Station, 2011.

Weber, R.J., Guo, H., Russell, A.G., Nenes, A., 2016. High aerosol acidity despite declining atmospheric sulfate concentrations over the past 15 years. Nat. Geosci. 9, 282-285.

Whitburn, S., Van Damme, M., Clarisse, L., Bauduin, S., Heald, C.L., Hadji-Lazaro, J., et al., 2016. A flexible and robust neural network IASI-NH_3 retrieval algorithm. J. Geophys. Res. Atmos. 121, 6581-6599.

Wimalasekera, R., 2015. Role of Seed Quality in Improving Crop Yields. in: Hakeem K.R., ed. Crop Production and Global Environmental Issues. Cham: Springer International Publishing.

Xu, R.T., Tian, H.Q., Pan, S.F., Prior, S.A., Feng, Y.C., Batchelor, W.D., et al., 2019. Global ammonia emissions from synthetic nitrogen fertilizer applications in agricultural systems: Empirical and process-based estimates and uncertainty. Global Change Biol. 25, 314-326.

Yahya, K., Wang, K., Campbell, P., Chen, Y., Glotfelty, T., He, J., et al., 2017. Decadal application of WRF/Chem for regional air quality and climate modeling over the U.S. under the representative concentration pathways scenarios. Part 1: Model evaluation and impact of downscaling. Atmos. Environ. 152, 562-583.

Yang, D., E. Cooter, L. Ran, V. Benson, J. Bowden, K. Talgo, A. Hanna., 2017. FEST-C 1.3 & 2.0 for CMAQ Bi-directional NH_3, Crop Production, and SWAT Modeling. 16th Annual CMAS Conference, Chapel Hill, NC, October 23 - 25, 2017.

Yarwood, G., Sunja, R., Mark, Y., Gary, Z.W., 2005. Updates to the carbon bond chemical mechanism: CB05. Report to the U.S. Environmental Protection Agency. http://www.camx.com/publ/pdfs/cb05_final_report_120805.pdf.

Ye, D., Klein, M., Mulholland, J.A., Russell, A.G., Weber, R., Edgerton, E.S., et al., 2018. Estimating Acute Cardiovascular Effects of Ambient $PM_{2.5}$ Metals. Environ. Health Perspect. 126, 027007.

Zeng, L.X., Ruan, M.Y., Liu, J.X., Wilde, P., Naumova, E.N., Mozaffarian, D., et al., 2019. Trends in Processed Meat, Unprocessed Red Meat, Poultry, and Fish Consumption in the United States, 1999-2016. J Acad Nutr Diet. 119(7), 1085-1098.

Zhang, L., Chen, Y.F., Zhao, Y.H., Henze, D.K., Zhu, L.Y., Song, Y., et al., 2018a. Agricultural ammonia emissions in China: reconciling bottom-up and top-down estimates. Atmos. Chem. Phys. 18, 339-355.

Zhang, L., Jacob, D.J., Knipping, E.M., Kumar, N., Munger, J.W., Carouge, C.C., et al., 2012. Nitrogen deposition to the United States: distribution, sources, and processes. Atmos. Chem. Phys. 12, 4539-4554.

Zhang, R., Thompson, T.M., Barna, M.G., Hand, J.L., McMurray, J.A., Bell, M.D., et al., 2018b. Source regions contributing to excess reactive nitrogen deposition in the Greater Yellowstone Area (GYA) of the United States. Atmos. Chem. Phys. 18, 12991-13011.

Zhang, X., Davidson, E.A., Mauzerall, D.L., Searchinger, T.D., Dumas, P., Shen, Y., 2015. Managing nitrogen for sustainable development. Nature. 528, 51-59.

Zhang, Y., Seigneur, C., Seinfeld, J.H., Jacobson, M., Clegg, S.L., Binkowski, F.S., 2000. A comparative review of inorganic aerosol thermodynamic equilibrium modules: similarities, differences, and their likely causes. Atmos. Environ. 34, 117-137.

Zhang, Y.Q., Mathur, R., Bash, J.O., Hogrefe, C., Xing, J., Roselle, S.J., 2018c. Long-term trends in total inorganic nitrogen and sulfur deposition in the US from 1990 to 2010. Atmos. Chem. Phys. 18, 9091-9106.

Zhao, S., Russell, M.G., Hakami, A., Capps, S.L., Turner, M.D., Henze, D.K., et al., 2019. A Multiphase CMAQ Version 5.0 Adjoint. Geosci. Model Dev. https://doi.org/10.5194/gmd-2019-287.

Zhou, Q.T., Driscoll, C.T., Sullivan, T.J., Pourmokhtarian, A., 2015. Factors influencing critical and target loads for the acidification of lake-watersheds in the Adirondack region of New York. Biogeochemistry. 124, 353-369.

Zhu, C., Byrd, R., Lu, P., Nocedal, J., 1997. Algorithm 778: L-BFGS-B: Fortran subroutines for large-scale bound-constrained optimization, ACM T. Math. Software, 23(4), 550-560, https://doi.org/10.1145/279232.279236.

Zhu, L., Henze, D.K., Cady-Pereira, K.E., Shephard, M.W., Luo, M., Pinder, R.W., et al., 2013. Constraining U.S. ammonia emissions using TES remote sensing observations and the GEOS-Chem adjoint model. J. Geophys. Res. Atmos. 118, 3355-3368.

Zhu, L.Y., Henze, D.K., Bash, J.O., Cady-Pereira, K.E., Shephard, M.W., Luo, M., et al., 2015. Sources and Impacts of Atmospheric NH_3: Current Understanding and Frontiers for Modeling, Measurements, and Remote Sensing in North America. Curr. Pollut. Rep. 1, 95-116.

Zhu, Z., Bergamaschi, B., Bernknopf, R., Clow, D., Dye, D., Faulkner, S., et al., 2010. A method for assessing carbon stocks, carbon sequestration, and greenhouse-gas fluxes in ecosystems of the United States under present conditions and future scenarios. Scientific Investigations Report 2010-5233. Reston, VA: US Geological Survey. 188 p.

Zuend, A., Marcolli, C., Booth, A.M., Lienhard, D.M., Soonsin, V., Krieger, U.K., et al., 2011. New and extended parameterization of the thermodynamic model AIOMFAC: calculation of activity coefficients for organic-inorganic mixtures containing carboxyl, hydroxyl, carbonyl, ether, ester, alkenyl, alkyl, and aromatic functional groups. Atmos. Chem. Phys. 11, 9155-9206.